UNIVERSITY OF OSLO
Department of Informatics

Environmentally Adaptive Sonar on an Autonomous Underwater Vehicle

Master thesis

Ole Jacob Lorentzen

November 2012

Environmentally Adaptive Sonar on an Autonomous Underwater Vehicle

Ole Jacob Lorentzen

November 2012

Acknowledgements

I would like to express my sincere gratitude to my supervisors, Senior Scientist Stig A. V. Synnes (FFI[1]), Associate Professor Kyrre H. Glette (UiO[2]) and Scientist Martin S. Wiig (FFI[1]) for their suggestions, constructive feedback and taking the time to review and comment on my work.

I would like to thank the Norwegian Defense Research Establishment, and especially Adjunct Associate Professor Roy E. Hansen, for giving me the opportunity to work with the HUGIN team in the first place, as well as his kind gesture to let me use a desk in his office throughout the year of writing this thesis.

I would also like to thank Kongsberg Maritime and everyone involved for taking the time to record and provide experimental data.

I would like to mention my fellow students and the student community Robotica Osloensis for being an inspiration throughout my education at the University of Oslo.

Finally, I would like to express my gratitude to family and friends for support and patience throughout my work with this thesis.

Ole Jacob Lorentzen, Oslo, November 2012

[1]Norwegian Defense Research Establishment (*Forsvarets forskningsinstitutt*)
[2]University of Oslo

Abstract

When imaging in shallow waters with an active sidescan sonar system, the performance is limited by signal returns that have been reflected multiple times off the sea surface and the sea floor. These are known as *multipaths*, referring to the multiple alternative paths the signal can travel to arrive back at the sonar sensor. These multipath signals can not be distinguished from the direct path signals on a single sonar sensor, but their presence can be indicated by the *coherence* from an interferometric sonar sensor.

This thesis addresses the multipath problem by proposing, analyzing and implementing an environmentally adaptive sonar method using an interferometric sidescan sonar on an autonomous underwater vehicle. The method is comprised of first estimating the ocean environment from a measurement, and then adapting to the environment using simulations provided by a sonar performance model for shallow waters. An electronically shapable transmit beam, made possible by a vertical transmitter array, is used in order to adapt the emitted energy to the current environment.

The analyses in this thesis show that the ocean environment can be estimated with sufficient precision to accurately predict sonar performance for other sonar settings. The accuracy of these predictions are verified by real measurements. Furthermore, the sonar settings which give the best results in simulations for these environments are found. Search algorithms for such improved settings are analyzed and discussed, and a proof of concept algorithm is proposed, implemented and successfully tested on real measurements.

Contents

Part I

Introduction

Chapter 1

Environmentally Adaptive Sonar

Environmentally adaptive sonar (EAS) is a concept of automatically adapting the sonar measurements to the current ocean environment. This may include controlling the sonar sensor parameters, like beam widths and beam directions, controlling the altitude, depth and other vehicle behavior in order to improve performance. For example, the maximum range can be increased by controlling the sonar sensor parameters, and the coverage rate can be improved by automatically adapting the track spacing to utilize the achieved range.

This thesis aims to suggest and investigate a method intended to improve the sonar sensor performance, i.e. the swath width and signal strength. The method is based on simulating the sonar in its current environment and controlling the sonar sensor parameters and vehicle altitude.

In this chapter, the motivation for adapting to the environment is presented first, followed by an introduction to the proposed method for environmentally adaptive sonar and its application. Finally, the outline of this thesis is presented.

1.1 Motivation

Sidescan sonar imaging has become a much used and studied technology since being introduced in the early 1960s (Lurton 2002). Both civilian and military applications of sidescan sonar imaging and bathymetry (underwater topography) are numerous. Civilian applications include high-resolution sea floor mapping and imaging, ocean exploration and monitoring, marine geological surveys, inspection of subsea structures and pipelines, as well as archaeological search operations. Military applications also include imaging, mapping and many of the other applications mentioned as civilian. A special and important military application is mine counter measures (MCM), which uses high resolution imagery to identify mines.

Modern sidescan sonar systems perform well in deep water with imaging at ranges hundreds of meters away from the sensor (Lurton 2002). With the synthetic aperture principle, introduced in Chapter 2, high along-track resolution is maintained even

at maximum range (Hansen 2011). In shallow water, however, the imaging range is limited by *reverberation* (Synnes et al. 2009). Reverberation is the effect that gives cathedrals and caves their well known acoustic signature where the sound takes a long time to die away. This is fine for a cathedral choir, which utilizes it to bring a sense of depth to the voices, but poses a problem when we are trying to detect a coherent sound signal. To illustrate this, imagine that we send out a controlled sound signal in a cathedral. Suppose that we received an echo of this signal. We measured the time it took from when we sent it until the echo was received. Because we know how fast the sound travels through the air, we are able to calculate from just how far away the echo originated. Then, some instants later, we receive another echo. Since this echo arrived later than the first one, we assume that it is from a source further away. How do we know that this echo isn't in reality from the same source as the one we received a few instants earlier - bounced off one or two cathedral walls? Unfortunately, the answer is that we don't.

Under water the sea floor and the sea surface serves as cathedral walls reflecting the sound. An example of this effect on a sonar image can be seen in Figure 3.2 on page 19, where the imaging range is good on a day of bad weather, but significantly degraded on another day of fair weather. This is because the flatter sea surface facilitates the reverberation effect. Active sonar imaging usually assumes that the received signals have traveled the direct path to the target reflector on the sea floor and back again. With reverberation we have several other paths that the sound can travel and arrive back at the receiver at the same time instant, e.g. to a closer point on the sea floor and back via the surface. All these other paths are referred to as *multipath* signal returns, or multipaths (MPs) for short.

The natural question to pose in relation to the reverberation or multipath problem is how it can be mitigated. Previous attempts to do this are studied in Chapter 3, all of which are post-processing methods or require specialized sonar antennas for use in shallow water. This might be because traditional sonar system have lacked a method of automatically estimating performance, the computing power to do it on the fly during data collection, and the ability to sufficiently steer and control the transmit and receive beam patterns. With a few of the leading state-of-the-art available sonar systems currently in the process of overcoming these challenges, the next step is to explore possibilities of automatically sensing and adapting to the present reverberation (Hansen et al. 2011). This is the main subject of this master thesis: dynamically adapting the sonar settings to the sensed environment in order to improve performance.

1.2 Concept

This thesis aims to propose and analyze an environmentally adaptive sonar method comprised of estimating the ocean environment and adapting to it using an interferometric sidescan sonar on an autonomous underwater vehicle (AUV).

The ocean environment estimation is achieved by fitting the parameters of a sonar

performance model to initial measurements. The adaptation is achieved by means of controlling a shapable transmit beam and the altitude of the sonar carrying vehicle. This concept for environmentally adaptive sonar is based on using the sonar performance model to simulate the performance with other sonar settings than the ones that are currently being used, in order to choose how the transmit beam should be shaped. The intention is to find sonar settings tailored to the current, local ocean environment which will improve the measurement substantially.

This process begins by predicting the ocean environment based on one or several measurements with generic sonar settings. When the ocean environment has been resolved, a search for new sonar settings that simulate improved performance begins. A simple flowchart of such a process, with swath width as the measure to be improved, is shown in Figure 1.1.

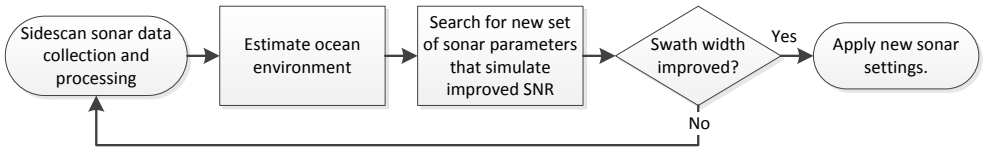

Figure 1.1: Conceptual flowchart of the environmentally adaptive sonar process.

1.3 Application

The environmentally adaptive sonar concept suggested in this thesis is inspired by the capabilities of the sonar sensor HISAS 1030 carried by the HUGIN autonomous underwater vehicle. HUGIN is an underwater vehicle developed by Kongsberg Maritime (KM) and the Norwegian Defense Research Establishment (*Forsvarets forskningsinstitutt*, FFI). HISAS 1030 is a state-of-the-art interferometric synthetic aperture sonar that is capable of high resolution imaging and bathymetric mapping of the sea floor. Typical system specifications for the HISAS 1030 sonar are listed in Table 1.1, and an image of a HISAS 1030 sonar sensor is shown in figure 1.2.

Table 1.1: Typical system specification for the HISAS 1030 interferometric SAS.

Center frequency	100 kHz
Wavelength	1.5 cm
Bandwidth	30 kHz
Total frequency range	50-120 kHz
Along-track resolution	3 cm
Cross-track resolution	3 cm
Maximum range (at 2 m/s)	200 m
Area coverage rate	2 km^2/h

Figure 1.2: Photo of a HISAS 1030 sonar sensor on HUGIN 1000 KM3. Picture taken after the data collection, and the AUV is still wet from the dive.

1.4 Outline

The chapters in this thesis are sorted in different parts. Part I, *Introduction*, contains this introductory chapter. Part II, *Background*, contains both an overview of sonar technology, as well as a survey of existing literature on multipath reduction in the ocean environment, where existing methods for multipath reduction are surveyed and discussed. Part III, *Modeling the ocean environment*, describes how the environment modeling is performed. Part IV, *Adapting to the ocean environment*, describes how the simulations of new settings are done, and discusses how the search should be conducted, e.g. with respect to which search criteria should be considered. Part V, *Implementation*, contains a chapter describing a simple implementation of a full environmentally adaptive sonar algorithm. Part VI, *Conclusion*, contains a final chapter which sums up results and conclusions in this thesis.

Chapter 1: ***Environmentally Adaptive sonar,*** which you are reading right now, is an introduction to the subjects and concepts that are the main topics in this thesis. The concepts of sonar imaging, multipath and environmental adaptation are mentioned to prepare the reader for the background chapters and the rest of the thesis.

Chapter 2: ***Active Sonar*** introduces the principle of active sonar along with an overview of the imaging process. Synthetic aperture imaging is explained and the coverage rate of sidescan and synthetic aperture sonar imaging is discussed.

Chapter 3: ***Multipath*** defines multipath and describes the problem it presents to active sonar imaging. The second half of the chapter is a survey of existing literature on the subject of multipath reduction in the ocean environment. The final section introduces the multipath modeling software used in this thesis.

Chapter 4: ***Search Algorithms*** provides a description of search algorithms used in this thesis, as well as a description of a curve fitting technique used in the environment estimation.

Chapter 5: ***Measurements*** presents a description of the datasets recorded for this thesis and details how they are organized for later reference.

Chapter 6: ***Environment Estimation*** describes in detail how the environment estimation is performed by fitting simulated signal to noise ratio to the measured one. Section 6.1 covers the method of calculating the signal to noise ratio from a measurement. Section 6.2 discusses which criteria should be used for choosing which simulated signal to noise ratio best describes the measured one, and describes the challenges of this process. Section 6.3 describes which model inputs are required. Finally, Section 6.4 sums up and present some thoughts on which parts could benefit from further improvements.

Chapter 7: ***Environment Estimation Results*** presents results and analyses on all the aspects of the environment modeling. The results are divided into two analyses. The first is a test of curve fitting performed in order to decide how to choose which area of the measured SNR curve should be used for curve fitting. The second analysis is sea floor and sea state estimation.

Chapter 8: ***Modeling SNR with New Parameters*** describes the parameters altitude, beam width and electronic steering of the beam that are varied in order to improve performance, as well as other inputs needed for the simulator in Section 8.1. Which metrics can be used as fitness criteria, and how well are they expected to work, is discussed in Section 8.2. Finally, Section 8.3 sums up the observations and present some thoughts on which parts could benefit from further improvements.

Chapter 9: ***Adaptation Results*** presents results and analyses on adaptation. First, a model verification analysis is performed, where each line is isolated and used to predict all the other measured lines. This way real measurements are available to confirm whether the simulations are correct. The second analysis is a brute force search in order to investigate how some of the different fitness criteria described in Section 8.2 work, and which sonar settings gives the best results.

Chapter 10: ***Adaptive Sonar Algorithm*** describes how a simple implementation of a full algorithm has been done. A few results from running it on the available datasets are provided, and the performance and suggested improvements of the algorithm is discussed.

Chapter 11: ***Conclusion*** sums up the important results and conclusions in this thesis, and suggests topics that could be investigated further in future work.

There are also appendices attached to the thesis. Appendix A contains tables with results from the curve fitting tests in Chapter 7. Appendix B contains tables with results from the bottom type and sea state estimation in Chapter 7.

Part II

Background

Chapter 2

Active Sonar

Sonar, or **so**und **n**avigation **a**nd **r**anging, is based on using sound to detect or locate objects. In passive sonar, we listen passively to the sound of the environment. In active sonar, we actively transmit a sound pulse of some kind and use the received echo to detect and locate objects. Note that, unless otherwise stated, all uses of the word *sonar* in this thesis refer to sidescan sonar, an active sonar looking to the side of the vehicle's travel direction.

In this chapter, the principle of active sonar is introduced along with an overview of the imaging process. Synthetic aperture imaging is explained and the coverage rate of sidescan and synthetic aperture sonar imaging is discussed.

2.1 Sound Ranging

In principle, sound ranging is a simple process where we emit a sound signal and measure the amount of time it takes to travel to the target, reflect off the target and travel back to the receiver. Given the sound velocity in the medium and the sensor geometry, we can calculate the range to the target. This range, the physical properties of the medium and the strength of the returned signal enable the estimation of the reflectivity of the target. This process is described thoroughly in several books, for example by Urick (1983), Burdic (1984) and Lurton (2002).

2.2 Imaging

Sonar imaging is to estimate the reflectivity for each resolution cell from the received data. This is illustrated in Figure 2.1. There are several methods to do this with an array sensor, including delay and sum beam forming (DAS, also known as back projection) and wavenumber-domain beam formers. Imaging is described well by Urick (1983), Burdic (1984) and Lurton (2002). Beamforming is thoroughly covered by Johnson and Dudgeon (1993).

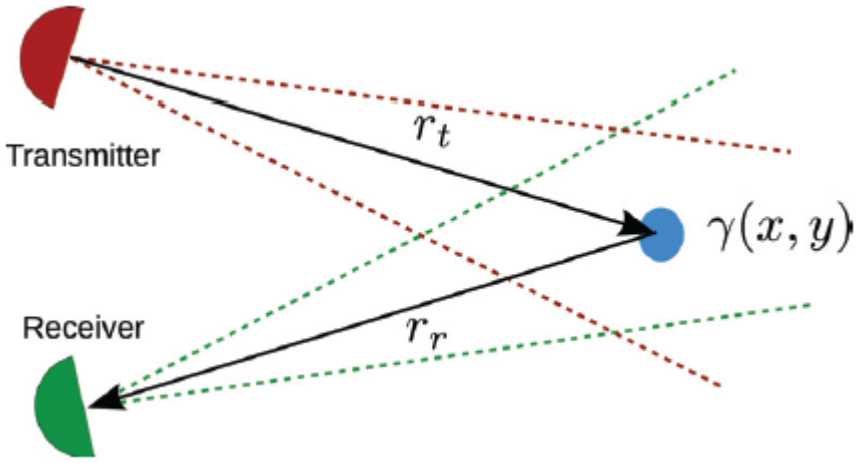

Figure 2.1: Basic imaging geometry. Figure adopted from Hansen (2011).

The resolution of a sonar image is defined on two axes: along-track resolution in the direction of the platform movement, and across-track resolution in the range direction (Lurton 2002). The across-track resolution δr for sidescan sonar imaging is proportional to the pulse bandwidth B and the propagation speed in the water c, and is given by $\delta r \approx \frac{c}{2B}$, assuming that the signal processing technique known as *pulse compression* is performed. The along-track resolution δx depends on the length of the sensor array L and the wavelength λ, which determines the angular resolution $\beta = \frac{\lambda}{L}$. The obtained along-track resolution is then the width of this beam at the imaging range, given by $\delta x = \frac{\lambda}{L} r$.

2.3 Synthetic Aperture Sonar

We can maintain desired resolution at far ranges by increasing the antenna size, but even at medium ranges this gets impractical due to platform limitations. Instead of increasing the physical antenna, the aperture can be built synthetically by moving the antenna and sampling in space as well as time (Hayes and Gough 2009; Hansen 2011). Such sampling is illustrated in Figure 2.2. By doing this, the along-track resolution's dependence on range is eliminated as a longer synthetic aperture can be used when the range increases. The along-track resolution without range dependence then becomes $\delta x_{SAS} = \frac{d}{2}$ for any r, where d is the size of an element in the array. This does not, however, enable imaging at unlimited range, due to the signal attenuation in the medium.

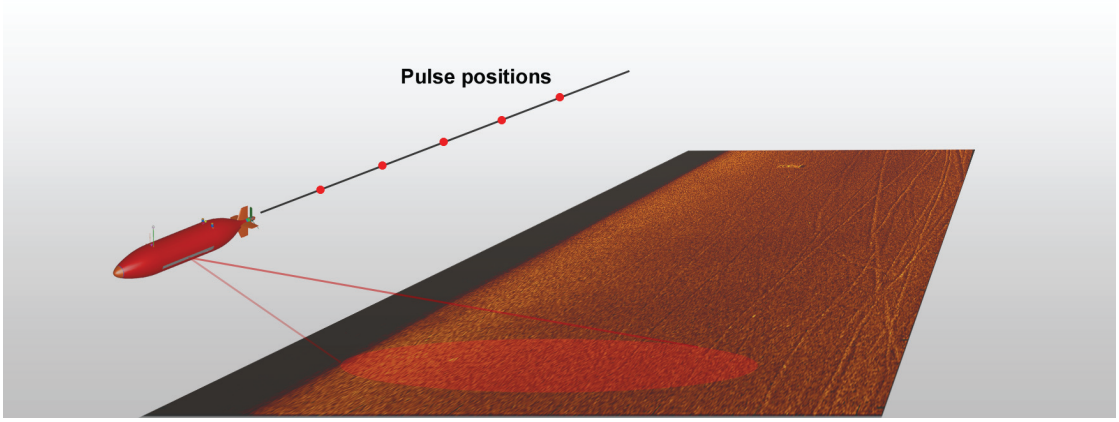

Figure 2.2: Data acquisition geometry for synthetic aperture sonar. Figure adopted from Hansen (2011).

2.4 Sea Floor Coverage

Sidescan sonars look sideways, and thus have a blind zone directly underneath the vehicle. Due to travel time ambiguities if looking downwards, filling this gap is not possible for such a sonar. We will always be left with a blind zone. Hence, without a gap-filler based on another system, it is necessary to run overlapping lines to cover the blind zones to achieve full coverage. Since every other line will cover each others' blind zones, it is only necessary to run two close lines before taking a double swath width spacing and running two new close lines. This pattern is illustrated in Figure 2.3, where the vehicle traveling into the page is illustrated by orange dots and the swath area of each line is layered for easy separation. From this figure we see that the coverage for each two close lines is $2x_{swath} + (2x_{gap} + x_{swath}) = 3x_{swath} + 2x_{gap}$, with the condition that $2x_{gap} < x_{swath}$ and x_{swath} is a conservative estimate of range.

This result indicates that best coverage is achieved when $x_{gap} = \frac{x_{swath}}{2}$. While the point is valid, it does not account for the fact that the signal to noise ratio (SNR) is often higher at shorter range. In other words, the image is often of better quality at shorter range. Therefore it can be desirable to limit the width of the blind zone, while at the same time maximizing the swath width.

If it is possible to add a sensor that could fill in the gap, e.g. a high resolution multibeam echosounder, this could increase the coverage rate per two lines from $3x_{swath} + 2x_{gap}$ to $4x_{swath} + 4x_{gap}$. This would likely impose a constraint on vehicle altitude above the sea floor, which in turn affects the sonar range, so the real gain might not be as large.

Figure 2.3: Illustration of two-sided sidescan sonar coverage.

2.5 Interferometric Processing

Using two sonar sensors spatially offset by a perpendicular baseline (an *interferometer*), the angular direction of an arrival signal can be measured (Hanssen 2001; Sæbø, T. O. 2010). With knowledge of the range, the angular direction and the geometry, the bathymetry can be resolved. This method is called interferometry and uses the phase information in the signals to accurately determine the distance difference between the sensors and the resolution cell. With knowledge of the sensors' geometry (the baseline) and the difference in range to the target from each sensor, the third dimension (height) can be resolved.

2.6 Sound Speed Profile

The sound speed in the ocean is not constant, but varies with temperature, salinity and depth (Lurton 2002). For simplicity, it is usually assumed that the sound speed can be represented as a function of depth, i.e. that the variations in salinity and temperature at the same depth are small. The *sound speed profile* (SSP) can then be presented by speed as a function of depth.

The variations are often local and need to be recorded at the time and place of the sonar measurements. This can be done either with a probe from a mother ship or, for the current depth, on the sonar sensor itself. Preferably, both methods are used and combined for a best-guess sound speed. The former is the most precise method for the entire water column, since it is not prone to platform navigation errors and can provide measurements of the entire sea column. On the other hand, it can not account for local variations in the sound speed like an AUV's own measurement can. Both these options can be utilized at the same time, computing a most likely combination of the two.

2.7 Self-noise

Self-noise is a term that includes several noise sources (Lurton 2002). Thermal, or electronic, noise is present in all electronic circuits, also for sonar systems. In addition to the thermal noise, there are also several other sources of platform self-noise. These include the acoustic noise radiated by the platform and received by the

transducer, mechanical vibrations to the transducer from the platform, hydrodynamic noise generated around the transducer and the platform, and noise radiated by other electrical devices on the platform.

In some cases, the self-noise is a visible interference in the signal. An example is if a harmonic from a frequency band used by another acoustic system on the platform is present in the sonar's frequency band. Apart from such interference, which can be detected and removed or avoided, it is assumed that the mentioned sources of self-noise are stable and can be described by a noise floor. With an example like the acoustic noise radiated by the platform and received by the sonar sensor, the self-noise level must be a function of the antenna beam pattern. Similarly, with an electronically steerable array, the self-noise level must be a function of the current steered beam pattern.

Chapter 3

Multipath

In this chapter multipath is defined and the problem it presents to active sonar imaging is explained. Section 3.1 defines multipath, while the notation used in this thesis to describe it is presented in Section 3.2. Section 3.3 presents the problem multipath poses to sonar imaging, and Section 3.4 discusses different methods to reduce multipath in both data collection and data processing. In Section 3.5 an overview is given of the sonar performance model *SMURF*, which is used in this thesis.

3.1 Definition of Multipath

In the context of sea floor imaging by active sonar, multipath is defined as all signal returns that are not direct returns. By direct it is meant that the sound goes directly from the transmitter to the target and gets reflected back to the receiver, which is usually in roughly the same position as the transmitter. Not all energy is reflected back towards the receiver. Most is scattered in different directions, depending on the scattering properties of the target. First order multipath occurs either when the energy is scattered towards the surface and back to the transmitter, or when the energy reflects off the surface and is scattered back to the receiver. This is illustrated by the *Bs* path in Figure 3.1. Second order multipath introduces a third reflection, e.g. a bottom to surface to bottom travel. Some multipaths that impact sonar images are illustrated in Figure 3.1.

A concise, yet precise definition of multipath is provided by Fish and Carr in *Sound Reflections*: *Multipaths are Sonar signals arriving at a target, or the sonar vehicle, from a single source but along different paths* (Fish and Carr 2001).

3.2 Notation

The notation used when referring to multipath returns indicates the sequence and type of scatterings. The scatterings are described using *s* for surface and *b* for bottom reflection. Small letters are specular (mirror-like) reflections and uppercase letters are non-specular (diffuse) scattering.

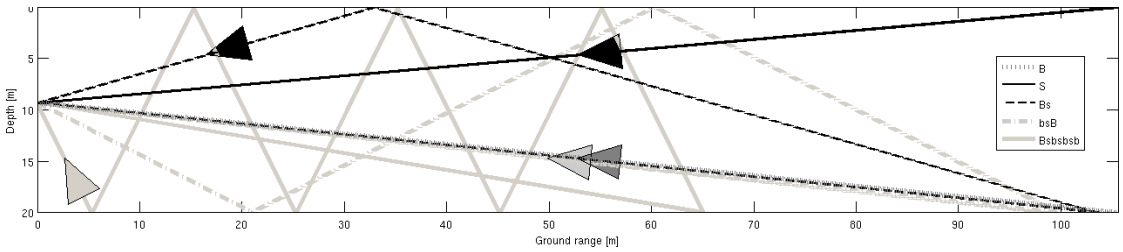

Figure 3.1: A few example multipaths of various order.

3.3 The Multipath Problem

Mapping of the sea floor was traditionally done from ships with either down-looking single-beam echo-sounders, or with multibeam echo-sounders (Blondel 2009). These devices have varying sea floor footprint depending on the water depth and local bathymetry. While the resolution they can provide is sufficient for some applications, AUVs using sidescan sonars and the synthetic aperture method can provide superior performance for high resolution sea floor mapping in some situations.

Sidescan sonars transmit a beam on each side that is broad in the vertical plane and narrow in the horizontal plane. In shallow water we have a channel between the reflecting sea surface and the sea floor. In this channel the signal may be reflected a number of times back and forth and make it back to the receiver, as illustrated in Figure 3.1. This is the multipath propagation described in Section 3.1.

One of the fundamental challenges in high-resolution imaging of the sea floor in shallow waters is multipath reflections off the sea surface (Hansen et al. 2011). The sea surface acts as a reflector to the sound and scatters all the incident energy back into the ocean. A flat sea surface will have more specular reflection than a rough surface, and thus give more energy in a received multipath signal. This leads to a lower Signal to Multipath Ratio (SMR) (Synnes et al. 2009). Because of this, we have the intuitively surprising result that bad weather (rougher sea surface) is actually better for sonar imaging in shallow waters. In bad weather conditions with high water currents it is, however, harder to maintain vehicle stability, which can cause severe image degradation (Hansen et al. 2011).

An example of multipath in two sonar images of the same scene taken in windy conditions (upper image) and calm conditions (lower image) is shown in Figure 3.2.

3.4 Methods to Reduce Multipath

There exist several general methods for reducing the effect of multipath, and varying implementations of each method. Here they have been organized into two main groups based on whether they deal with data processing or with the actual data collection. An analysis of some relevant methods is performed by reviewing literature for each of them. Specifically it is the data collection method of *adjusting transmit beam* that is

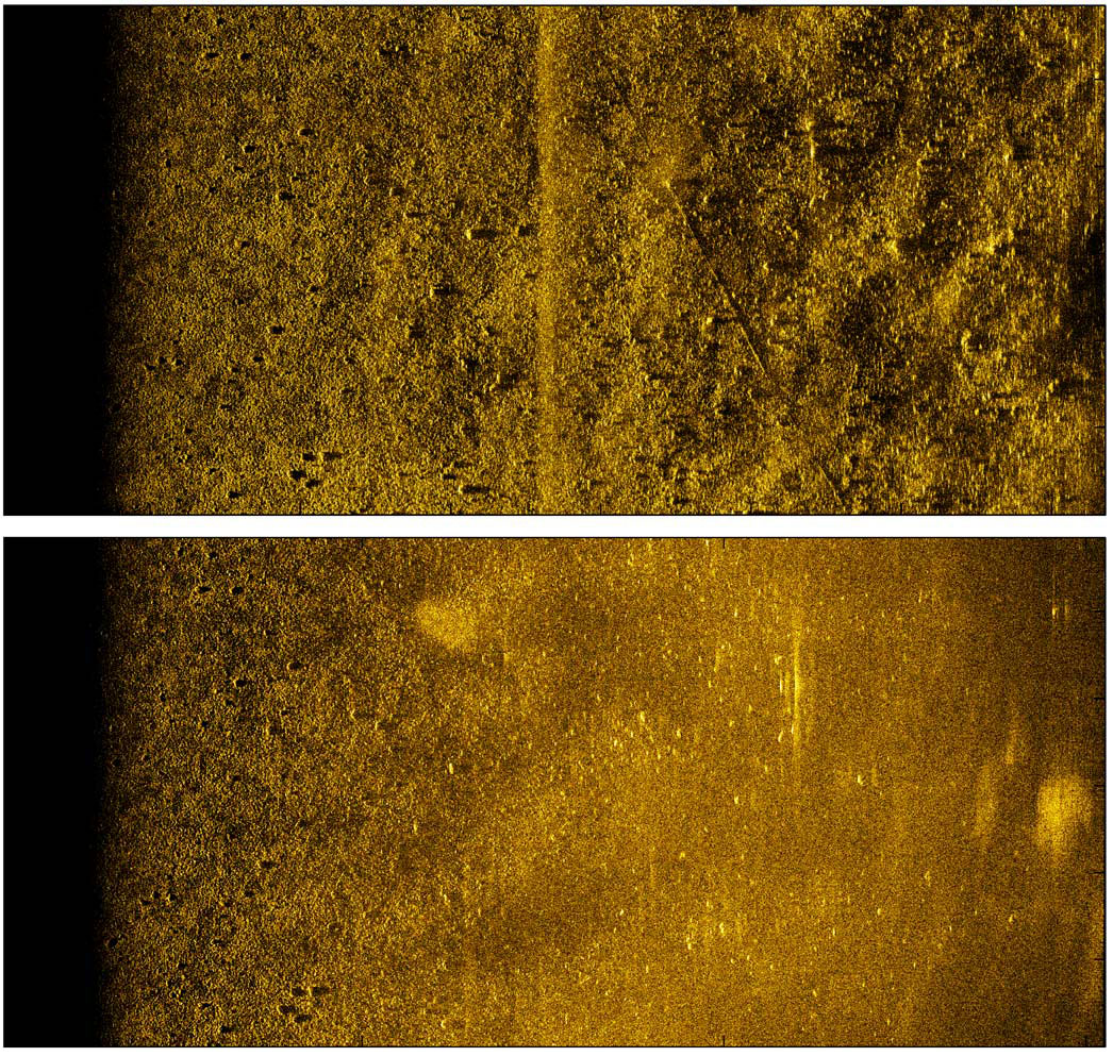

Figure 3.2: The figure is adopted from Hansen et al. (2011). Original description: *Effect of multipath in shallow waters. The two images are from close-to-identical vehicle tracks taken one week apart. The wind speed was relatively high during data collection for the upper image, whereas, during the data catch for the lower image, the sea was calm. The range interval is 0-150 m (left to right), and the along-track image size is 60 m. The water depth is only 9 m, and the vehicle depth is 3 m. Notice that the line about midrange in the upper image is an artifact caused by interference from other acoustic sensors on the AUV.*

investigated in this thesis.

3.4.1 Data Collection

This section investigates methods to reduce multipath in the data collection.

Multiple Sensors

Pinto et al. (2004) has proposed a synthetic aperture sonar system using two separate beams for both transmitting and receiving. The concept is derived from theory backed by measurements supporting that a wide beam is better at short range, while a narrow beam is better at long range. This seems sensible when considering that a small beam will concentrate the energy better and reduce the possibilities for multipath returns, while the second, wider beam for short range maintains the necessary coverage.

Pinto claims to show by simulation and experimental data that the *bsB* multipath is the most important multipath at long ranges because the incident angle is nearly identical to that of the direct signal return. By not ensonifying the sea floor at short range when imaging at longer ranges, the generation of the *bsB* multipath can be avoided. To achieve this, a two sensor setup is proposed with two sonars working simultaneously in different frequency bands. One sonar has a wide beam pattern to ensonify a larger portion of the near range and maintaining area coverage, while the second sonar has a narrow beam which avoids the most destructive multipath, and thus increases the range. This setup is illustrated in Figure 3.3(a).

The results from a simulation of the performance of this setup is shown in Figure 3.3(b). It is evident that when choosing the best signal to noise ratio of the lines corresponding to the wide and narrow beams, the effective range is increased compared to the conventional beam pattern, shown as the darkest line. Which beam pattern constitutes a *conventional beam* is not properly defined in the article. Note that this article uses a different sonar performance model, named *ESPRESSO*, than the one used in this thesis.

While this method seems to have potential to improve sonar range in shallow waters, it requires a complex set up and imposes a limitation on the bandwidth available for each beam. This bandwidth reduction reduces the across-track resolution of the system, given by $\delta r = \frac{c}{2B}$ from Section 2.2.

A flat sea floor is assumed in the design. The narrow beams might limit performance in rough bathymetry, e.g. with a steep uphill sea floor where, for example, a higher and wider beam might be more effective. In such cases adaptive techniques might be better suited.

Adjusting Transmit Beam

The spatial coherence from the real aperture interferometer is a good quality measure of the collected data, as detailed later in Chapter 6. It is suggested by Hansen et al. (2011)

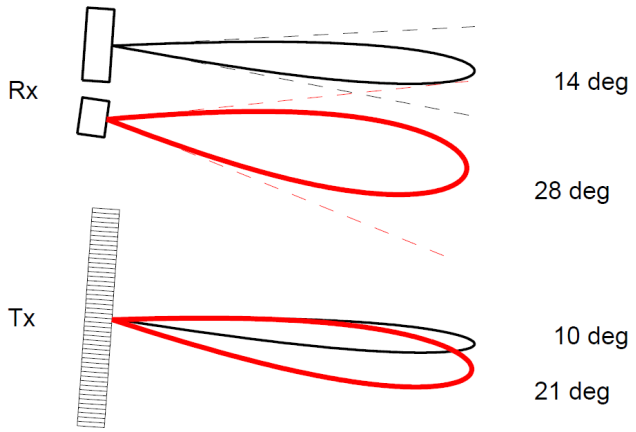

(a) Illustration of the suggested beam patterns in a multiple sensor setup. Different frequency bands are used for the wide and narrow beams.

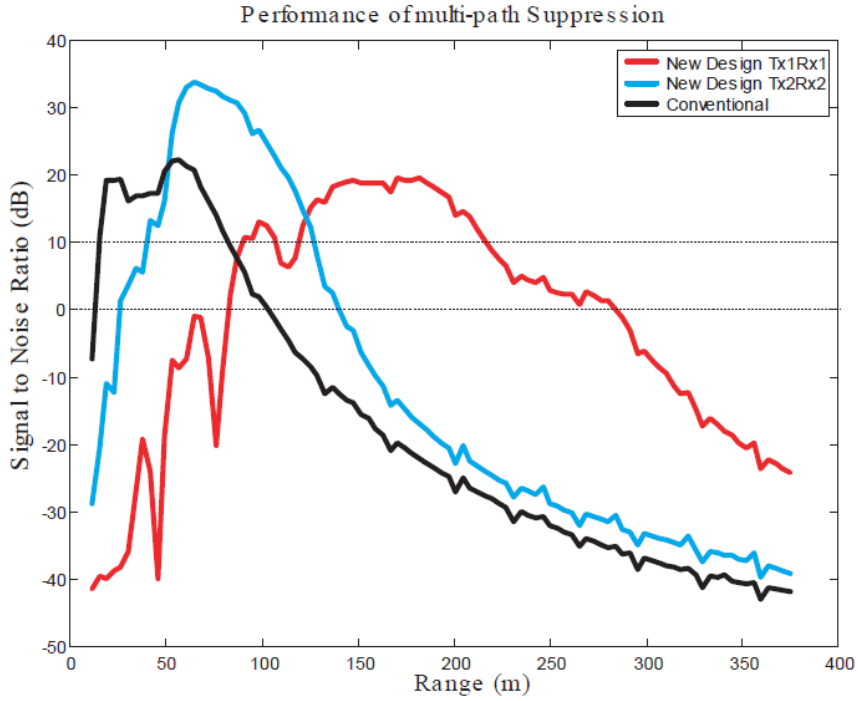

(b) Performance prediction of the suggested multiple sensor setup. The line with the highest peak value is the near-range beam, corresponding to the wide beams in Figure 3.3(a). The line which peaks at about 200 meters range is the far-range beam, corresponding to the narrow beams in Figure 3.3(a). The black line is a conventional beam, which is roughly explained to have a beam width of 40° centered around a direction of about 20°.

Figure 3.3: A simulated example of how a multiple sensor setup can improve the SNR. Both figures are adopted from Pinto et al. (2004).

that it can be used to adaptively adjust the sensor settings and the vehicle track to optimize data quality on collection.

Synnes (2009) has shown that a 60 % increase in shallow water imaging range could be achieved by varying the vehicle altitude and adjusting the receiver antenna angle and the electronically steerable transmit beam. This increase in range is achieved by using the multipath model Signal to Multipath Ratio of FOCUS Toolbox (SMURF) to estimate the settings which give best SNR (Synnes 2011). This will vary with varying ocean environment, i.e. weather conditions, sea floor and bathymetry. Therefore it is suggested that on-the-fly optimization of vehicle altitude and the transmitter beam pattern is desirable for best possible imaging range (Hansen et al. 2011).

The optimal sensor settings and altitude is estimated by, first, using the measured SNR and estimating the sea state and the bottom type. These impact how the emitted energy is reflected. Then, the sonar settings and altitude is tuned, and the resulting SNR is simulated.

As opposed to the multiple sensor method, this method cannot avoid ensonifying the sea floor at short range. Therefore, it is not possible to avoid the presumed most important *bsB* multipath in the same way. However, we can use the entire bandwidth of the system for all ranges, and thus get better across-track resolution.

This method requires a vertical transmitter array so that the beam can be electronically steered.

For synthetic apertures, applying new sonar settings on the fly can be done on a per line basis, but when using a delay-and-sum type algorithm it is trivial to apply different sonar parameters for each ping. This makes it possible to adapt the sonar parameters inside of a synthetic aperture.

3.4.2 Data Processing

This section investigates methods to reduce multipath in the data processing.

Conventional Delay and Sum Beam Forming

By having two or more vertically displaced antennas making up a vertical antenna array, it is possible to use signal processing techniques like delay and sum (DAS) beam forming to direct the antenna beam pattern (Johnson and Dudgeon 1993).

If we can estimate the expected angle of arrival and direct the beam towards it, we can dampen the noise from multipath returns coming from other directions (Blomberg et al. 2012). Delay and sum beam forming is done by applying a delay to the receiver antennas to steer and focus the beam in a given direction. Increasing the number of elements in the array enables the creation of a narrower beam, which is more directive.

The conventional delay and sum beam forming requires a number of receiver antennas to get the resolution required to distinguish direct signal from multipath returns, especially at long range. Adding receiver antennas is an expensive option and is limited by the size of the platform.

Additionally, this method requires a priori knowledge of what is the expected direct reflection angle. This is given by the sea floor bathymetry, meaning that a priori information about the bathymetry is required. A bathymetry can be obtained by the interferometric sonar sensor itself by calculating a rough sidescan bathymetry.

Super-resolution Techniques

Super-resolution techniques is a set of signal processing techniques that utilize a small vertical array (typically three or more elements) and various properties to overcome the limitations of angle of arrival estimation on a small vertical array (Chen et al. 2009). The main difference from the conventional delay and sum beam forming is that these techniques attempts to place nulls in the beam pattern at the angles of the multipath returns (Blomberg et al. 2012).

These are techniques such as the minimum variance distortionless response beam former (MVDR) (Capon 1969; Blomberg et al. 2012), the low complexity adaptive beam former (LCA) (Synnevåg et al. 2008; Blomberg et al. 2012), coherent source direction estimation (CSDE) (Xu and Stewart 1999), computed angle-of-arrival transient imaging (CAATI) (Kraeutner and Bird 1999), Bayesian MAP based estimation (Hayes 2004), blind separation (Kirsteins 2003) and robust Capon (minimum variance) beam forming (RCB) (Li et al. 2003; Blomberg et al. 2012). These mentioned methods are applicable to narrowband signals, but can be adapted for wideband applications (Van Trees 2002; Chen et al. 2009). Examples of such adaptions are wideband robust Capon beam forming (WRCB) which extends the RCB to the wideband application by dividing the signal into narrowband frequency bins, and a variant of it named steered robust Capon beam forming (SRCB) (Chen et al. 2009).

Image Enhancement: Multipath Removal by Image Interpolation

For those working with automated target recognition (ATR) or other image processing, removal of multipath by different methods of locating likely multipath contributions in the already formed image and removing them by interpolation has been successful and useful (Le Bas et al. 1995; Crosby and Cobb 2005; Blondel 2009). However, these methods dispose of data that may have contained useful information from the actual sea floor had the multipath been reduced or removed in an earlier processing step. It is a method of determining which data should be disregarded. Thus it does not improve the data, but rather enhances the image for easier human or machine inspection. Therefore it is not a viable candidate in this thesis and has not been investigated further.

3.4.3 Summary

Several methods to approach the multipath problem have been reviewed. They are organized into two groups: data collection and data processing. See Table 3.1 for a summary.

Table 3.1: Overview of methods to reduce multipath.

	Data Collection
Multiple sensors	Design the sonar system with multiple beams using different frequency bands to illuminate far ranges with a more narrow beam than near ranges.
Adjusting transmit beam	Adjust the transmitted beam pattern electronically in such a way that multipath noise is reduced.
	Data Processing
Conventional delay and sum beam forming	Use delay and sum beam forming on a vertical antenna array to maximize the signal received from the expected angle of arrival.
Super-resolution techniques	Use signal processing techniques on a small vertical antenna array to improve the delay and sum method.
Image enhancement	Multipath removal by image interpolation.

The main difference between these groups is that the data collection methods work closer to the measurement than the data processing methods, which work on already collected data. The data collection methods have some special requirements. The multiple sensor method requires a special setup with two more or less separate sonars. The adjusting transmit beam method requires both an advanced transmitter array, an interferometric receiver and a robust and responsive way to sense and adapt to the environment. The data processing methods include the angle of arrival estimation and super-resolution techniques, which both require a few vertical sensors to collect the required data. They do not, however, require to change anything during the actual data collection process. They might seem easier to implement than the data collection methods, but the physical and cost limitations of adding numerous receiver antennas can be prohibitive to the effectiveness of these methods. The last technique discussed, image enhancement, is furthest away from the source of the data. It is only a method of classifying which data is bad and disregard it. This does not improve the data quality, so it is not interesting in terms of multipath reduction. It is, however, useful in fields like automated target recognition and other image analysis.

The methods discussed can be combined to exploit their different strengths. We can, for example, have an adjustable transmit beam on the multiple sensor setup. Or, we can add a few receiver arrays to any of the setups and use super-resolution techniques.

After creating the final image products it can be edited for different purposes by image enhancements methods. How well these techniques work together and the limitations of such combinations is not obvious and should be investigated further.

When data has already been collected, we can improve the end result by processing it in the right way. However, this processing improvement is at some point limited by what information is actually available in the data we have collected. Therefore, it is an important point that it is desirable to improve quality as close to the data source as possible. It is better to collect good quality data and then try to improve it even further, than to collect flawed data and try to improve that. Hence, more work should be put into improving the data collection methods. Data processing methods are still important because they can be combined with data collection methods to improve the end result even further.

Among the data collection methods, the adjustable transmit beam method with a model for multipath simulation looks promising in simulations and experimental data (Synnes et al. 2009; Synnes 2011). It has yet to be detailed, implemented and documented to improve data collection automatically. This method is the subject of this thesis.

3.5 Multipath Modeling with the SMURF Model

The *adjustable transmit beam method* requires a model for multipath simulation. In this thesis, the multipath modeling software Signal to MUltipath Ratio of Focus toolbox, SMURF, will be used to model multipath. This section briefly describes the inner workings of the SMURF model, as documented in *Sonar performance modeling for sea floor imaging in shallow waters - concept and implementation in SMURF 1.0 and SPRAY 1.0* (Synnes 2011).

In order to simulate the path of sound in the water, many different aspects of how pressure waves travel through viscous media need to be considered. Sound in water does not travel in a straight line, but refracts due to variations in the water. These deviations vary with both the sound signal itself and with changing properties in the medium. For example, the refraction varies with frequency, but it is also a function of the sound speed which changes with salinity, pressure and temperature. After traveling through the medium, the sound waves hits an interface and reflection, scattering and transmission needs to be taken into account. With multipaths there may be interactions with several interfaces and several paths through the water column. It is not an easy task to simulate what the result will be.

The model assumes that only a single non-specular scattering can be included. This is based on the specular reflections being much stronger than the non-specular ones, so that too much energy is lost if multiple non-specular scatterings are undertaken (Synnes 2011). This simplification considerably reduces the number of possible paths, and thus the number of computations needed if trying to calculate all the paths for a simulation.

The SMURF model is a 2-dimensional model, i.e. depth and range. It uses four different sub-modules to predict the signal to noise ratio as a function of distance. These

are named the ray tracing module, the scattering module, the ray management module and the sonar equation module. A simplified flowchart of how these modules work together to simulate the sonar performance is shown in Figure 3.4.

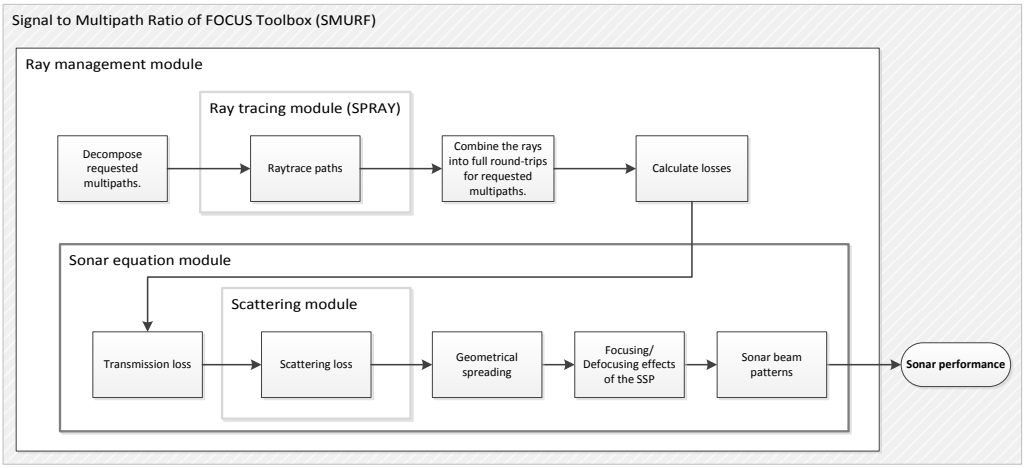

Figure 3.4: Flowchart of how the multipath modeling software SMURF works.

The ray tracing module of SMURF calculates the ray paths in the water by an analytic solution for sound speed profiles of piecewise constant gradient (Synnes 2011). The implementation is based on the solution in Section 6.2 of Ziomek (1985).

The scattering module of SMURF consists of different scattering models for sea floor and sea surface scattering, based on the values of *High-frequency ocean environment acoustic models handbook* (APL-UW 1994).

The ray management module attempts to optimize the code by not retracing ray paths that have already been traced, but rather combining simpler paths into higher order paths (Synnes 2011).

While the other modules concern themselves with the ray paths, the sonar equation module is there to compute the signal level of each ray at receive time (Synnes 2011). From the other modules, the complete round-trip distances and the reflectivity for each of the scatterings and specular reflections of the multipaths are available to the sonar equation module. The reflectivities are multiplied together to obtain the total reflection loss. Geometrical spreading and focusing or defocusing of rays induced by the sound speed are compensated for, and absorption loss is computed using the model of Urick (1983).

An example of a simulated SNR from the SMURF-model is shown in Figure 3.5. In the upper plot, the red line is a measured SNR and the blue line is the simulated SNR that best matched the bright red part of the measured one. From the measured SNR we cannot read out which multipaths contribute. The simulated SNR, however,

is a result of the ratio between the direct signal return and the multipaths, called the *signal to multipath ratio*. These can be read in the lower plot where all the signal returns are plotted as relative intensity. The red line is the direct signal return. The yellow line is the estimated self-noise level, and the other lines are various orders of multipaths, as listed in the legend. The blue simulated SNR in the upper plot is simply given by the ratio between the red direct signal return and all the multipaths, plus self-noise, shown in the lower plot.

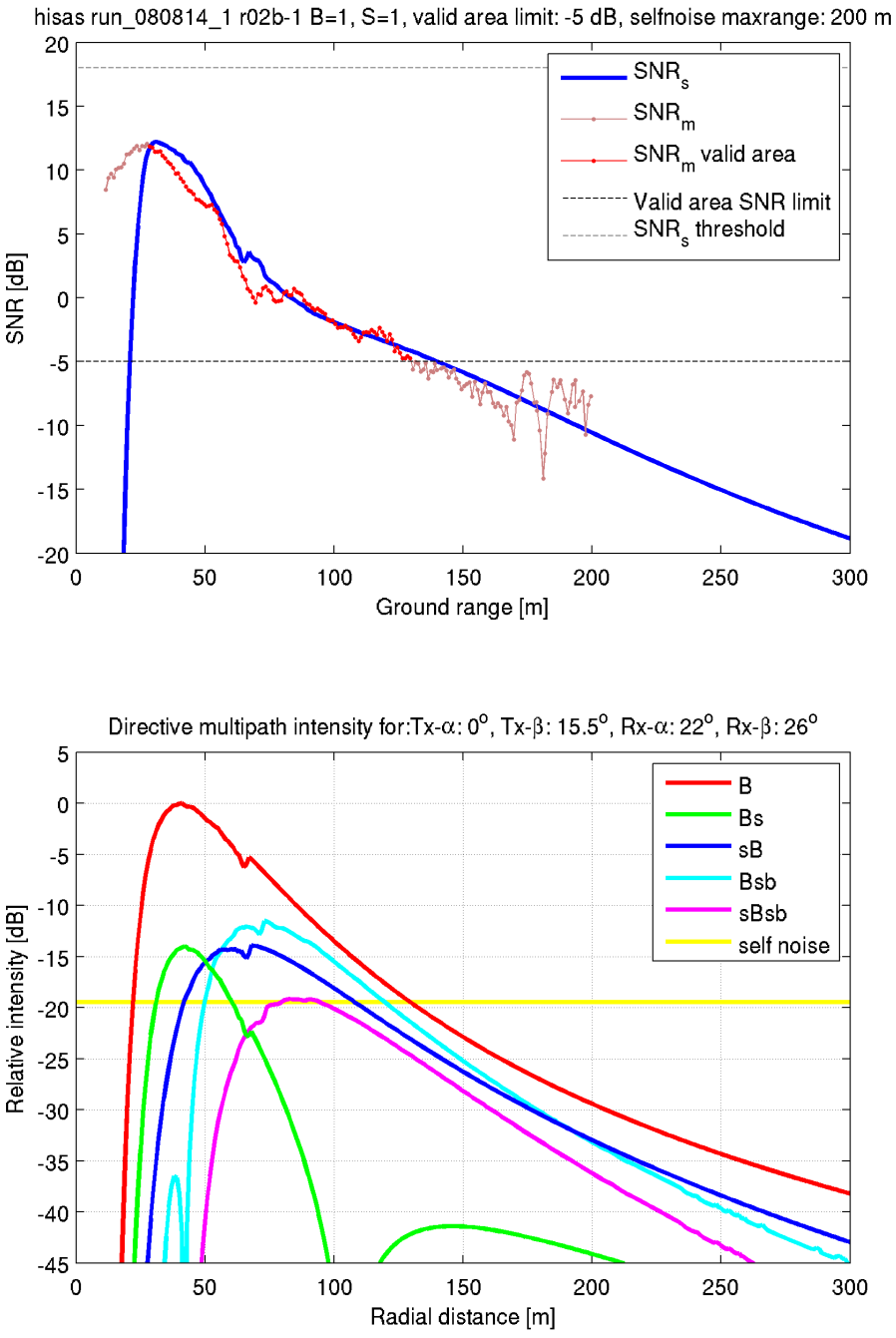

Figure 3.5: Example of a simulated SNR from the SMURF-model.

Chapter 4

Search Algorithms

This chapter provides descriptions of search algorithms used for adaptation in this thesis, as well as a description of a curve fitting process used for estimating the environment.

Curve fitting is done by the method of least squares, in which function parameters are selected in order to minimize the sum of squared error between measurements and the function value.

The first search algorithm described is a straightforward brute force search, in which all possibilities are tried out. Then, the slightly more sophisticated search algorithms hill climbing and steepest descent search are described, where the algorithms try to slightly change the function parameters and move in the direction which is better, under the assumption of a search space without discontinuities.

The brute force search is used primarily for analysis purposes throughout the thesis, but is not intended to be a part of the final algorithm. Hill climbing and steepest descent search, on the other hand, are search algorithms that should have the potential for decent performance. The hill climbing search algorithm is used in the implementation in Chapter 10.

4.1 Curve Fitting

Curve fitting refers to finding the parameters for a function so that it best fits a measurement. In the particular application of this thesis it involves finding the sonar performance model parameters that best models the measured SNR.

Curve fitting in this thesis is done by the least squares method of minimizing the squared difference between a measurement and a function value. This is a common technique and is covered in several books, e.g. Kay (1993), Marsland (2009) and Burden and Faires (2010).

The mathematical expression for the error is shown in Equation 4.1, where y_n is the discrete measurement at index n, $\bar{x}$ is a vector of the function parameters, $\tilde{y}_n(\bar{x})$ is the function value for parameters $\bar{x}$ corresponding to the measurement at index n, and N

represents all the indexes that will be used for fitting.

$$\epsilon(\bar{x}) = \sum_{n=1}^{N} \left(y_n - \tilde{y}_n(\bar{x})\right)^2 \tag{4.1}$$

The expression for the actual least squares curve fitting is then simply to find the function parameters $\bar{x}_{\text{LSE}}$ that minimizes the squared error $\epsilon(\bar{x})$ as shown in Equation 4.2.

$$\bar{x}_{\text{LSE}} = \arg\min_{\bar{x}} \epsilon(\bar{x}) \tag{4.2}$$

As a performance measure describing how well the least squares curve fitting worked, the root mean squared error (RMSE or $\sqrt{\text{MSE}}$) will be used as shown in Equation 4.3.

$$\text{RMSE} = \sqrt{\frac{1}{N}\epsilon(\bar{x}_{\text{LSE}})} \tag{4.3}$$

A smaller RMSE-value means that there is less error between the measurement and the function given the fitted parameters. Since it is normalized by the number of samples fitted to, i.e. averaged, it can be used to compare the fits for different measurements. The squared error sum $\epsilon(\bar{x}_{\text{LSE}})$ can not be used in the same manner when there are varying number of samples used for curve fitting. For a function being fitted to a single measurement, however, minimizing the squared error sum and minimizing the mean squared error is equivalent, as the only difference is the constant factor N.

4.2 Brute Force Search

Brute force search, also known as exhaustive search, is a trivial search algorithm that is guaranteed to come up with the best solution (Marsland 2009).

The brute force search works by trying out every solution to the problem at hand and picking the best one. The major drawback of the brute force search is that it is impractical for all reasonably sized problems. The computational cost will either require too much time or too much computational capacity.

In this thesis, the brute force search has been used extensively for analysis purposes. This is because it has been useful to explore the entire search spaces for the given problem and analyze them before choosing which search algorithm to apply in the final algorithm. It is not trivial to develop and implement multiple objective search algorithms, but with the brute force search results, multi-objective solutions can be analyzed.

4.3 Hill Climbing

Hill climbing is a greedy local search algorithm that starts with an initial solution and incrementally changes single elements in the solution (Marsland 2009). If the new solution is better, it is accepted. Note that this differs from gradient descent methods, which will change *all* the elements in the solution together according to the gradient of the hill. This may lead to faster convergence, but requires calculating the gradients.

For example, in a 2D Euclidean space, the hill climbing algorithm can be as simple as attempting to move 1 step north, south, east and west, giving four function evaluations per iteration. The best new function value is picked, and the algorithm repeats. If the new solutions are not better than the current one, a local maximum has been found and the algorithm will usually terminate.

The main drawbacks of hill climbing is that it is prone to getting stuck at local maxima and plateaus (Marsland 2009). Therefore, the starting point of the hill climbing algorithm is a crucial parameter in order to avoid getting stuck in a local maximum or on a plateau.

Note that even though hill climbing is described as a maximization algorithm here, the difference between maximization and minimization is simply a minus sign. Therefore, it can be used for both maximization and minimization problems.

4.4 Steepest Descent

Steepest descent search, also known as gradient descent search, works much in the same way as hill climbing in that it moves one step in the best direction, but it relies on estimating the gradient of the function and moving in the steepest direction by a step where the step size is proportional to the steepness (Marsland 2009). Note that moving a step may involve changing all the elements in the solution together, as opposed to the hill climbing algorithm which only changes one element at a time.

The main advantage of steepest descent method over hill climbing is that it can potentially skip some steps in a steep area because it adapts the step size according to the improvement in the objective function.

Defining steepest descent is problematic in discrete search spaces because it relies on the objective function being continuous in order for it to be differentiable, at least numerically. Hill climbing does not observe the same limitation.

Chapter 5

Measurements

This chapter presents a description of the two datasets *120515_1* and *120918_2* recorded by Kongsberg Maritime for this thesis, as well as a third dataset *080814_1* with measurements performed in shallow water in 2008 for another project. All the datasets contain measurements performed with multiple sonar settings and altitudes.

For each dataset, the method of performing the measurements is described, as well as the organization of the data, including the indexing used in the results sections of this thesis. Relevant notes are also included, e.g. weather measurements and known sources of noise. Figures of the navigation and measured bathymetries are also included.

All the measurements were performed from Kongsberg Maritime's M/K Simrad Echo shown in Figure 5.2. The measurements were performed with HUGIN vehicles carrying a HISAS 1030 sonar, shown in Figure 5.1.

This thesis is about making a method and a model work with real measured data. The measurements are not separable or supplemented with a correct answer of everything that contributes to the measured value, and therefore such measurements will always have irregularities. Noise will be present, both white and colored, from known and unknown sources. Software have bugs, and with physical measurements hardware bugs and calibration errors are also issues. So are possible human errors in planning the mission, and actions taken by the operator during the data collection. It is not possible to find exact results with a simplified model, and it is prohibitively hard to try and develop an ocean environment model without any simplifications. Thus, exact accuracy is not achievable, nor is it the aim of this thesis. The aim is rather to achieve sufficient accuracy to attain the goal of finding better sonar parameters and altitudes for the current measurement.

Figure 5.1: Photo of HUGIN 1000 HUS in the water. The rope from the nose leads to the nose cone, which has been released to recover the AUV.

Figure 5.2: A photo taken on 18.9.2012 of the Kongsberg Maritime's Simrad Echo used as the mother ship on all the data collections.

5.1 Deep Water Dataset 120515_1

The deep water dataset 120515_1 was designed and collected for this thesis in May 2012. It was collected with the kind help of Kongsberg Maritime using the HUGIN 1000 KM3-vehicle equipped with a HISAS 1030 sonar.

The mission area is located outside Horten at about 190 meters depth. The area has relatively flat bathymetry, which is plotted from the collected data in Figure 5.3. The weather conditions for this run, from measurements on the weather station at Gullholmen, was a moderate breeze of about 6 m/s from the south (The Norwegian Meteorological Institute 2012). This corresponds to approximately 4 on the Beaufort scale, but since we are near land, the sea state converted to the Beaufort scale under the assumption of fully developed sea is expected to be lower.

The vehicle depth was varied by setting the control system to a given altitude. For each attempted altitude above the sea floor, six different sets of sonar settings were applied for the duration of 36 pings each. A simple overhead view of the mission navigation is shown in Figure 5.4.

The lines are marked as a*dd*t*ss*b*b*-1. The letters dd are replaced by the requested altitude, e.g. 05 for 5 meters above the sea floor. The letters ss are replaced by the electronic steering, e.g. 10 for 10° electronic steering in addition to the 22° mechanical steering for a total of $22° - 10° = 12°$ down from the horizon. The letters bb are replaced by the beam width, e.g. 20 for 20°. Additionally, the lines are numbered from 1 through 30 for easy reference. The lines, along with sonar settings, depths and swath widths, are listed in Table 5.1.

The actual mean altitude above the sea floor is measured to be a few meters higher than the requested altitude, as can be seen in Table 5.1.

Images of the measured swath width for dataset 120515_1 as a function of altitude and beam direction are shown for beam widths 10° and 20° in Figure 5.5. The best swath width is obtained with 10° beam width, 30 meters altitude and a beam directed 17° down from the horizon.

Table 5.1: List of all the lines in dataset 120515_1. Measured swath width and swath lower and upper limits (LL and UL) in meters, measured as the area with estimated SNR higher than 0 dB, as described in Chapter 6. Beam width centered around the beam direction, which is defined positive down from the horizon.

Line	Beam width [°]	Beam dir. [°]	Altitude [m]	Depth [m]	Swath [m]	LL [m]	UL [m]
1: a05t0510-1	10	17	9	188	161	14	175
2: a05t0520-1	20	17	7	190	133	13	146
3: a05t1010-1	10	12	7	189	123	14	137
4: a05t1020-1	20	12	6	190	129	15	144
5: a05t1510-1	10	7	7	190	110	11	121
6: a05t1520-1	20	7	6	191	114	14	128
7: a10t0510-1	10	17	16	182	184	16	201
8: a10t0520-1	20	17	11	185	157	13	170
9: a10t1010-1	10	12	13	184	174	14	189
10: a10t1020-1	20	12	11	186	159	13	172
11: a10t1510-1	10	7	11	185	133	13	146
12: a10t1520-1	20	7	11	186	146	18	164
13: a15t0510-1	10	17	20	177	204	26	230
14: a15t0520-1	20	17	17	180	196	17	214
15: a15t1010-1	10	12	18	179	189	19	209
16: a15t1020-1	20	12	17	180	188	17	206
17: a15t1510-1	10	7	17	180	163	17	181
18: a15t1520-1	20	7	17	180	174	15	190
19: a20t0510-1	10	17	30	166	271	0	271
20: a20t0520-1	20	17	23	174	212	22	234
21: a20t1010-1	10	12	28	169	221	29	250
22: a20t1020-1	20	12	22	175	196	23	219
23: a20t1510-1	10	7	25	172	194	25	219
24: a20t1520-1	20	7	22	175	195	20	215
25: a30t0510-1	10	17	33	162	230	42	272
26: a30t0520-1	20	17	32	163	239	31	270
27: a30t1010-1	10	12	33	162	226	36	262
28: a30t1020-1	20	12	32	164	233	31	264
29: a30t1510-1	10	7	32	163	204	34	238
30: a30t1520-1	20	7	32	164	226	32	258

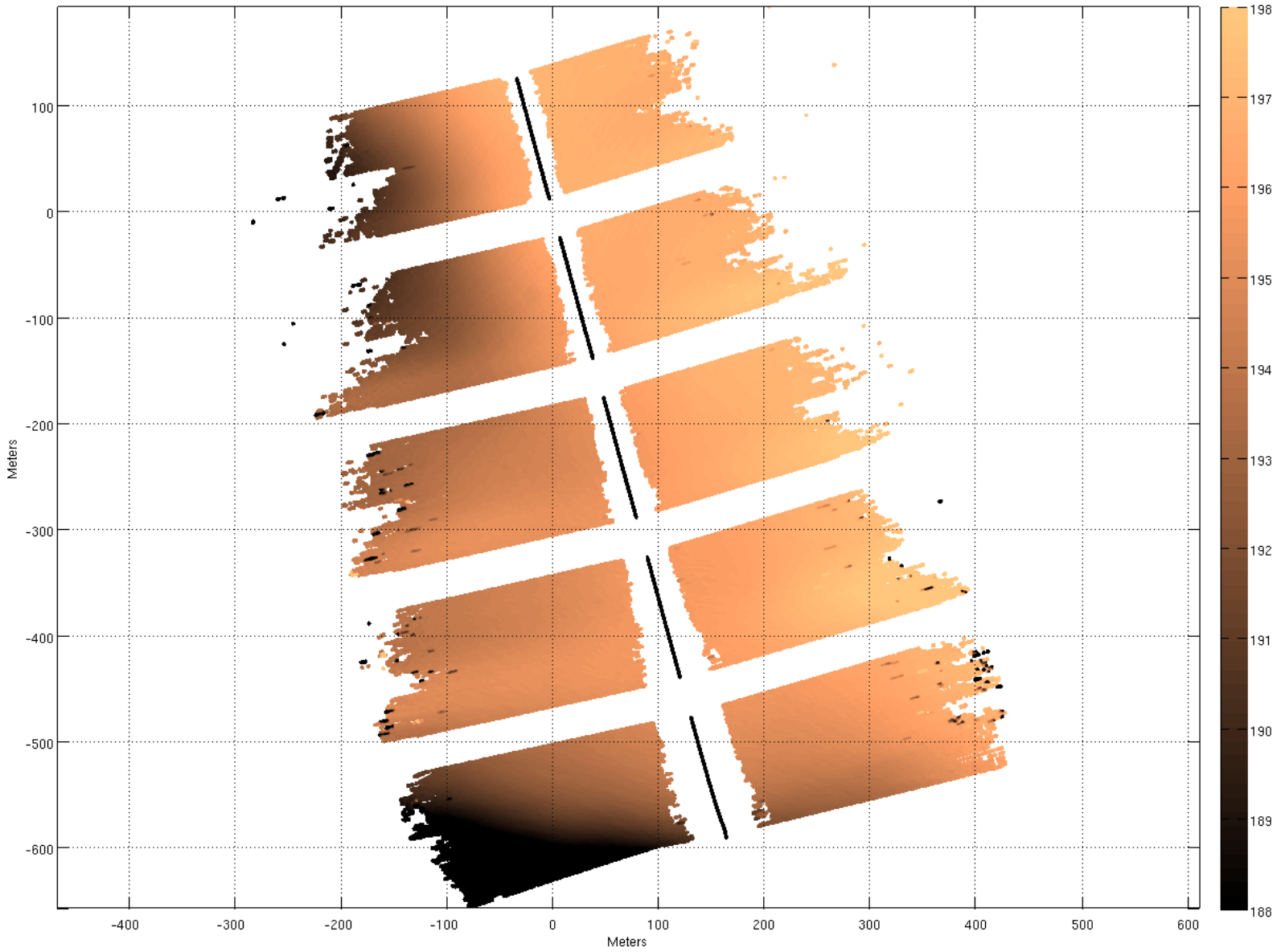

Figure 5.3: Bathymetry mosaic of dataset 120515_1. Values on all axes in meters.

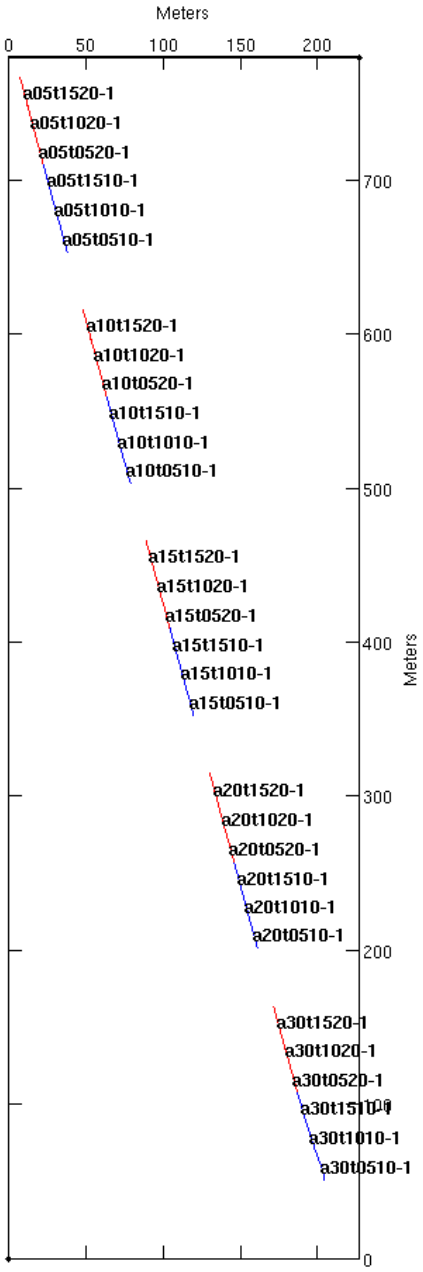

Figure 5.4: Navigation overview of all lines in dataset 120515_1

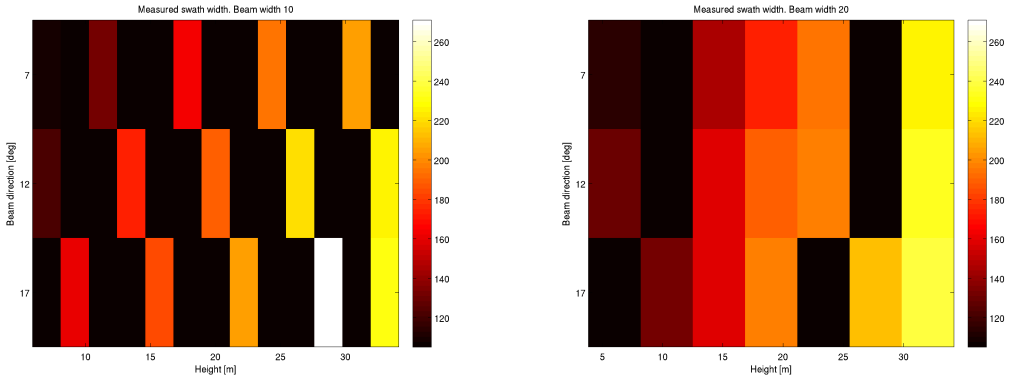

(a) Beam width 10°

(b) Beam width 20°.

Figure 5.5: Measured swath width for dataset 120515_1 as a function of depth and beam direction for beam widths 10° and 20°. Black squares represent missing data, which are there because of slight errors in the altitude caused by the control system.

5.2 Shallow Water Dataset 120918_2

After working with the deep water dataset 120515_1 at about 190 meters depth, a similar measurement in shallow water was needed. Dataset 120918_2 was designed and collected for this thesis in September 2012, again with the kind help of Kongsberg Maritime and the same HUGIN 1000 KM3-vehicle equipped with a HISAS 1030 sonar.

The mission area is located at about 16 meters depth outside Horten. The area has relatively flat bathymetry, which is plotted from the collected data in Figure 5.7. The vehicle depth was this time controlled by depth settings, with which the control system proved more accurate than the previous attempt to request an altitude. A sketch of the navigation for this mission is shown in Figure 5.8. For each depth, six different sonar settings were applied for the duration of about 79 pings each. The ping repetition rate was set lower than what is usual in shallow water to make sure that the range of the measurements was not limited by this.

The weather conditions were observed from the mother ship during the run. Fair weather with a gentle breeze of 5 m/s was recorded on the ship bridge at 13:20. This corresponds to approximately 3 on the Beaufort scale, but since we are near land, the sea state converted to the Beaufort scale under the assumption of fully developed sea is expected to be lower. The picture in Figure 5.6 is included to aid in finding the sea state converted to the Beaufort scale under the assumption of fully developed sea to be about 2. The wind direction was approximated to be 180°. On measurements from the weather station at Gullholmen, the weather log for the same time indicates a fresh breeze of about 8 m/s from the south (The Norwegian Meteorological Institute 2012).

The lines are marked as *n*d*m*t*ssbb*-1. The letter n is replaced with either the number 1 or 2 to represent which of the two lines it is. The letter m is replaced by the requested depth, e.g. 2 for 2 meters depth. The letters ss are also here replaced by the electronic steering. The letters bb are replaced by the beam width. Additionally, the lines are numbered from 1 through 41 for easy reference. The lines, along with sonar settings, depths and swath widths, are listed in Table 5.2. Note that the first measurement, 1d2t0510, is not included. This is due to the mother ship staying directly to the side of the line, which contaminated the data from this line since it was run at only two meters depth.

Images of the measured swath width for dataset 120918_2 as a function of altitude and beam direction are shown for 10° and 20° beam widths in Figure 5.9. The best swath width is obtained with 10° beam width, 9 meters altitude and a beam directed 17° down from the horizon.

There were some unresolved issues with what looks like noisy bathymetry for this run. The effect can be quite easily seen in the bathymetry mosaic in Figure 5.7.

Figure 5.6: A photo of the ocean during the data collection on September 18th 2012. The sea state under the assumption of fully developed sea corresponds to about 2 on the Beaufort scale.

Table 5.2: List of all the lines in dataset 120918_2. Measured swath width and swath lower and upper limits (LL and UL) in meters, measured as the area with estimated SNR higher than 0 dB, as described in Chapter 6. Beam width centered around the beam direction, which is defined positive down from the horizon.

Line	Beam width [°]	Beam dir. [°]	Altitude [m]	Depth [m]	Swath [m]	LL [m]	UL [m]
1: 1d2t0520-1	20	17	10	2	72	17	90
2: 1d2t1010-1	10	12	10	2	74	16	90
3: 1d2t1020-1	20	12	10	2	76	15	91
4: 1d2t1510-1	10	7	10	2	67	14	81
5: 1d2t1520-1	20	7	10	2	73	17	90
6: 1d4t0510-1	10	17	9	4	88	12	100
7: 1d4t0520-1	20	17	8	4	73	19	92
8: 1d4t1010-1	10	12	9	4	81	14	95
9: 1d4t1020-1	20	12	9	4	78	15	93
10: 1d4t1510-1	10	7	8	4	72	12	84
11: 1d4t1520-1	20	7	9	4	76	14	90
12: 1d6t0510-1	10	17	6	6	73	11	84
13: 1d6t0520-1	20	17	6	6	78	13	91
14: 1d6t1010-1	10	12	6	6	79	13	92
15: 1d6t1020-1	20	12	6	6	69	11	81
16: 1d6t1510-1	10	7	6	6	66	11	77
17: 1d6t1520-1	20	7	6	6	74	15	89
18: 1d8t0510-1	10	17	3	8	57	10	67
19: 1d8t0520-1	17	3	8	53	10	63	
20: 1d8t1010-1	10	12	3	8	55	10	65
21: 1d8t1020-1	20	12	3	8	45	12	57
22: 1d8t1510-1	10	7	3	8	42	11	53
23: 1d8t1520-1	20	7	3	8	54	15	69
24: 2d2t0510-1	10	17	9	3	79	13	92
25: 2d2t0520-1	20	17	9	2	98	16	114
26: 2d2t1010-1	10	12	10	2	99	13	112
27: 2d2t1020-1	20	12	9	2	83	14	97
28: 2d2t1510-1	10	7	10	2	82	13	95
29: 2d2t1520-1	20	7	9	2	87	12	99
30: 2d4t0510-1	10	17	9	4	111	11	122
31: 2d4t0520-1	20	17	8	4	103	13	116
32: 2d4t1010-1	10	12	9	4	108	12	120
33: 2d4t1020-1	20	12	8	4	88	11	99
34: 2d4t1510-1	10	7	7	4	84	12	96
35: 2d4t1520-1	20	7	7	4	89	9	98
36: 2d6t0510-1	10	17	5	6	96	9	105
37: 2d6t0520-1	20	17	5	6	94	8	102
38: 2d6t1010-1	10	12	5	6	91	9	100
39: 2d6t1020-1	20	12	4	6	84	7	91
40: 2d6t1510-1	10	7	5	6	80	7	87
41: 2d6t1520-1	20	7	4	6	80	8	88

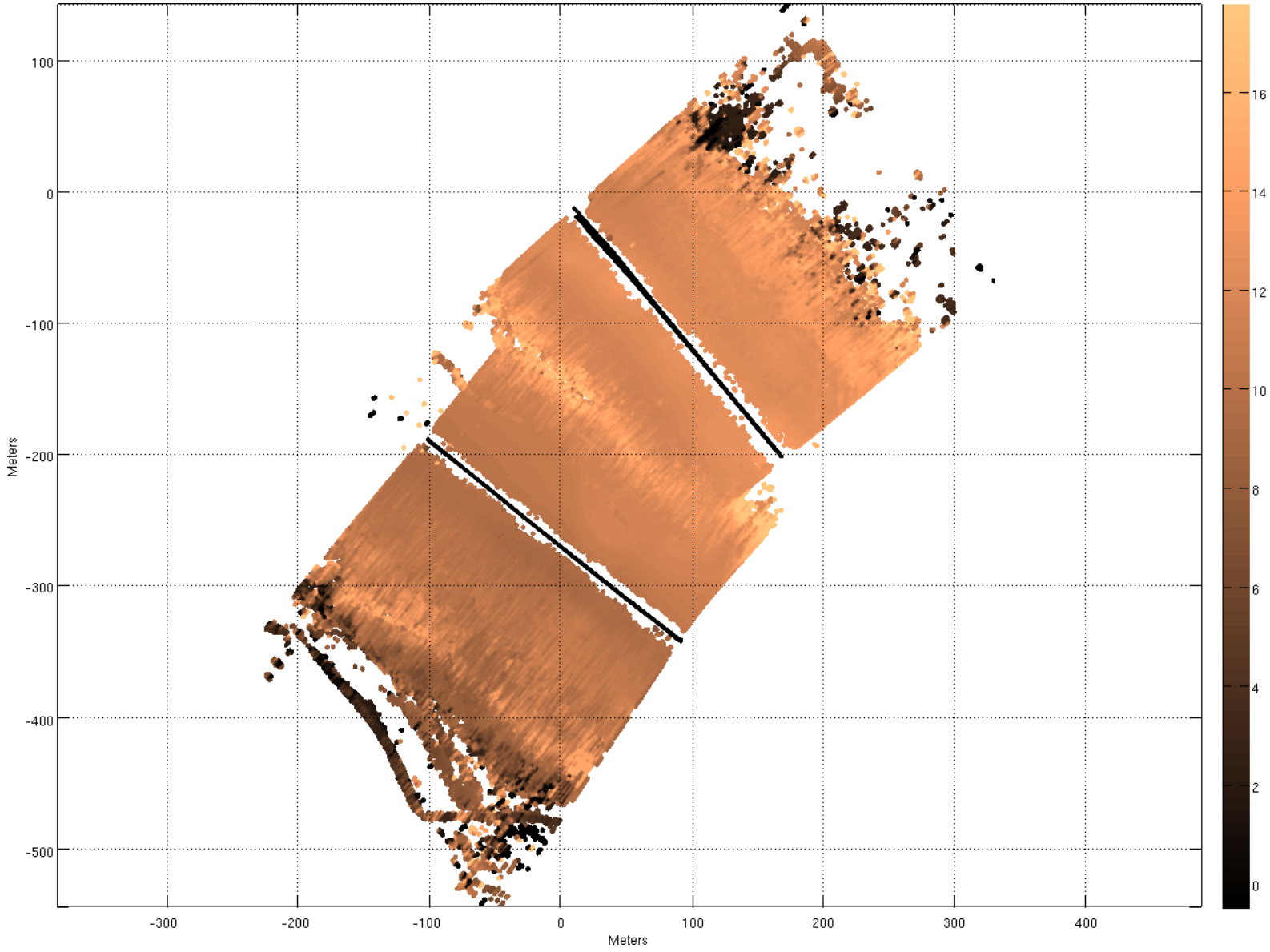

Figure 5.7: Bathymetry mosaic of dataset 120918_2. Values on all axes in meters.

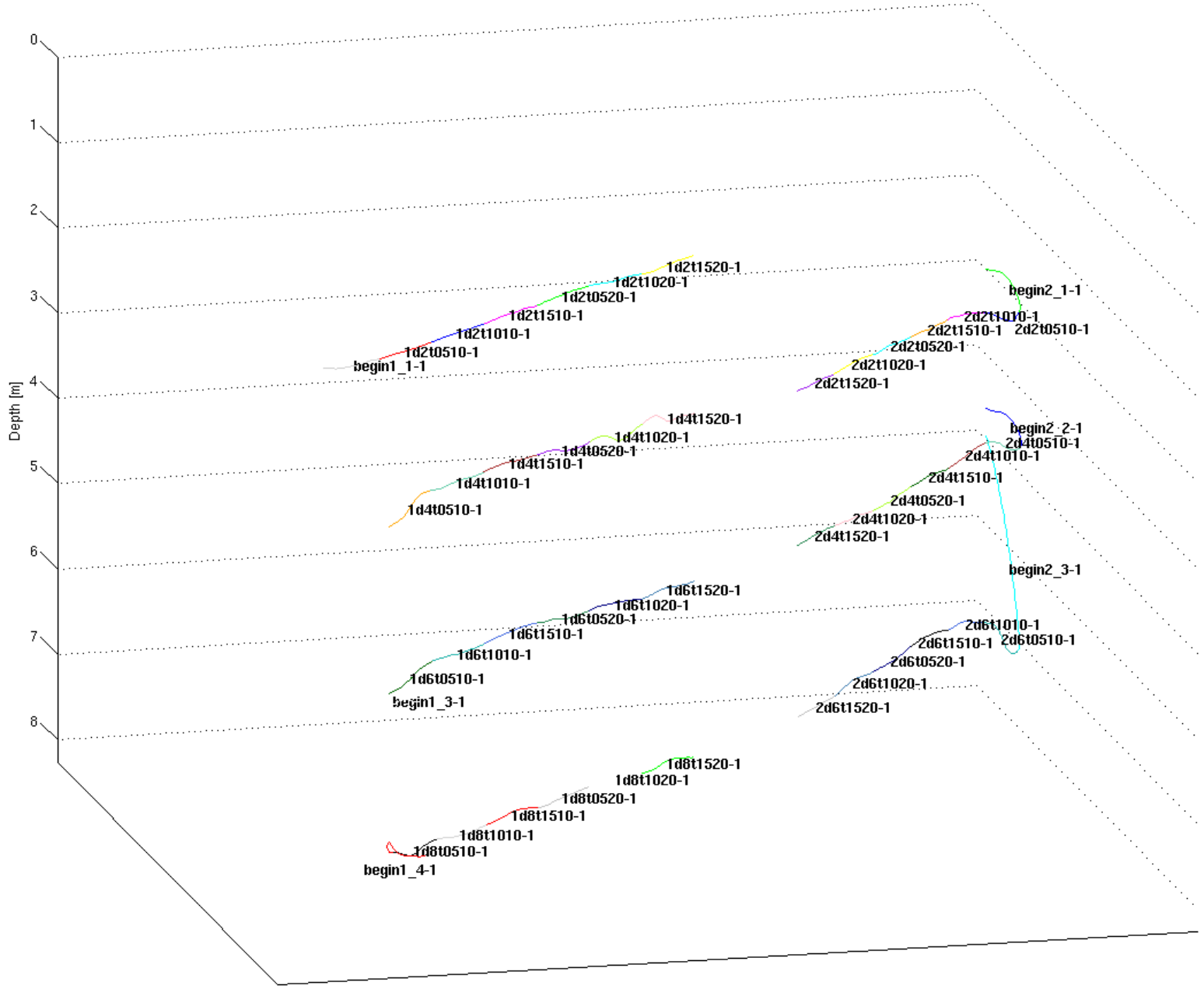

Figure 5.8: Navigation overview of all lines in dataset 120918_2.

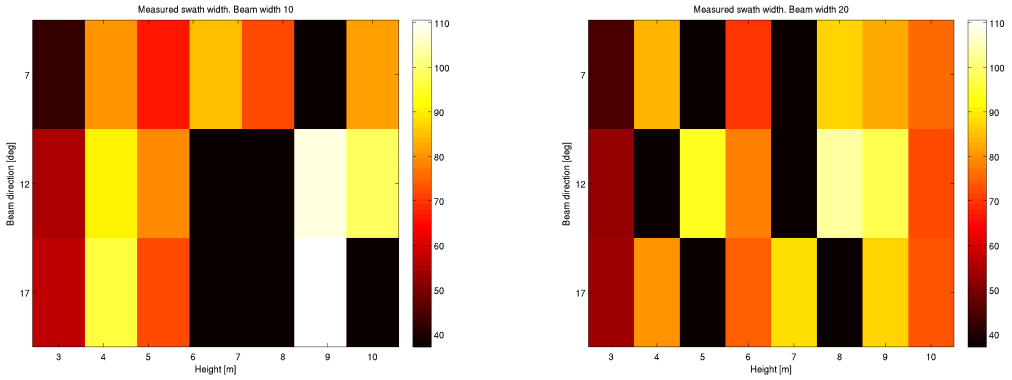

(a) Beam width 10°

(b) Beam width 20°.

Figure 5.9: Measured swath width for dataset 120918_2 as a function of depth and beam direction for beam widths 10° and 20°. Black squares represent missing data, which are there because of slight errors in the altitude caused by the control system.

5.3 Shallow Water Dataset 080814_1

The shallow water dataset 080814_1 was collected by the Norwegian Defense Research Establishment in 2008 intended to be used for analyzing the performance of various sonar settings and altitudes, work which relates to the development of the SMURF model (Synnes et al. 2009).

The sea floor depth is about 16 meters. The area has relatively flat bathymetry, displayed in Figure 5.10. A sketch of the navigation for this mission is shown in Figure 5.11. Notice the three distinctly different depths that have been repeated several times.

The weather conditions for this run was recorded at a later time using logs from the weather station at Gullholmen. It shows fair weather with a gentle breeze of about 4.3 m/s blowing from 225°, approximately a south-west wind direction (The Norwegian Meteorological Institute 2012). This corresponds to 3 on the Beaufort scale, but since we are near land, the sea state converted to the Beaufort scale under the assumption of fully developed sea is expected to be lower.

The lines are marked as r*nn*b-1 where the letters nn are replaced by line numbering from 1 through 12. All lines were collected with a beam width of 15.5°. The lines, along with sonar settings, depths and swath widths, are listed in Table 5.3.

An image of the measured swath width for dataset 080814_1 as a function of altitude and beam direction is shown in Figure 5.12. The best swath width is obtained with 12 meters altitude and a beam directed 15° down from the horizon.

Table 5.3: List of all the lines in dataset 080814_1. Measured swath width and swath lower and upper limits (LL and UL) in meters, measured as the area with estimated SNR higher than 0 dB, as described in Chapter 6. Beam width centered around the beam direction, which is defined positive down from the horizon.

Line	Beam width [°]	Beam dir. [°]	Altitude [m]	Depth [m]	Swath [m]	LL [m]	UL [m]
1: r01b-1	16	15	10	6	63	10	73
2: r02b-1	16	22	12	4	57	12	69
3: r03b-1	16	19	12	4	83	11	95
4: r04b-1	16	15	12	4	92	12	103
5: r05b-1	16	22	10	5	56	10	66
6: r06b-1	16	19	10	6	81	10	91
7: r07b-1	16	15	10	6	89	10	99
8: r08b-1	16	12	10	6	91	9	100
9: r09b-1	16	19	8	8	64	8	72
10: r10b-1	16	15	8	8	84	8	92
11: r11b-1	16	12	8	8	79	8	87
12: r12b-1	16	15	10	6	90	10	100

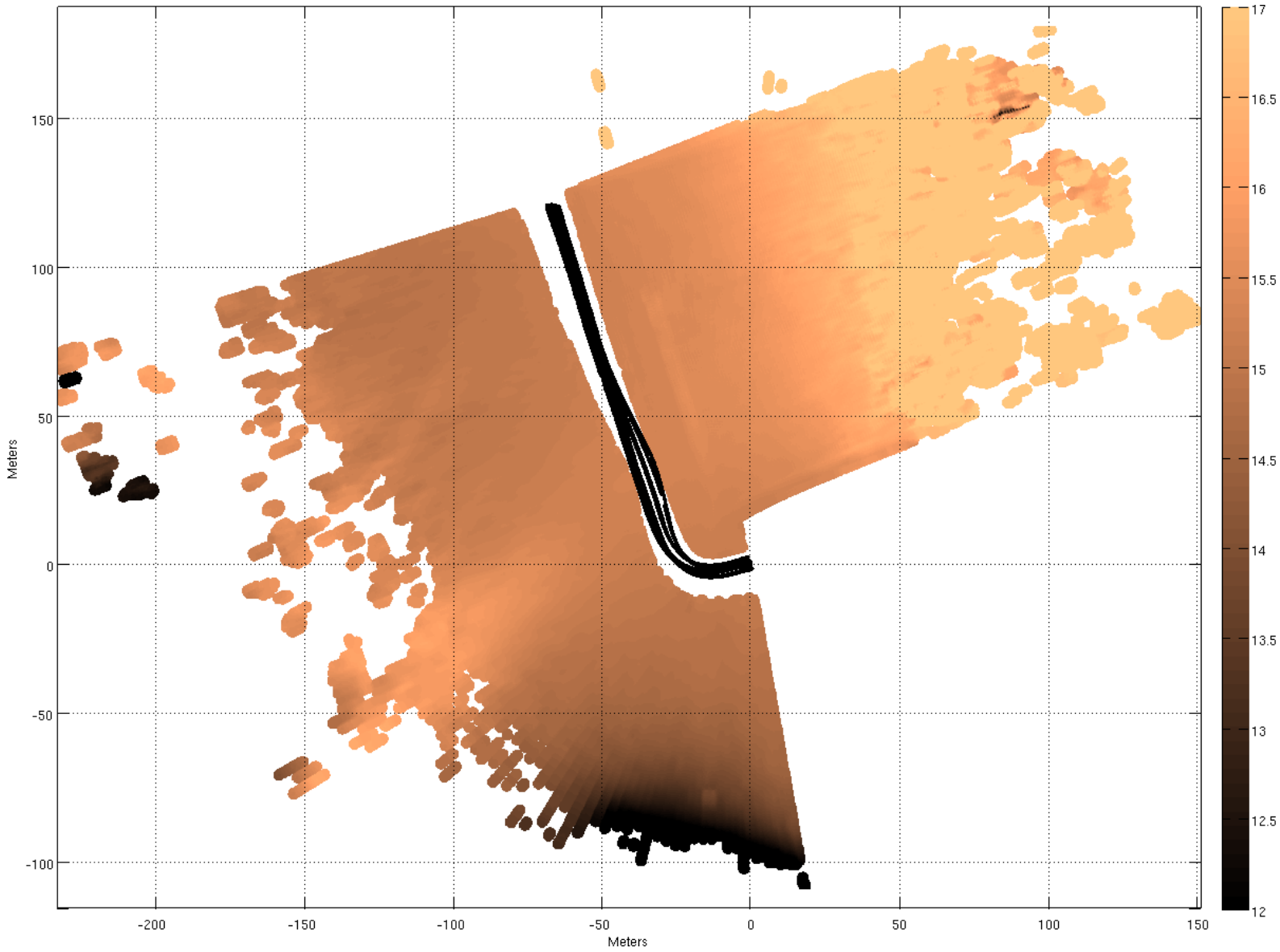

Figure 5.10: Bathymetry mosaic of dataset 080814_1. Values on all axes in meters.

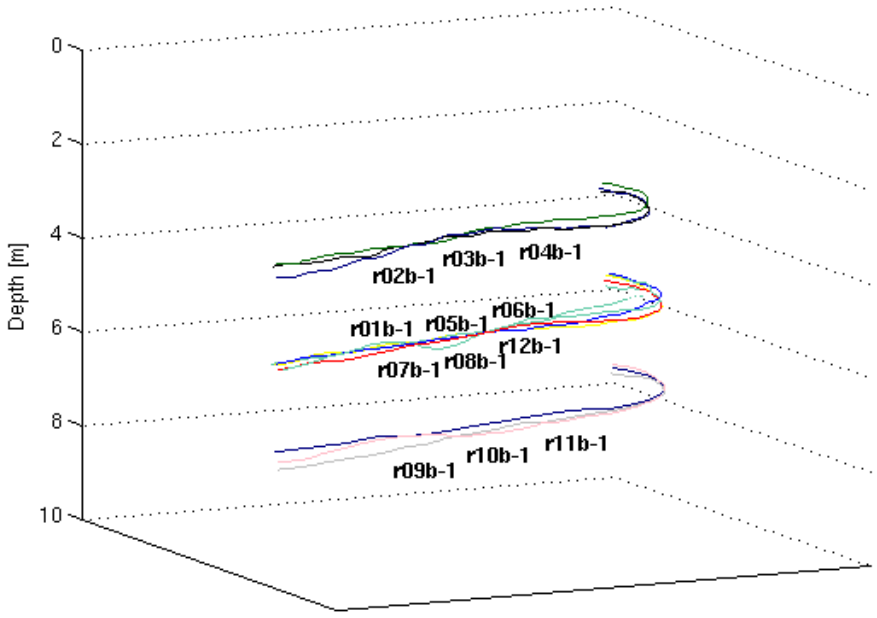

Figure 5.11: Navigation overview of all lines in dataset 080814_1. Note the three distinctly different depths and the repeated passes, applying different sonar settings each time.

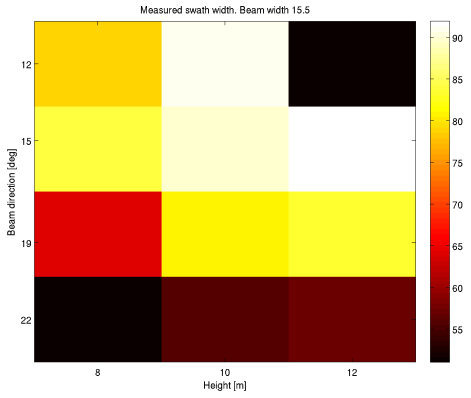

Figure 5.12: Measured swath width for dataset 080814_1 as a function of depth and beam direction for beam width 15.5°. Black squares represent missing data, which are there because of slight errors in the altitude caused by the control system.

Part III

Modeling the Ocean Environment

Chapter 6

Environment Estimation

The environmental parameters to be estimated are the sea state and the bottom type. The sea state describes the roughness of the sea surface by the surface waves or, indirectly, by the wind speed. The bottom type expresses the roughness and reflectivity of the sea floor, and is here represented through the mean grain size.

A few measurements are collected to estimate these parameters. The SNR as a function of range is estimated from these measurements. Next, a model is run with the parameters used for the measurements, and sea state and bottom type parameters are varied to simulate a SNR as close as possible to the measured SNR.

The method of calculating the SNR from a measurement is covered in Section 6.1. In Section 6.2, the criteria for choosing which simulated SNR best describes the measured one, and challenges met in this process, are discussed. The inputs required for the simulation are covered in Section 6.3. Finally, the chapter concludes by summing up observations and suggestions on which parts could benefit from further improvements in Section 6.4.

6.1 Measured SNR

The signal to noise ratio of measurements can be estimated from the coherence, which in this context is the normalized cross-correlation of the two coregistered images from an interferometric setup (Hansen et al. 2011). The coherence contains information about the similarity of the two images collected by the two different sensors in the interferometric setup. In other words, the coherence expresses the ratio of coherent energy between the signals, as illustrated later in Equation 6.4. A higher coherence value means that the noise part N is small compared to the signal part S. If the coherence is low, the noise part must be large compared to the signal part, which means that the measurement is of lower quality since it does not have a strong, coherent signal present.

Assuming local stationarity, it is possible to express the coherence of two signals s_1 and s_2 as shown in Equation 6.1 (Hanssen 2001):

$$\gamma(\tau) = \frac{\mathrm{E}\left[s_1(t)s_2^*(t+\tau)\right]}{\left(\mathrm{E}\left[|s_1(t)|^2\right]\mathrm{E}\left[|s_2(t)|^2\right]\right)^{1/2}} \tag{6.1}$$

The phase corrected coherence is equivalent to the zero-lag coherence of two coregistered images. It can usually be expressed as the peak value in the coherence function, as shown in Equation 6.2. This is to say that the phase shift that results in the maximum coherence between the two signals is the shift that makes them coregistered.

$$|\gamma| = \max_{\tau} |\gamma(\tau)| \tag{6.2}$$

Consider the two coregistered signals s_1 and s_2. They should both contain the same signal s, but different, uncorrelated noise components n_1 and n_2 as illustrated in Equation 6.3 (Zebker and Villasenor 1992). The noise components contain noise from several sources, including multipath.

$$\begin{aligned} s_1 &= s + n_1 \\ s_2 &= s + n_2 \end{aligned} \tag{6.3}$$

Since the signal and noise are uncorrelated, we can evaluate the correlation between s_1 and s_2 as in the zero-lag (already coregistered, i.e. $\tau = 0$) case of Equation 6.1. This results in an expression of the coherence by the signal and noise power:

$$|\gamma| = \frac{|s|^2}{|s|^2 + |n|^2} = \frac{S}{S+N} \tag{6.4}$$

By manipulating Equation 6.4 using the definition of $SNR = \frac{S}{N}$, the coherence can be expressed in terms of the SNR:

$$|\gamma| = \frac{S/N}{(S+N)/N} = \frac{SNR}{SNR+1} \tag{6.5}$$

An estimate of the SNR of a measurement can thus be expressed by the coherence after manipulating Equation 6.5 (Zebker and Villasenor 1992; Hanssen 2001):

$$SNR = \frac{|\gamma|}{1-|\gamma|} \tag{6.6}$$

This SNR estimate is a good measure of signal to multipath ratio in shallow waters (Synnes et al. 2009). It also corresponds to the SNR simulated by the SMURF model, which makes direct comparison possible.

The coherence has a known bias towards higher values because the correlation is performed with data series of a finite number of samples. An expression for this bias and its variance exists, and shows that the bias increases with decreasing number of samples (Carter et al. 1973; Hanssen 2001). Because the coherence in Equation 6.2 is estimated through a maximum operator, the value with the highest total process coherence and bias is found. Thus, the estimated coherence value will be in the upper range of the bias variance, which justifies performing bias compensation in order to

achieve a more accurate estimate of the actual process coherence. Bias compensation is performed by the SMURF model used in this thesis.

6.2 Curve Fitting

The objective of the environment estimation is to find the model parameters that result in a simulated SNR that best fits the measured one. To obtain these parameters, the least squares method described in Section 4.1 is applied. The error, which will be named ϵ_{SNR}, is calculated only over an area considered valid.

One of the criteria for a valid area is measured SNR higher than a threshold. This value should be chosen wisely. The lower the SNR, the more dependent it becomes on the coherence bias correction, thus making the estimate less confident. A too high threshold will throw away data that contains usable information. A threshold set too low will use all recorded information regardless of its quality, and might result in parameters for a curve that does not capture the trends in the measured SNR, but is still the least squares fit. Brute force simulations to find the best fits for all the data was performed and analyzed manually since there is no simple metric that accurately can describe which results are good fits. The conclusion of the analysis is that, while there is no universal answer, a threshold of less than 0 dB should be used, e.g. -5 or -10 dB which have varying rates of success.

In the simplified case of flat bathymetry, the minimum range was limited to $r > \frac{h}{tan(45^\circ)} = h$, where r is the range and h is the altitude of the vehicle above the sea floor. This implements a rule of thumb maximum look angle of 45°. Since this algorithm is mostly applicable to shallow waters with low altitudes, this limitation will usually not matter. If it comes into play, it disregards the shortest ranges, which are normally lower than 0 dB either way.

Problems with the curve fitting was encountered during the experiments in this thesis because the modeled SNR does not perform realistically at short ranges. Therefore, an ad-hoc fix is applied that limits the lower edge of the valid area to the maximum value of the measured SNR. While doing this does throw away some information from the measured SNR, the model has not proven to be valid in this area, so the data only puts the result off. This fix normally eliminates the need for the first rule-of-thumb range-limit.

The final expression for ϵ_{SNR} is shown in Equation 6.7. $\text{SNR}_m(r)$ is the measured SNR at discrete range intervals, and $\text{SNR}_s(r)$ is the simulated SNR at the same intervals.

$$\epsilon_{\text{SNR}} = \sum_r \left[\text{SNR}_m(r) - \text{SNR}_s(r)\right]^2, \ \forall r \text{ where } \text{SNR}_m(r) \geq -5\text{dB} \wedge r \geq \arg\max_r \text{SNR}_m(r) \tag{6.7}$$

The parameters that have the smallest ϵ_{SNR} are considered the best fit, as described by Equation 4.2. An illustrative plot of a measured SNR with valid area and its threshold limit is shown in Figure 6.1. The swath width is defined as the largest

continuous range interval where the measured SNR is larger than 0 dB, as marked by the thick horizontal line at 0 dB. The lower and upper limits (LL and UL) are marked by circles. The valid area of the measured SNR, as defined in Equation 6.7, is highlighted. This is the data which will be used for curve fitting.

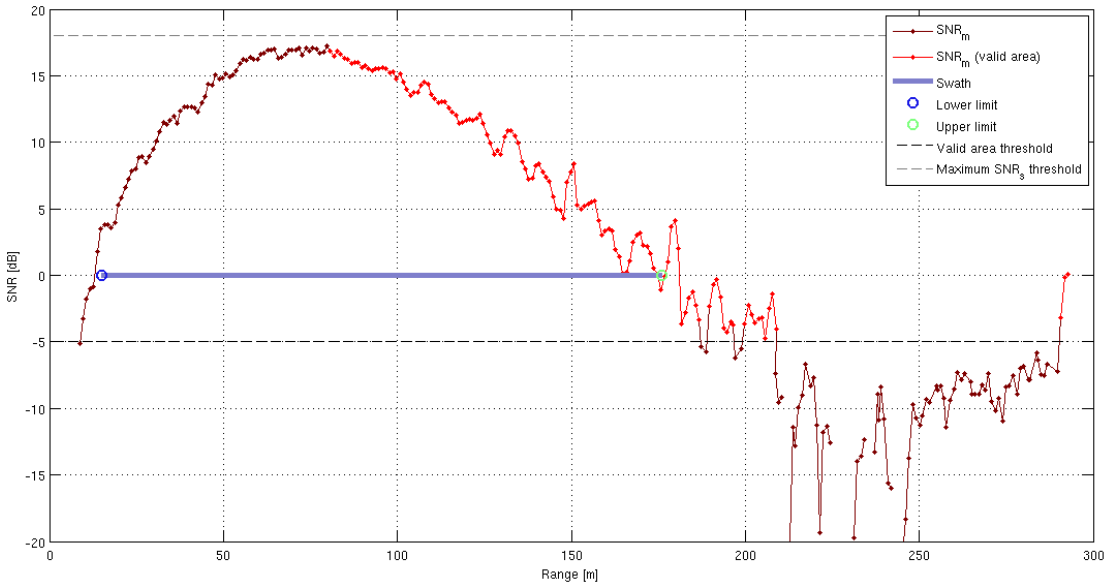

Figure 6.1: Example of a measured SNR, plotted in decibel as a function of range in meters. The valid area, which will be used for curve fitting is highlighted. The swath width, which limits are measured at 0 dB, is marked by a thick line with the lower and upper swath limits marked by circles. A gray dashed line marks the 18 decibel limit, at which a simulated SNR is thresholded. A black dashed line marks the attenuation threshold, in this case at -5 dB.

6.3 Model Parameters

The different model parameters are described in this section. These include the number of multipaths to consider, a bathymetry, a sound speed profile, and the two ocean environment parameters, the sea state and the sea floor roughness.

For bathymetry input, the sidescan bathymetry is readily available from the interferometric processing. It is averaged over all the pings, in the same manner as with the coherence, in order to reduce the noise level. The sound speed profile is important for the ray tracing in the SMURF-model, and is described in Section 2.6. It must be measured for every mission, as it varies locally.

6.3.1 Number of Multipaths

The number of multipaths to calculate is an important model parameter. Which multipaths that are dominating is generally unknown, so calculating more orders of multipath returns is generally better. Up to a point, there is a trade-off between accuracy and number of calculations, which is often dictated by the available computational power and the required computational time. The calculation cost increases approximately linearly with the number of multipaths calculated. Multipath returns of very high order are unlikely, but there is no way to predict how many are needed, as this will vary for different environments and setups, i.e. different bathymetry, sound speed, sea floor roughness and sea state, as well as sonar settings and platform position. Even if no significant multipaths exist for a certain order, higher order multipaths could potentially be stronger.

In most of the simulations, only multipaths up to third order have been considered due to calculation speed issues. A few comparisons with multipaths up to sixth order was done, and the results did not vary considerably. Multipaths past sixth order (e.g. bsbsBsbs, which is seventh order) are unlikely to have an impact because the attenuation and scattering loss is expected to be large after such a long travel through the water.

6.3.2 Sea State

The sea state is described on the Beaufort scale. This might seem odd since the Beaufort scale is a scale of wind speed, but under the assumption of *fully developed sea* the value on the Beaufort scale is converted to a sea state for open sea and constant wind strength over time (LeBlond and Mysak 1978; Synnes 2011).

Wind speed measurements close to land should not be estimated correctly by the model, since a lower sea state than the one given by the conversion is the right answer.

The 13 different levels from 0-12 (Stewart 2009) are listed in Table 6.1. The Beaufort scale gives a discrete range of sea states, which is practical when performing a search. More granular or continuous measures of the sea states directly could be better if implementing e.g. machine learning algorithms or genetic search algorithms. The Beaufort scale can in this case be extended to a continuous measure, because the equations for converting a value on the Beaufort scale to a sea state can still be used.

6.3.3 Sea Floor Roughness

The sea floor scattering model needs to be provided with the correct sediment properties. The sediment type is expressed through the bulk grain size, denoted Mz (Synnes 2011).

The bulk grain size is a logarithmic measure of the mean grain size and it is directly calculated as shown in Equation 6.8 from the mean grain size d in millimeters and a reference length $d_0 = 1$ mm (APL-UW 1994).

Table 6.1: Beaufort scale. Extract from Stewart (2009).

Beaufort	Description	Wind speed	Wave height
0	Calm	0.0 - 0.2	0.0
1	Light air	0.3 - 1.5	0.1
2	Light breeze	1.6 - 3.3	0.2
3	Gentle breeze	3.4 - 5.4	0.6
4	Moderate breeze	5.5 - 7.9	1.0
5	Fresh breeze	8.0 - 10.7	2.0
6	Strong breeze	10.8 - 13.8	3.0
7	Near gale	13.9 - 17.1	4.0
8	Gale	17.2 - 20.7	5.5
9	Strong gale	20.8 - 24.4	7.0
10	Storm	24.5 - 28.4	9.0
11	Violent storm	28.5 - 32.6	11.5
12	Hurricane force	32.7.0 -	14.0

$$\mathrm{Mz} = -\log_2 \frac{d}{d_0} \approx -3.32 \log_{10} \frac{d}{d_0} \tag{6.8}$$

The mean grain size can thus easily be calculated from the Mz value as shown in Equation 6.9.

$$d = d_0 2^{-\mathrm{Mz}} \approx d_0 10^{-\frac{\mathrm{Mz}}{3.32}} \tag{6.9}$$

The bulk grain size is a continuous scale, but has been listed with commonly named sediment types in Table 6.2. This is practical when trying to characterize the sea floor. As with the sea state, this value can be discretized or used as a continuous parameter depending on the algorithm in use.

6.3.4 Self-noise

The self-noise is a flat noise level that is supposed to represent the sonar's own noise level, as described in Section 2.7. Here it is defined as the self-noise max-range in meters. It is the range where the echo level is 0 dB for a 100 kHz sonar on sandy bottom of constant depth 30 meters and sonar depth 5 meters. The sonar geometry is 15° beam width centered around 12° down from the horizon on the transmitter, and 45° beam width centered around 22° down from the horizon on the receiver (Synnes 2011).

6.4 Further Improvements

Suggestions for further improvements to the environment estimation are described here, as well as a few known issues with the SMURF model used.

Table 6.2: Bulk grain size (Mz), mean grain size (d) and sediment names. Extract from APL-UW (1994)

Mz	d [mm]	Sediment name
-5	32.0000	
-4.5	22.6274	
-4	16.0000	
-3.5	11.3137	Gravel, pebble and rock
-3	8.0000	
-2.5	5.6568	
-2	4.0000	
-1.5	2.8284	
-1	2.0000	Sandy gravel
-0.5	1.4142	Very coarse sand
0	1.0000	Muddy sandy gravel
0.5	0.7071	Coarse sand/Gravelly mud
1	0.5000	Gravelly muddy sand
1.5	0.3536	Medium sand
2	0.2500	Muddy gravel
2.5	0.1768	Fine sand/Silty sand
3	0.1250	Muddy sand
3.5	0.0884	Very fine sand
4	0.0625	Clayey sand
4.5	0.0442	Coarse silt
5	0.0313	Sandy silt/Gravelly mud
5.5	0.0221	Medium silt
6	0.0156	Sandy mud
6.5	0.0110	Fine silt/Clayey silt
7	0.0078	Sandy clay
7.5	0.0055	Very fine silt
> 8	< 0.0039	Silty clay

The simulated SNR is often overestimated by several decibel at short range using the SMURF model. The reason for this is not known, but is a result of either overestimating the signal strength or underestimating multipath returns. It is currently resolved by thresholding the simulated SNR at an 18 dB threshold. There are examples in the measurements used in this thesis where the maximum measured SNR is closer to about 20 dB, but the result of thresholding at 18 dB seems to fit reasonably most of the time. Further work into accurately simulating the SNR for short ranges would allow the use of more data, and thus improve the overall accuracy.

When the SMURF model faces small grazing angles, the model used for calculating reflectivity is no longer valid. Therefore, a constant value, the Del Balzo plateau, is used instead (APL-UW 1994; Synnes 2011). The SMURF model is thus less accurate for smaller grazing angles, which are common in shallow waters because the altitudes are usually low. Further work in scattering theory investigating sea floor scattering properties for small grazing angles would benefit sonar performance modeling.

The antenna beam patterns used in the SMURF model are believed to not correspond precisely to the real beam patterns (Synnes et al. 2009). For the transmitting antenna, tank measurements have been available when modeling the beam pattern, but not for the most recent antenna model. Further work should be done to correct this in order to make the model more accurate.

In the tank measurements for the transmit antenna it has been seen that there is an offset between the requested and the real, tank-measured beam width. An ad-hoc fix for this could be to map the requested beam width to the corresponding tank-measured beam width. A more permanent fix is to make this correction directly in the beam pattern correction. Either way, a study on how the beam pattern varies with requested beam width and electronic steering, as well as a more thorough tank measurement, would be required.

Improved ways of performing the bottom type estimation should be looked into. This is discussed briefly in the *High-frequency ocean environment acoustic models handbook* (APL-UW 1994).

Chapter 7

Environment Estimation Results

Two different analyses will be carried out in this chapter. The first analysis is a test of curve fitting, performed in order to decide how to choose which area of the measured SNR curve should be used for curve fitting. The second analysis is sea floor and sea state estimation, investigating how the self-noise levels and the number of pings used affect the result, as well as analyzing the consistency of the estimated environment.

7.1 Curve Fitting

Since the SNR is calculated from the coherence, the accuracy of the coherence estimator is of interest when choosing the threshold. The coherence has a known increasing bias with lower values, as discussed in Section 6.1. When this error grows too large, the SNR, along with the coherence estimate, is not as trustworthy. Three different SNR thresholds will be tried out here: 0 dB, -5 dB and -10 dB. These thresholds correspond to coherence values of 0.5, 0.24 and 0.09 respectively, calculated by Equation 6.5. The bias correction at a coherence of 0.1 (or even at 0.25) is not negligible, but that does not necessarily mean that the curve fitting will work better with a threshold at 0 dB.

The actual estimation of the bottom type and the self-noise level was done as described in Chapter 6.

All the lines from datasets 120515_1 and 080814_1, as well as the 23 first lines of dataset 120918_2 are used for this analysis. The reason for using only 23 lines from the last dataset is simply that the number of figures for visual inspection is already large, and the processing time required made it impractical to include all 41 lines. The measurements are described in Chapter 5. For each line, the least squares curve fitting was performed in six different ways for all combinations of thresholds 0 dB, -5 dB and -10 dB, and self-noise max-ranges of 200 meters and 400 meters. A more fine-grain selection of thresholds and self-noise max-ranges is not included because the analysis of the curve fits will be done manually, which gets impractical with too many variables.

For each dataset, the average bottom type, sea state, RMSE-value and upper limit errors are plotted with standard deviations in Figures 7.1 and 7.2. The results are also listed in appendix A.

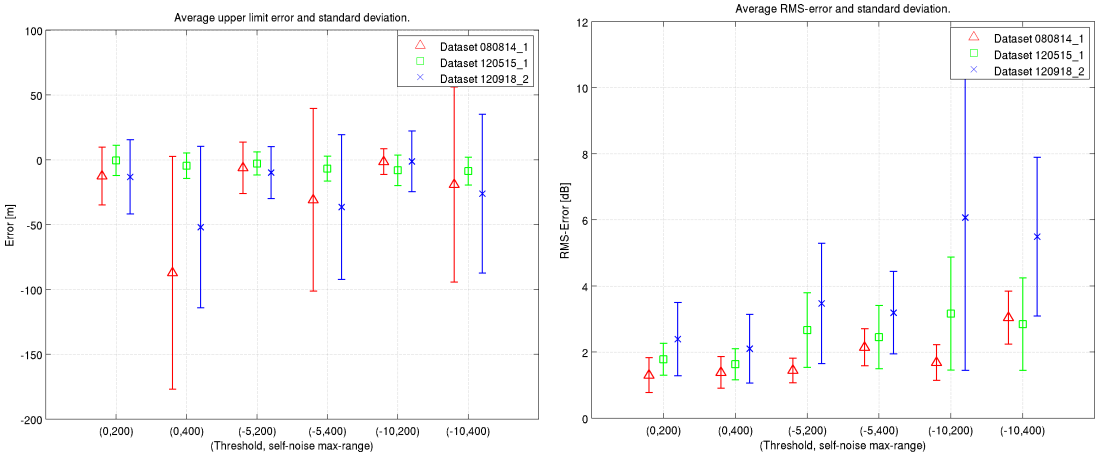

(a) Upper limit (UL) error.

(b) RMS-Error.

Figure 7.1: Curve fitting upper limit and RMS errors for all datasets.

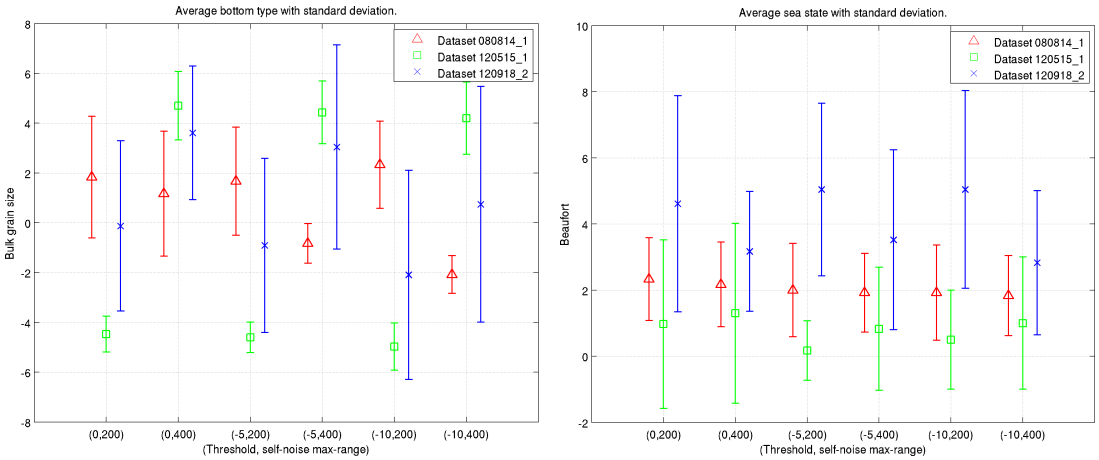

(a) Average bottom type.

(b) Average sea state.

Figure 7.2: Curve fitting average environment estimations with standard deviations.

7.1.1 Deep Water Dataset 120515_1

For the deep water dataset 120515_1, the upper limit errors are good in all cases, as seen in Figure 7.1(a). This is because there are no multipaths in deep water, which means that only the direct signal return needs to be correctly simulated. The settings that stand out with the lowest bottom type variation is a threshold of -5 dB and self-noise max-range of 200 meters. Note how the RMSE-value in Figure 7.1(b) increases with lower valid area thresholds, even though the curves look similar upon inspection. This increase in RMSE-value happens because lower thresholds take more data into account, which makes it harder to make good fits. Therefore, the RMSE-values are not directly comparable when varying the valid area threshold.

7.1.2 Shallow Water Dataset 080814_1

Dataset 080814_1 has an average sea floor depth of about 10 meters, so multipath returns should be present. The upper limit error is much lower with a self-noise max-range of 200 meters rather than 400 meters, as can be seen in Figure 7.1(a). Inspection of the actual fitted curves show that this is because the low self-noise (400 meters) tends to extend the curve with an unrealistically high SNR. An example of this effect can be seen in Figure 7.3(b). With a self-noise max-range of 200 meters, a threshold of 0 and -5 dB results in lower RMSE-values compared to a threshold of -10 dB, as shown in Figure 7.1(b). The increasing RMSE-values with decreasing thresholds is, again, partly because more data is taken into account. When taking the standard deviations of the upper limit errors into account, it seems that the best combination based on this dataset is a threshold of -10 dB with a self-noise max-range of 200 m. On the other hand, the standard deviation for the bottom type is far better with self-noise max-range of 400 meters, which could be important in avoiding too large variations in the results.

7.1.3 Shallow Water Dataset 120918_2

Dataset 120918_2 has an average sea floor depth of about 16 meters, so multipath should be present. As with dataset 080814_1, the upper limit error shown in Figure 7.1(a) is much lower with a self-noise max-range of 200 meters. The lowest upper limit error is achieved with a valid area threshold of -10 dB, while the variation in the bottom type and sea state estimation is lower with a valid area threshold of 0 and -5 dB. The mean RMSE-values are higher than for the other datasets. After examining the individual curve fitting results manually, it is found that the multipaths' intensities drops quicker than the direct return intensity, which often leads to curious results like the one in Figure 7.6(b). The bottom type and sea state values are extreme (-8 and 8 respectively), which is far away from the expected values of sandy bottom and calm sea. So the conclusion is that these examples are lines where the environment modeling, i.e. the curve fitting, fails.

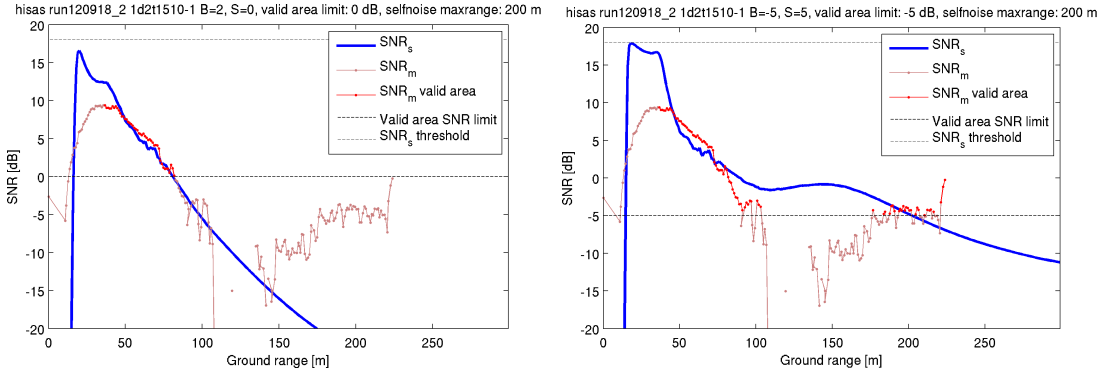

(a) Threshold: 0 dB.

(b) Threshold: -5 dB.

Figure 7.3: Example of a line where a threshold of 0 dB worked well, while a threshold of -5 dB did not.

7.1.4 Curve Fitting Summary

A few comparisons of lines where the curve fitting result was different with different thresholds are shown in Figures 7.3, 7.4, 7.5 and 7.6. Observing that different thresholds can give the best results under different circumstances, it is not possible to conclude with one being universally best. The results show that the upper limit error is best estimated (in all but the deep water dataset) by setting the threshold to -10 dB, which is an agreeable result since it also means including the most data in the curve fitting. Since the upper limit error is considered as an important optimization criteria later on it is an important value to estimate well, which should be taken into account when choosing a threshold for the valid area used with the curve fitting. On the other hand, there is less variation in the estimated bottom type and sea state with a threshold of 0 and -5 dB. For robustness, less variation is desirable in order to have less variation in the final result. Lower SNR values are also less confident, because the lowest simulated SNR values are dependent on the bias correction, as discussed in Section 6.1. Visual inspection of the curves generated showed that the combination of threshold -5 dB and self-noise max-range 200 meters gave subjectively better fits than threshold -10 dB and self-noise max-range 200 meters.

An example of a low threshold resulting in a bad least squares fit is shown in Figure 7.6. The simulated curve does not fit the measured values after about 100 meters range, and when these measurements are taken into account the result is not a good fit. Note that this is an example where the RMSE-value will be large for the bad fit compared to the good one, and could thus be a good measure of how well the curve fitting worked.

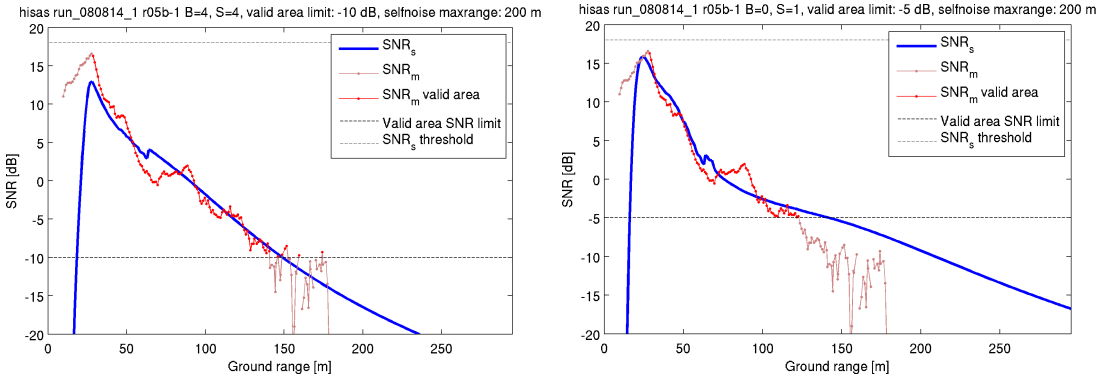

(a) Threshold: -10 dB.

(b) Threshold: -5 dB.

Figure 7.4: Example of a line where a threshold of -10 dB worked well, while a threshold of -5 dB did not. Note that the first fit is considered good because it fits well when measuring swath limits at 0 dB. These two examples fit well for different parts of the measured SNR. This is often the case, and which one results in the least squares solution is not obvious upon inspection.

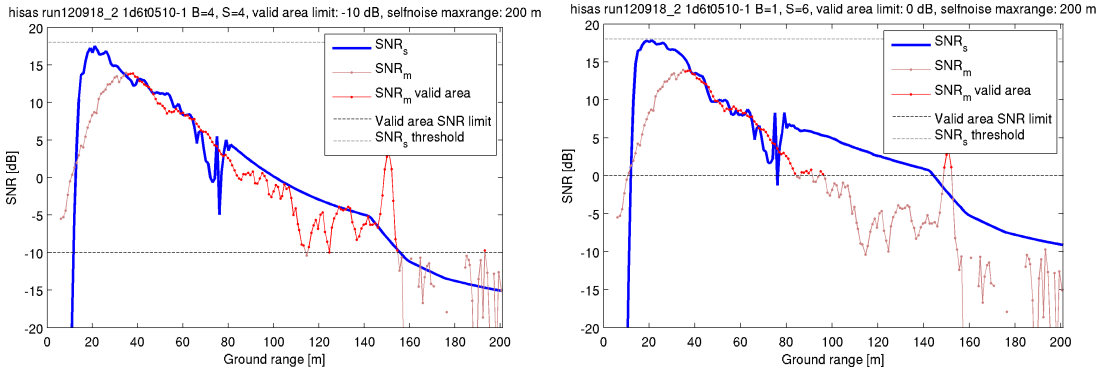

(a) Threshold: -10 dB.

(b) Threshold: 0 dB.

Figure 7.5: Example of a line where a threshold of -10 dB worked well, while a threshold of 0 dB did not.

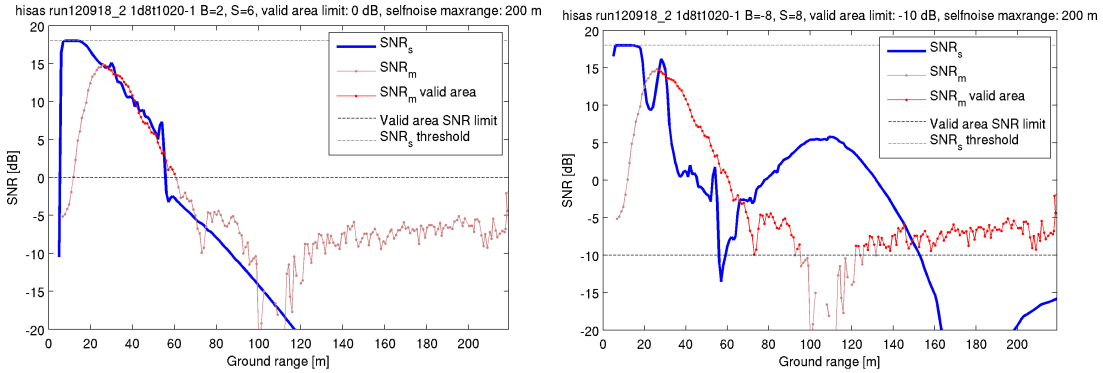

(a) Threshold: 0 dB

(b) Threshold: -10 dB

Figure 7.6: Example of a line where a threshold of 0 dB worked well, while a threshold of -10 dB did not. A threshold of -5 dB for this line looks similar to the -10 dB example.

7.2 Sea Floor and Surface Estimation

The objective of this analysis is to model the ocean environment in deep and shallow water. The analyses are undertaken in order to investigate which self-noise levels provide the most reliable and reasonable results, how consistent the bottom type and sea state estimations are, and how averaging a varying number of pings affect the results.

The estimation of the bottom type and sea state was done as described in Chapter 6. The bottom type was allowed to vary discretely from -8 to 9. The sea state was allowed to vary discretely from 0 to 12.

The self-noise level is assumed constant for the sonar sensor, but the actual level varies with the sonar settings applied. Therefore the self-noise level is described by the self-noise max-range for a standard setting, as described in Sections 2.7 and 6.3.4. The self-noise max-range setting should be constant, but it's value is unknown. Therefore, several values are compared in an attempt to fix this parameter.

7.2.1 Self-noise Estimation

The objective of this analysis is to estimate a value for the self-noise max-range. This is done by modeling the ocean environment by tuning the self-noise max-range level, the bottom type and the sea state.

The self-noise level, bottom type and sea state should be constants for a measurement within a small homogeneous area. Therefore the first part of this analysis involves fixing first the self-noise level, then the bottom type, while varying the others. Then, the self-noise level, bottom type and sea state are all varied simultaneously in order to investigate if this will turn out reasonable mean values. Since there is no solid a priori knowledge of what these values should be at, a wide range of values are tried. For the self-noise max-range this includes values ranging from 150 to 500 meters. For the bottom type this includes values ranging from -8 to 9. For the surface this includes values on the entire scale from 0 to 12.

A number of pings are averaged into a single coherence and bathymetry for each line. The number of pings used is based on how many pings are available for each dataset. For dataset 120515_1, 30 pings per line were used. For dataset 080814_1, 250 pings per line were used. For dataset 120918_2, 60 pings per line were used.

The number of discrete levels for the self-noise max-range was limited for the shallow water datasets 080814_1 and 120918_2 due to the time it takes to run these simulations with multipath.

Deep Water Dataset 120515_1

The results of fixed self-noise max-range are included in Appendix B, Tables B.1, B.2 and B.3 for 0, -5 and -10 dB valid area thresholds respectively.

When varying the self-noise level the model tries to compensate by varying the reflectivity of the sea floor, i.e. varying the bottom type. This is another way of saying

that to achieve the measured result with more self-noise, the sea floor must be more reflective in order to give a stronger signal back, which intuitively makes sense. Looking at the trends of the errors, the results are the same regardless of valid area threshold. The RMSE-values are lowest for self-noise max-range values of 320-450, while the upper limit errors are smallest for much lower self-noise max-range values of 190-220 meters. For the lower self-noise max-range values, the bottom types estimated are unexpected at -5 to -6, which corresponds to very rocky bottom. For the higher self-noise max-range values, the bottom types estimated are 0 to 5, which corresponds to bottom types ranging from gravel, through sand, to silt. The bottom types of 0 to 5 are more likely with regards to the expected bottom type in the mission area. The lowest upper limit errors were achieved with a valid area threshold of 0 dB.

The results of fixed bottom type are included in Appendix B, Tables B.4, B.5 and B.6 for 0, -5 and -10 dB valid are threshold respectively.

The trends of the errors here are pretty much the same regardless of valid area threshold, as they were with the fixed self-noise. The lowest upper limit errors are found for bottom types -3 to -6, with self-noise max-range at about 200 meters. The lowest RMSE-values are found for bottom types 2-4 with self-noise max-range at about 400 meters. This is consistent with the previous result from locking the self-noise level. The lowest mean upper limit errors were achieved with a valid area threshold of -5 dB.

The results of varying both bottom type and self-noise level at the same time are included in Appendix B, Tables B.7, B.8 and B.9 for 0, -5 and -10 dB valid area threshold respectively.

The lowest upper limit error are achieved with a valid area threshold of 0 dB, the second lowest at -5 dB and the worst at -10 dB. Regardless of valid area threshold, the mean self-noise max-range is about 400 meters and the mean bottom type is about 3, which corresponds to muddy sand.

This is in accordance with the last two simulations with locked self-noise and locked bottom type, since these values had the lowest RMSE-values. It is, however, interesting that the best curve fit is achieved with a self-noise max-range of about 400 meters, while the lowest upper limit errors are achieved with a self-noise max-range of 200 meters.

Shallow Water Dataset 080814_1

The results of fixed self-noise max-range are included in Appendix B, Tables B.10, B.11 and B.12 for 0, -5 and -10 dB valid area threshold respectively.

Regardless of the valid area threshold, the smallest upper limit errors are found for low self-noise max-ranges, i.e. 150-200 meters. For valid area threshold of -5 dB, the self-noise max-range of 200 meters have both the smallest upper limit error and the smallest RMSE-value, and since the upper limit error is smaller than for the other valid area thresholds, this seems to be the best result in this case. The estimated sea state of about 2 is within what was expected based on the weather measurements.

The results of varying bottom type, sea state and self-noise level at the same time are included in Appendix B, Table B.13 for valid area threshold of -5 dB.

The mean self-noise max-range is estimated to slightly less than 200 meters, resulting in a mean upper limit error of about 10 meters. The bottom type is estimated to be about 1 and the sea state about 2.

Shallow Water Dataset 120918_2

The results of fixed self-noise max-range are included in Appendix B, Tables B.14, B.15 and B.16 for 0, -5 and -10 dB valid area threshold respectively.

Regardless of the valid area threshold, the lowest upper limit errors are found for low self-noise max-ranges, i.e. 150-200 meters. For valid area thresholds 0 and -5 dB, the RMSE-values are smaller for 200 and 250 meters self-noise max-range, while the upper limit errors are smallest for 150 meters self-noise max-range. For valid area threshold -10 dB, the upper limit error is smallest for 200 meters self-noise max-range. The estimated sea state of about 5 is too high compared to what was expected based on the weather measurements. The sea states fit better at higher self-noise max-ranges like 400-500 meters, but the upper limit errors are too large to be useful in these cases at more than 40 meters.

The results of varying bottom type, sea state and self-noise level at the same time are included in Appendix B, Table B.17 for valid area threshold of -5 dB.

The mean self-noise max-range is estimated to about 260 meters, resulting in a mean upper limit error of about 16 meters. The bottom type is estimated to be about 3 and the sea state about 3.5.

7.2.2 Number of Pings

A certain number of pings are used in the average to reduce noise in the coherence. The objective of this analysis is to investigate how varying the number of pings used affect the variance of the resulting environment parameters. The hypothesis is that averaging a larger number of pings should give better results, as it reduces the noise level, but this may be affected by strong reflectors on the sea floor, or by bathymetry variations, since an increasing number of pings cover a larger area on the sea floor. Additionally, a cost and benefit analysis is performed with respect to simulating multiple times on smaller spans of the available pings versus averaging all the pings into a single coherence, and thus performing the simulation only once.

The self-noise max-range is fixed at 200 meters and the valid area threshold at -5 dB. The bottom type was allowed to vary from -8 to 9 and the sea state from 0 to 12.

Using dataset 080814_1, ping spans of 10, 50, 100 and 250 were tried. Table 7.1 shows the averaged results of dividing the 250 available pings into different sections (spans) and estimating the environment from each of them. Table 7.2 shows the result of dividing the 250 available pings into different sections and estimating the environment only from the first section for each line. In this case less data is used with smaller ping span sizes, so the results should improve approximately linearly with the increasing amount of pings included.

The upper limit error decreases with increasing ping span size. Splitting the 250 pings into smaller sections, and simulating for each of them, does not seem to improve the estimated environment with respect to which parameters results in the best upper limit error. The actual curve fitting also fits better with one large ping-span, rather than several smaller ones, as can be seen by the lower RMSE-value.

The conclusion of this is that averaging the coherence and bathymetry over more pings improves the estimate much more efficiently than simulating several times on smaller ping spans. The sea floor in this case has similar bathymetry for the entire measurement, which is believed to be favorable of this conclusion. The computational cost of performing more simulations is large, while the computational cost of averaging the coherence and bathymetry is small. This result justifies choosing the least computationally expensive method. On the other hand, gathering more pings takes more time depending on the ping repetition frequency, which also limits the maximum range. In other words, there is a trade-off between time and accuracy for the estimation and the following adaptation.

Table 7.1: Result of bottom type estimation on dataset 080814_1 with varying number of segments per line.

		Mz		Surface		UL error [m]		$\sqrt{MSE}$ [dB]	
Ping span size	Spans	Mean	STD	Mean	STD	Mean	STD	Mean	STD
10	25	0.08	1.69	2.99	1.22	21.77	17.22	2.23	0.55
50	5	0.88	1.56	2.85	1.32	16.43	12.14	1.87	0.62
100	2	1.46	1.46	2.50	1.59	11.84	8.89	1.69	0.61
250	1	1.67	1.50	2.50	1.38	8.02	6.30	1.39	0.66

Table 7.2: Result of bottom type estimation on dataset 080814_1 with one segment per line varying in size.

		Mz		Surface		UL error [m]		$\sqrt{MSE}$ [dB]	
Ping span size	Spans	Mean	STD	Mean	STD	Mean	STD	Mean	STD
10	1	1.08	1.88	2.83	1.53	17.66	9.75	2	0.41
50	1	2.17	2.29	2.17	1.40	10.03	4.59	1.48	0.47
100	1	1.92	1.98	2.08	1.56	11.08	7.18	1.64	0.50
250	1	1.67	1.50	2.50	1.38	8.02	6.30	1.39	0.66

7.2.3 Discussion

While the bottom type should only be constant in a homogeneous area on the sea floor, the self-noise max-range should be a constant linked to the sonar sensor. While

the actual self-noise level changes with beam forming, the self-noise max-range value should still be constant, and these variations should be compensated for. Therefore the variations in the self-noise should be deterministic, not a random process. Whether or not this compensation is done properly has not been investigated here, but the variation in these results could be an indication of how well it works.

From the self-noise estimation analysis in Section 7.2.1 the conclusion is that the overall best results are achieved with self-noise max-range of 200 meters and valid area threshold at -5 dB. The best curve fits, i.e. the lowest RMSE-values, does not always coincide with the lowest upper limit errors. Since the upper limit error is used as an optimization criteria for adaptation, it is considered more important than slightly lower RMSE-value. The deep water dataset 120515_1 had the most ambiguous results, but since the main objective here is to estimate the ocean environment in shallow water, this is overlooked. This result is in accordance with the results from the curve fitting analysis in Section 7.1. Based on this, the other simulations in this thesis are carried out with the self-noise max-range set to 200 meters and the valid area threshold set to -5 dB, unless otherwise stated. For an idea of the performance using these parameters, see the model verification in Section 9.1.

Note that a higher self-noise, i.e. a lower self-noise max-range, was found for the shallow water dataset 080814_1 compared to the other shallow water dataset 120918_2. This might be because the sonar sensor was updated between 2008, when dataset 080814_1 was recorded, and 2012, when dataset 120918_2 was recorded. The noise-level for the newest model is known to be better than it was in 2008.

The analysis on number of pings in Section 7.2.2 showed that the number of pings does indeed impact the spread in the results, and that it is better to include more pings. There is no benefit from performing a larger number of simulations, rather than averaging more pings. This means that there is no need to perform a larger number of simulations, which would have increased the processing time roughly by a factor of the number of sections to perform the simulations and curve fitting for.

Part IV

Adapting to the Ocean Environment

Chapter 8

Modeling SNR with New Parameters

When the environment is known, the model parameters can be tuned in order to find new sonar settings that improve performance in simulations. The new settings can then be applied to the next measurements and hopefully improve real performance.

The model parameters which will be tuned for improved performance are the altitude of the vehicle, the beam width and the electronic steering of the beam. These, and other input required for the simulation, are described in Section 8.1. Section 8.2 discusses which metrics could be used as optimization criteria, and highlights advantages and drawbacks of these. Finally, the chapter concludes by summing up observations and thoughts on which parts could benefit from further improvements in Section 8.3.

8.1 Model Parameters

The altitude, beam width and electronic steering of the beam will be used as model variables for adaptation. In order to put together a complete ocean environment, the model also needs to be supplied with a bathymetry and a sound speed profile, together with the sea state and bottom type estimated earlier.

For bathymetry input, the sidescan bathymetry is readily available from the interferometric processing. It is averaged over all the pings, in the same manner as with the coherence, in order to reduce the noise level. This is the same input as used for the environment modeling. This could give a poor result if the bathymetry varies significantly over the chosen number of pings. If the bathymetry changes from the area used as basis for the simulation, the improved settings will not be applicable. This should only be a concern in extreme environments, but no actual measurements to investigate this have been analyzed.

The sound speed profile is important for the ray tracing in the SMURF-model, and is described in Section 2.6. It must be measured for every mission, as it varies locally.

8.1.1 Altitude

The altitude is an important factor in the imaging geometry and has an impact on the obtained range. Too low, and the grazing angles at long range will be very small. Too high, and too much energy might be lost in the water column, or the blind zone under the vehicle might grow too wide.

The sea floor is usually not flat in the heading direction, and the bathymetry of the sea floor swath on each side of about 300 meters perpendicular to the heading direction can vary significantly. Echo sounders can sense the instant altitude relative to the sea floor directly underneath the vehicle, which makes it possible to maintain an altitude setting. For very rough bathymetry this can give bad results due to track linearity concerns for synthetic aperture processing, but on the other hand it can give better results if the sea floor is sloping in the along-track direction. Another parameter that can be used is the vehicle depth, which is defined relative to the current sea level. These parameters can be interchanged locally, as they are linked by the sea floor depth so that the mean depth and the mean altitude adds up to the mean sea floor depth.

8.1.2 Beam Width and Electronic Steering

The main lobe beam width[1] of the beam is given in degrees or radians, and is centered around the beam direction. The beam direction is given in degrees or radians positive down from the horizon, i.e. 0° at the horizon.

The transmit beam can be steered electronically due to the 16-element vertical transmitter array. Both the beam width and beam direction can be controlled. This is essential to the concept of environmentally adaptive sonar studied here, as the beam direction together with the beam width are the sonar parameters being tuned. Note that electronic steering will affect the beam pattern, i.e. change the side lobes of the beam. The effect of this is not specifically studied in this thesis.

The beam width and direction can also be changed mechanically. For the beam width this would mean changing the dimensions and geometry of the sensor itself. Mechanical steering can be achieved by mounting the sensor at a different angle. Mechanical steering might seem irrelevant when electronic steering can be applied in the desired direction, but this is not the case in the physical world. The mechanical steering will affect the beam pattern in a way that can not necessarily be achieved with electronic steering. A mechanical steering of 22° down from the horizon is the standard setting on HUGIN AUVs and has been used in this thesis in order to limit the number of variables. The resulting beam pattern should be different when steering electronically versus mechanically, but the effects of this have not been investigated.

[1] The abbreviation *BW* is used for beam width in some articles and books. This is misleading as it can easily be confused with bandwidth, which is abbreviated in the same way and occurs more frequently in signal processing literature. Therefore the beam width will not be abbreviated in this thesis.

8.2 Fitness Criteria

The metrics that can describe performance in this setting are the SNR and the swath width. The swath width is defined as the largest range interval that has a SNR larger than 0 dB. The swath width is limited by a lower limit (LL) and an upper limit (UL). In Table 8.1 some envisioned combinations of these are listed. It is built up by first listing a *first priority* criterion, which is applied first. For the possibly multiple solutions that fit this criterion, the *second priority* criterion is applied to select the winner. The difference between *maximize* and *maximum* is that, while maximize means *make something as large as possible*, maximum defines an upper limit. The value may be smaller than the maximum limit, but not larger. The same difference applies to *minimize* and *minimum*.

Table 8.1: Suggestions for possible combinations to apply the fitness criteria SNR and swath width (lower limit and upper limit, LL and UL).

	First priority	**Second priority**
1	Maximize swath width	Maximize SNR
2	Maximize SNR	Maximize swath width
3	Minimum swath width	Maximize SNR
4	Minimum SNR	Maximize swath width
5	Maximum LL and minimum UL	Maximize SNR
6	Maximum LL and minimum SNR	Maximize UL

The first combination maximizes the swath width as a first priority, and then selects the best SNR if there are multiple solutions with equal swath widths. At first glance this seems to be exactly what is desired, and it is not too far away, but there are a few pitfalls. First, this might leave the SNR just slightly above 0 dB, leaving little room for error in the simulation and limiting some processing that may require or benefit from a higher SNR. There is also processing that benefit from data at short range, for example correlation-based micro-navigation (Hansen et al. 2011). It is likely that a wide swath will be realized by the means of higher altitude, which can increase the lower swath limit. Still, the method of simply maximizing the swath width is easy to implement as a fitness function for a search and does tend to our main objective of increasing imaging performance.

The second combination maximizes the SNR as a first priority, and then maximizes the swath width. This might seem to address the issue of leaving no room for SNR-error in the simulation, but it is expected to, more often than not, find a solution with a beam directed down towards the sea floor. This will strongly illuminate a small swath and give a very high SNR, but leaving only a tiny swath width, either because the beam is narrow, or because directing a beam downwards can give strong reflections for multipaths. Such a result will often be useless when the swath is very narrow, and thus maximizing SNR as a first priority is not expected to be a good fitness criteria.

The third combination intends to set a minimum swath width as the first priority, and then choose the best SNR from the available solutions. This is a method that attempts to address the concern of stretching the swath too wide at the cost of SNR, but there is no control over the lower limit of the swath. It is expected that the solution of high SNR will also be achieved through a higher altitude, since larger grazing angles intuitively could improve SNR. Therefore, this combination faces the same problems related to a high swath lower limit as described before.

The fourth combination requires a minimum SNR level, and then attempts to maximize the swath width. This is a method that properly addresses the concern of stretching the swath too wide at the cost of SNR, but there is still no control over the lower limit of the swath. Therefore the same challenges are faced as with the third combination. This solution can, however, be effective with adaptive track spacing, because the swath width is maximized with a sufficient SNR. If the track spacing can be laid out accordingly, this should improve the coverage rate.

The fifth combination requires a maximum lower limit and a minimum upper limit, thus indirectly requiring a minimum swath width, while at the same time specifying what range the swath must begin at. Then, for all the solutions fulfilling this requirement, the one with the best SNR is selected. This addresses the problem of controlling the swath width, controlling the lower swath limit and facilitating a sufficient SNR.

The sixth combination attempts to combine the best of all worlds by requiring a maximum lower swath limit and a minimum SNR, and then trying to maximize the swath width while retaining the two requirements. While it does not try to maximize the SNR, it addresses all the other concerns that have been pointed out in this section, including the possibility to specify a minimum SNR, which could leave headroom for some error in the simulated SNR.

For the analysis in Chapter 9, the different possibilities have been explored by a brute force search, and the application of these suggested fitness criteria is discussed. When reaching implementation in Chapter 10, these fitness criteria represent a search with multiple objectives at the same time. This is known as multi-objective search, and is not trivial to implement (Marsland 2009). A multi-objective fitness function, in its simplest form, could have been used. This would have consisted of the weighted sum of various objectives, e.g. swath width and swath width mean SNR. It does not, however, allow any direct control of swath width and swath boundaries (LL and UL) as described here, and the weights will require tuning on top of the search algorithm. Therefore, the final example implementation has only considered a simple fitness criteria of maximizing the swath width.

8.3 Further Improvements

The success, and especially the accuracy, of the adaptation is dependent on the success of the environment estimation. Therefore, the suggestions discussed in Section 6.4 also apply here. As for the modeled beam pattern, it is even more important that it is

appropriate compared to the real beam pattern. Otherwise, the solutions found can not be expected to have the simulated performance in practice.

Varying bathymetry changes the results, but this is believed to only be a major factor in extreme cases. Sonar measurements, in extreme cases, are a challenge either way, but adaptive methods have the potential to improve performance in such environments. Further studies could investigate how extreme bathymetry can be adapted to, and what performance is achievable in such environments.

Chapter 9

Adaptation Results

This chapter presents results and analysis on adapting the sonar parameters and altitude to the estimated environment. First, in Section 9.1, a model verification analysis is performed, where each line is isolated and used to predict all the other measured lines. In this way, real measurements are used to verify whether the simulations are correct. The second analysis, in Section 9.2, is a brute force search in order to investigate how some of the different fitness criteria described in Section 8.2 work, and which sonar settings give the best results for the available measurements.

9.1 Model Verification

The model verification is done in a way that mimics the way an actual algorithm would work on a single measurement line. First, the bottom type and sea state is estimated from the measurement, as described in Chapter 6. Then, the other combinations that measurements exist for are simulated from this result, as described in Chapter 8. This is done for each line: estimating the environment and simulating all the other lines.

The results are plotted as measured and average simulated upper and lower swath limits. The upper and lower limits from each line is plotted in light gray color to indicate the variation in the results. This shows how well the simulations from a single measurement can predict the others. If the other measurements can be accurately predicted, the confidence in the model is improved. If the predictions are not accurate, they might still predict the general trend, i.e. they can predict when the swath width will increase and decrease, but can't accurately tell by how much. In this case the confidence in the simulation accuracy is lessened, but it is still useful for finding the best settings. If the result does not correlate to the measurements, the conclusion must be that the model is not a suitable one. In this case, the model parameters needs to be tweaked, or it needs to be changed for another model. Note that lines with the same estimated environment parameters are not identical because of the measured bathymetry, which is not exactly the same for the different lines. The analyses are presented separately for each dataset and then summed up in Section 9.1.4.

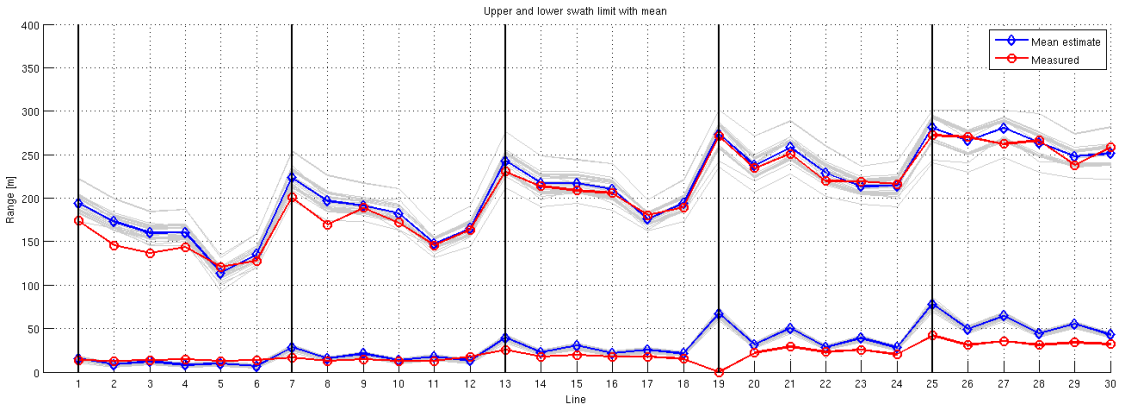

Figure 9.1: Comparison of measured and simulated upper and lower swath limits (from each line) for dataset 120515_1. The bottom type was estimated for each line separately with self-noise max-range 200 m and valid area threshold -5 dB.

9.1.1 Deep Water Dataset 120515_1

Figure 9.1 shows the model verification results for dataset 120515_1 of about 190 meters depth. The bottom type is estimated from each line separately. There is a good correlation between the measured and simulated swath limits. The lower limit increases with increasing altitude, i.e. with increasing line numbers in this case. The simulation seems to overestimate it at higher altitudes compared to the measured SNR, which might be due to the errors in the simulated SNR at short range. The upper limit, however, seems to become more accurate as the altitude increases. This might be because of increased model accuracy with increased grazing angles. It could also be related to the simulated beam pattern, which is discussed in Section 6.4.

The results for dataset 120515_1 were about the same both with varying self-noise levels and varying valid area thresholds, except for the actual value of the bottom type estimated. Because the water depth is about 190 meters, there are no multipaths in this case.

For comparison, estimating the bottom type by minimizing the total error, as described later in Section 9.1.3, resulted in bottom type -5 for this dataset.

9.1.2 Shallow Water Dataset 080814_1

Figure 9.2 shows the model verification results for dataset 080814_1 of about 10 meters depth. The bottom type and sea state are estimated from each line separately. Which lines the environment is estimated from is indicated by the numbered arrows. There is a good correlation between the measured and simulated swath limits. The mean trend looks fitting, even though it fails slightly to identify the best measurement from line 8, favoring line 4 instead.

The results seem to be grouped, and looking into this there are some estimated

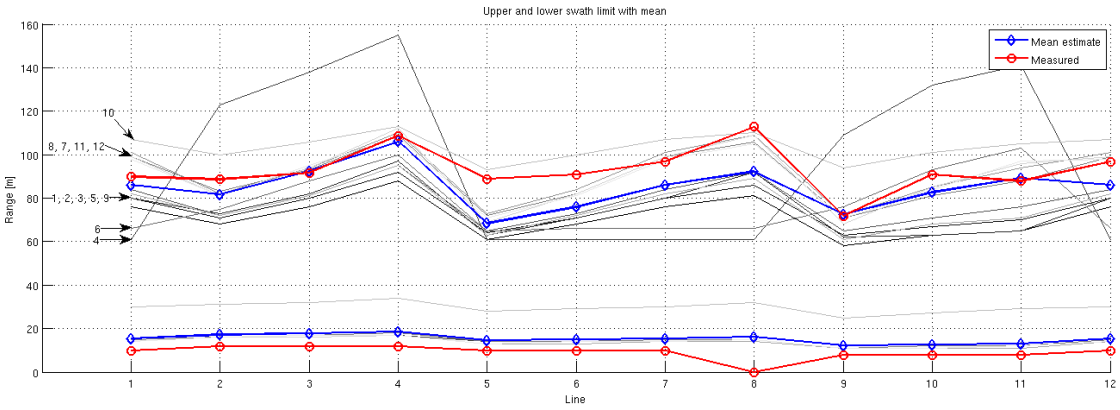

Figure 9.2: Comparison of measured and simulated upper and lower swath limits (from each line) for dataset 080814_1. The bottom type and sea state was estimated for each line separately with self-noise max-range 200 m and valid area threshold -5 dB. The arrows indicate which environment estimation the line is a result of as listed in Section 9.1.2.

environments that fit better than others. The estimations from line 7, 8, 11 and 12 seems to be the best fits, with bottom type and sea state pairs of (2,3), (3,1), (1,4) and (2,2) respectively. A lower bottom type, i.e. a higher sea floor reflectivity, seems to consistently underestimate the upper limit, but the bottom type and sea state pairs found still seem to represent the trend well. These are lines 1, 2, 3, 5 and 9, with bottom type and sea state (1,0), (1,1), (1,0) , (1,2) and (1,2) respectively. A larger bottom type, i.e. a lower sea floor reflectivity, does not seem to work well with lines 6 (4,4) and 10 (6,3). The best results are achieved with a bottom type of about 2 and a sea state of about 2-3. This sea state corresponds well with the weather measurements from the data collection.

For comparison, estimating the bottom type and sea state by minimizing the total error, as described later in Section 9.1.3, resulted in bottom type 2 and sea state 1 for this dataset.

9.1.3 Shallow Water Dataset 120918_2

Figure 9.3 shows the model verification results for dataset 120918_2 of about 16 meters depth. The bottom type and sea state are estimated from each line separately. The variation in bottom type and sea state estimation for this dataset is large, and the model verification result has a large variance as a consequence of this. Still, when looking at the mean estimate trend, there is a good correlation between the measured and simulated swath limits.

Because of high variance in the estimated bottom type and sea state, the analysis for this dataset was also repeated with bottom type and sea state chosen by minimizing the total error over all the lines. This is shown in Equation 9.1 where $\epsilon_i(\bar{x})$ is the error,

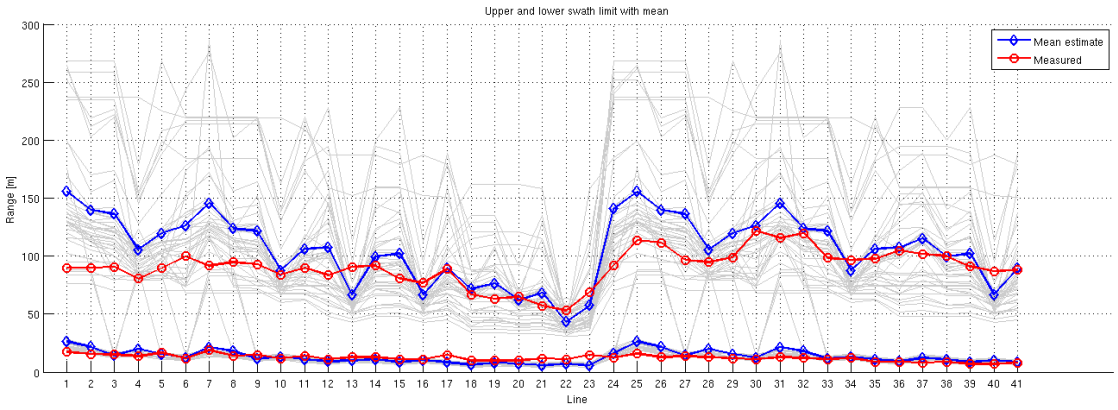

Figure 9.3: Comparison of measured and simulated upper and lower swath limits (from each line) for dataset 120918_2. Bottom type and sea state estimated for each line separately with self-noise max-range 200 meters and valid area threshold -5 dB.

as described in Section 4.1, for line i.

$$\bar{x}_{\text{TotalLSE}} = \arg\min_{\bar{x}} \sum_i \epsilon_i(\bar{x}) \tag{9.1}$$

As shown in Figure 9.4, this helped somewhat, especially for the lines with the lowest altitude, but the variance is still large. Further investigation indicated that this is caused by bathymetry errors, which can be seen in the bathymetry mosaic in Figure 5.7. It appears that this problem is less severe when the sonar is closer to the sea floor. In order to show that noisy bathymetry is the problem, the same simulations were carried out with a smoothed bathymetry, i.e. an average of the bathymetry over all the lines. The result is shown in Figure 9.5. Since the local bathymetry is important for an accurate estimate, the estimation accuracy suffers, but it shows that the large variations was indeed caused by the noisy bathymetry. The mean estimate trend looks very good in both these cases, except for the first couple of lines.

The reason for the noisy bathymetry measurement is being investigated, but no conclusion has been made at the time of writing this thesis. Such noise may be a part of the reason for why the model is often struggling to simulate the SNR at longer ranges in shallow water. Since only the bathymetry from the measurement is being used, it is harder to accurately simulate an increased range when the bathymetry can only be extrapolated assuming a flat sea floor from the last depth value, which in this case has proven to be noisy. Noisy variations in bathymetry can also cause strong echoes in the simulation because corners are strong reflectors, and these strong reflections might cause some simulated multipaths to be stronger.

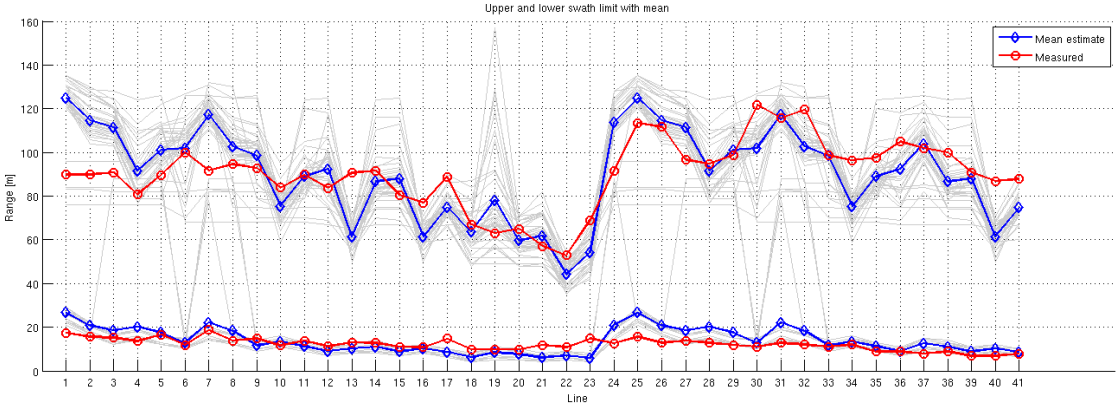

Figure 9.4: Comparison of measured and simulated upper and lower swath limits (from each line) for dataset 120918_2. Bottom type 2 and sea state 4 estimated by minimizing total error over all the lines. Self-noise max-range is 200 meters and valid area threshold is -5 dB.

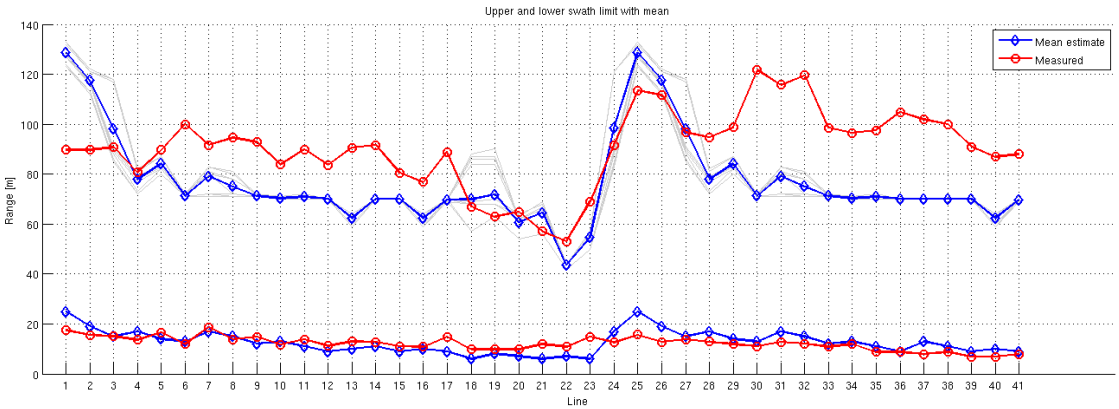

Figure 9.5: Comparison of measured and simulated upper and lower swath limits (from each line) for dataset 120918_2. Bottom type 2 and sea state 4 estimated by minimizing total error over all the lines. Self-noise max-range is 200 meters and valid area threshold is -5 dB. The bathymetry is averaged over all the lines.

9.1.4 Model Verification Summary

The simulation based on the deep water dataset 120515_1 of about 190 meters depth showed good results, even with different self-noise max-range values and valid area thresholds. The varying self-noise level can be compensated by adjusting the reflectivity of the sea floor, and this works well because only the direct return signal needs to be simulated in deep water. This can also be seen in the bottom type values obtained when varying the self-noise max-range, as discussed in Chapter 7.

The simulation based on the shallow water dataset 080814_1 of about 10 meters depth showed good results without too large variation and with clear trends. It looks like the environment estimation sometimes fail to produce parameters that simulate the other settings well. This shows that there is a need to take measures to decrease the variation in this result. This can be done by averaging multiple results, or by minimizing the total error, as shown for dataset 120918_2.

The simulation based on the second shallow water dataset 120918_2 of about 16 meters depth showed large variations in the results. It is believed that this is caused by noisy bathymetry estimations. It was shown that the model can predict the trends well, both by minimizing the total error for a single environment estimation and by smoothing the bathymetry over all the lines. This also illustrates the importance of the bathymetry used for an accurate result.

The importance of the bathymetry measurements, seen clearly with dataset 120918_2, is worrying. For the method to work well, it might be required to have a bathymetry of some detail available before it can be measured by the sensor itself. This is not necessarily prohibitive. For example, in a change detection scenario, where an already explored and mapped area is repeatedly surveyed looking for new objects, a detailed bathymetry of the full scene is available. Another example is using the bathymetry from the previous line, which can solve the problem at least for one side.

These model verification results show that, while the model can accurately represent the measurements, it is sensitive to errors in the estimated environment and the bathymetry.

9.2 Adaptation

The objective of this analysis is to use the estimated environment parameters in order to find improved settings which, in simulations, provides either better swath width, better SNR or, preferably, both.

The bottom type and sea state estimations were done as described in Chapter 6. The simulations were performed with SMURF as described in Chapter 8.

The adaptation was done for all datasets by simulating combinations of beam width, electronic steering and vehicle depths in a brute force manner. A scatter plot with lower swath limit on one axis and upper swath limit on the other illustrates all the solutions found for each dataset. The dots are colored according to the mean SNR level within the swath. The ideal solution is a bright yellow dot in the upper left corner of the

plot, indicating a 300-meter swath width with high SNR. A diagonal from (0,0) across to (50,50) would mark the edge of possible values, because the upper limit can not, by definition, be lower than the lower limit. The swath width is given by the difference between the upper and lower limits.

In pairs corresponding to a given depth, The swath width and valid area mean SNR are also plotted as functions of the beam width and the beam direction. Four pairs are listed for each dataset, corresponding to various altitudes. The intensity at each coordinate indicates the simulated swath width or mean SNR. Comparing these two images for the same depth shows what swath width and mean SNR level was achieved for different beam widths and beam directions.

The results are organized like this to allow for discussion of the performance of the optimization criteria, listed in Section 8.2. An important remark is that these results are applicable only for the current sea floor type, sea state, bathymetry and sound speed.

9.2.1 Deep Water Dataset 120515_1

Figure 9.6 shows a scatter plot of the swath mean SNR as a function of swath lower (LL) and upper (UL) limits. The characteristic lines of constant lower limits are caused by the altitude. This simulation was run with 12 different altitudes, whose values correspond to the 12 lines of constant lower limit seen in the plot. Notice that this effect is most noticeable at low altitudes, i.e. small lower limits.

To maximize the swath width, the lower and upper limit coordinates that are as far apart as possible needs to be found. This corresponds to the upper points in the scatter plot. It can be clearly seen that the SNR is higher for lower swath widths, but in this deep water case, high mean SNR values of about 12 dB are simulated even for the largest swath widths.

Maximizing SNR is analogous to picking the brightest yellow data point from the scatter plot. The trade-off between SNR and swath width can be seen, but in this case the SNR is still high for the widest swath widths. Picking the brightest dots, however, does not result in very large swath widths.

An equal diagonal from (0,0) to (150,150) illustrates the minimum possible swath width of 0 meters, represented by a gray, dashed line in Figure 9.6. Requiring a minimum swath width can be illustrated by raising this line up the number of meters required as a minimum swath width, e.g. 40 meters for a diagonal from (0,40) to (150,190). All data points above that line are within the requirement. Again, the SNR decrease amongst the available data points when this line is moved up. Solutions are found up to about 230 meters swath width.

Limiting the SNR and picking the best swath width available is illustrated by e.g. removing all reddish data points and selecting the best swath width as before. For this deep water case, high SNR is available even for the largest swath widths.

Requiring a maximum lower limit and a minimum upper limit is much like requiring a minimum swath, except that the limits of this swath is more controlled. It is illustrated by creating a vertical line for the lower limit and a horizontal line for the

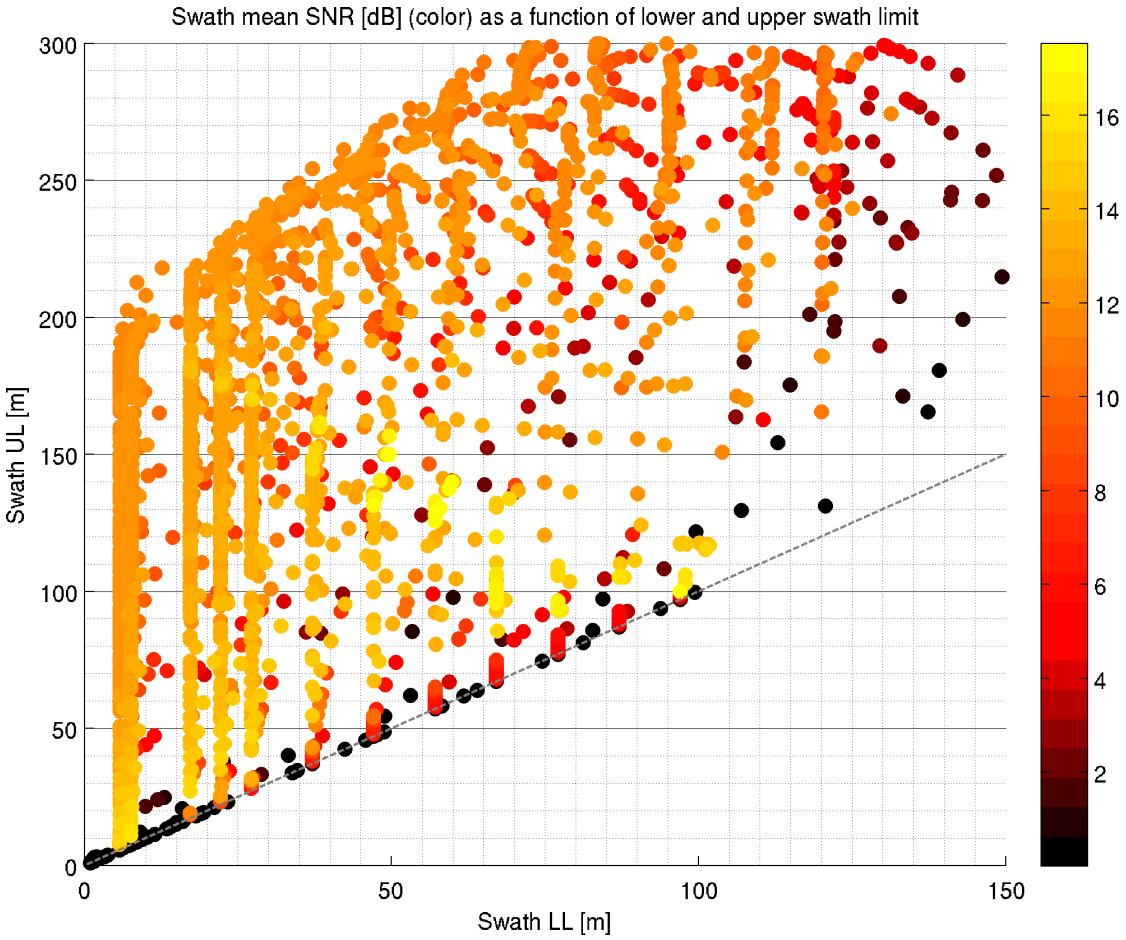

Figure 9.6: Result of brute force simulation for dataset 120515_1. Color indicates mean swath SNR [dB] plotted for swath lower limit (LL) and swath upper limit (UL). Ideal solution is top left with bright, yellow color.

upper limit. Data points that are above the horizontal line and to the left of the vertical line are within the requirement. Note that these solutions will vary in swath width, but will never have a swath width of less than the difference between the required limits.

Requiring a maximum lower limit and maximizing the upper limit is almost analogous to requiring a maximum lower limit and maximizing the swath width. It is illustrated by again creating a vertical line for the lower limit. Then the largest upper limit available to the left of this vertical line is chosen.

Figure 9.8 show the simulated swath width and valid area mean SNR as a function of beam width and beam direction for different depths.

The best swath widths are achieved at 46 meters altitude with a beam width of 10 degrees, steered slightly down from the horizon by 15-30 degrees. They are the white areas in the images. These do not, however, correspond to the highest SNR values, but

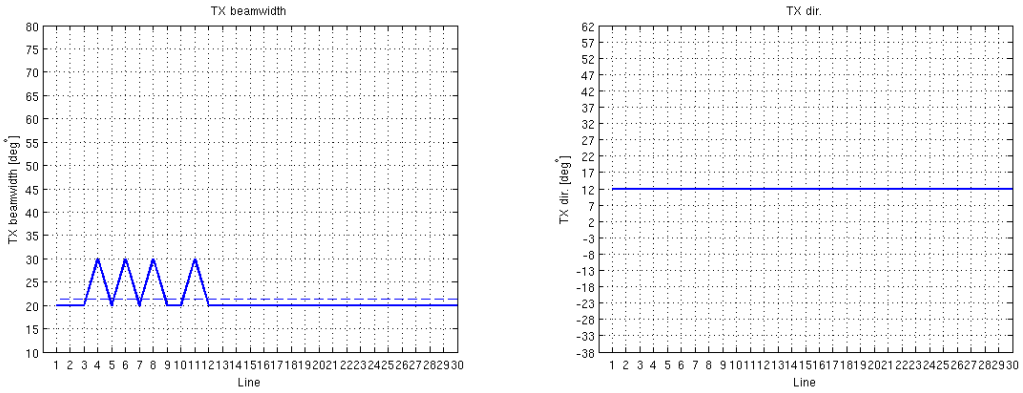

(a) Transmit beam width.

(b) Transmit beam direction.

Figure 9.7: Transmit beam sonar settings for overall best swath on each line for dataset 120515_1.

rather mean swath SNR of about 12 dB, as seen in the scatter plot before.

The best SNR values are achieved for narrow beam widths directed down towards the sea floor, but they are high for all settings in this deep water case, except for beam width and direction combinations that does not actually illuminate the sea floor, i.e. the top left corner in the images.

Picking the best simulated swath width from each line, which has varying solutions to the environment, the transmit beam width and electronic steering are shown in Figure 9.7. Ideally, these should have the same value for all lines. The result here is pretty consistent.

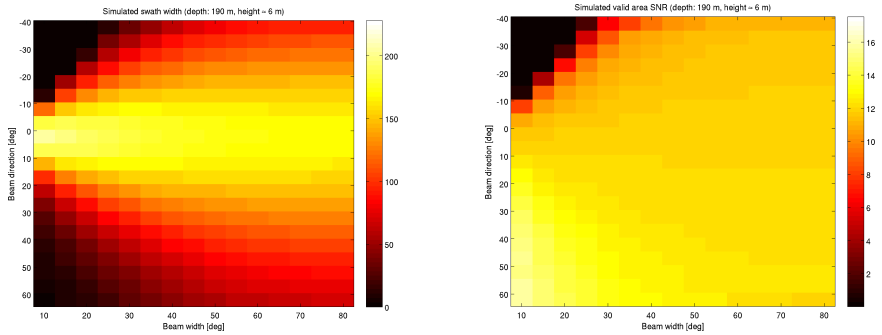

(a) Depth: 190 m. Altitude: 6 m.

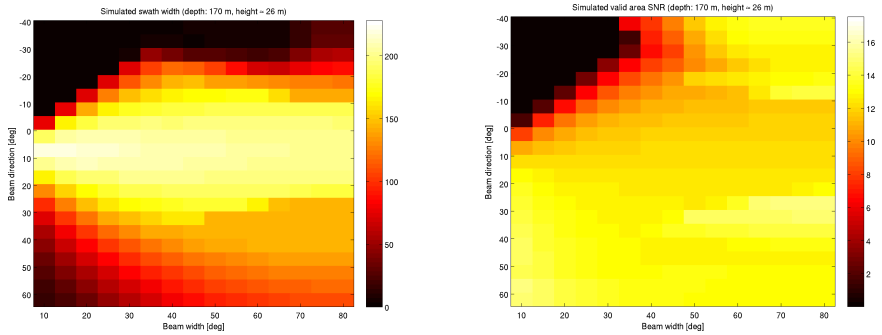

(b) Depth: 170 m. Altitude: 26 m.

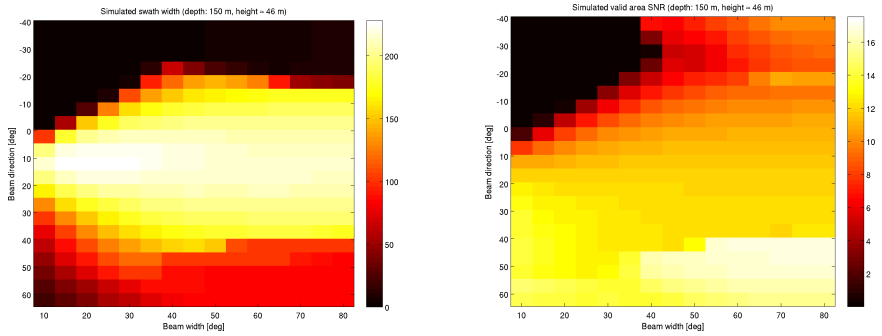

(c) Depth: 150 m. Altitude: 46 m.

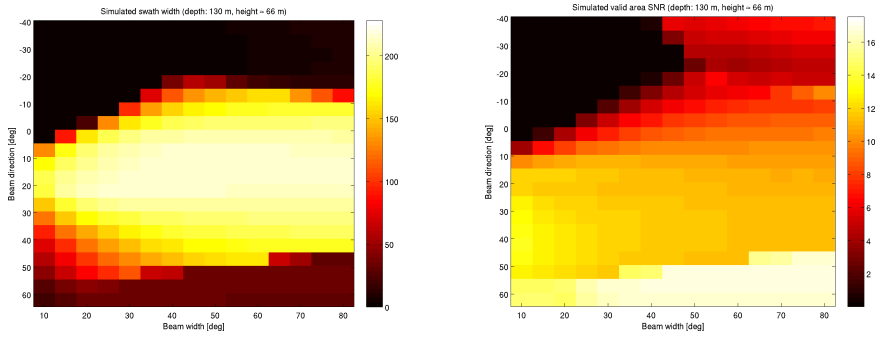

(d) Depth: 130 m. Altitude: 66 m.

Figure 9.8: Simulated swath width (left) and valid area mean SNR (right) for dataset 120515_1. The values are average values from estimations on each of the lines.

9.2.2 Shallow Water Dataset 080814_1

Figure 9.9 shows a scatter plot of the swath mean SNR as a function of swath lower (LL) and upper (UL) limits. Again, the characteristic lines of constant lower limits can be seen, caused by the altitude. This simulation was run with four different altitudes, whose values correspond to the four lines of constant lower limit seen in the plot.

To maximize the swath width, the lower and upper limit coordinates that are as far apart as possible must be found. This corresponds to the upper points in the scatter plot. Comparing this to the deep water result in Figure 9.6, the limitations in shallow water is clear. The highest mean SNR levels are achieved for very small swath widths. For the largest swath widths, the SNR level drops to around 4-5 dB, or even lower.

Maximizing SNR is analogous to picking the brightest yellow data point from the scatter plot. Again, the trade-off between SNR and swath width is clear, as it is hard to find a bright yellow dot with more than 10 meters swath width in this case.

For a minimum required swath width, the SNR decreases quickly, but swath widths of over 250 meters can be found with mean SNR values of more than 5 dB.

Limiting the SNR and picking the best swath width available is illustrated e.g. by removing all reddish data points and selecting the best swath width as before. Doing so for this shallow water case will quickly limit the available choices.

Figure 9.10 shows the simulated swath width and valid area mean SNR as a function of beam width and beam direction for different depths.

The best swath widths are achieved at 14 meters altitude, or 2 meters depth, with a beam width of 10-20 degrees, steered slightly down from the horizon by 0-10 degrees. They are the white areas in the images. These do not, however, correspond to the highest SNR values. The best SNR values are achieved at low altitudes for beam widths of 30-50 degrees, directed down towards the sea floor.

Picking the best simulated swath width from each line, which has varying solutions to the environment, the transmit beam width and electronic steering are shown in Figure 9.11. Ideally, these should be the same value for all lines. The result here is good with little variance, but keep in mind that the sample size is very small with only 12 lines.

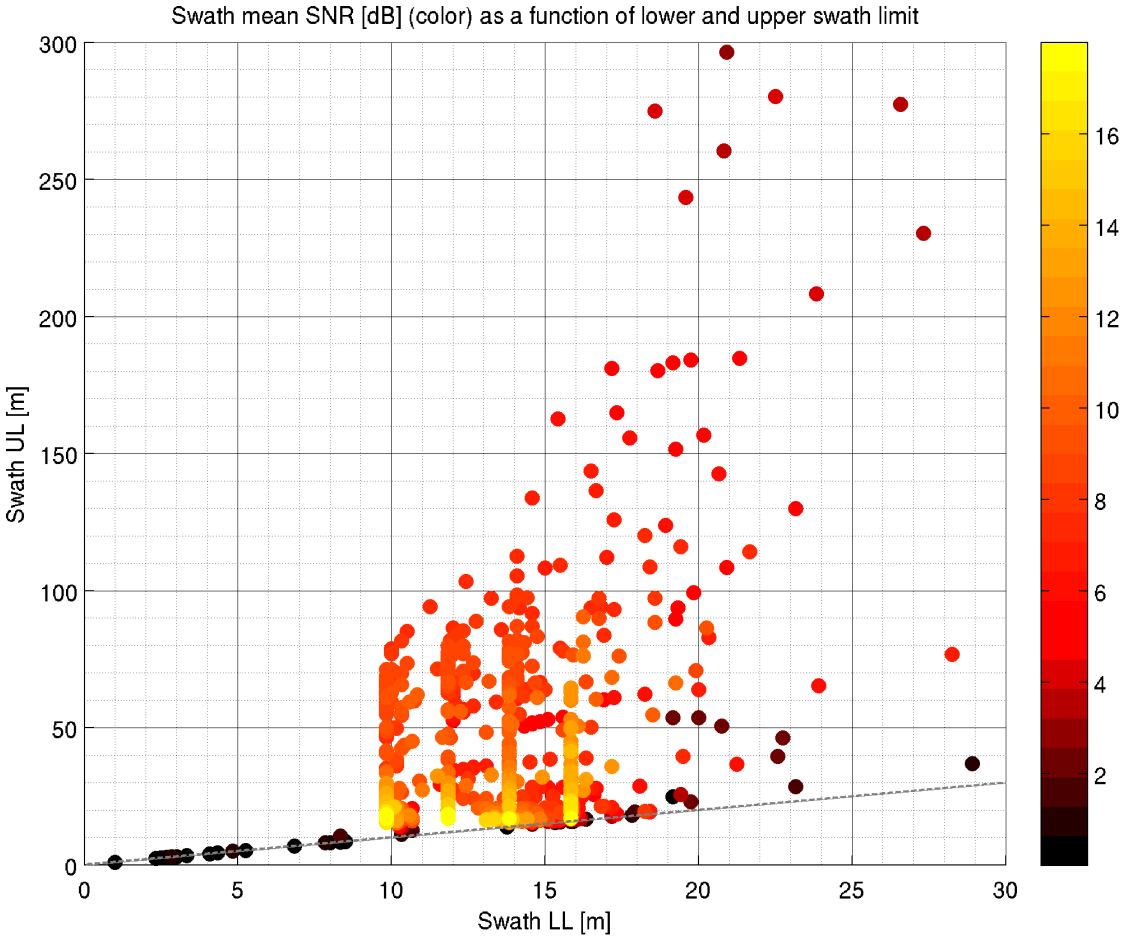

Figure 9.9: Result of brute force simulation for dataset 080814_1. Color indicates mean swath SNR [dB] plotted for swath lower limit (LL) and swath upper limit (UL). Ideal solution is top left with bright, yellow color.

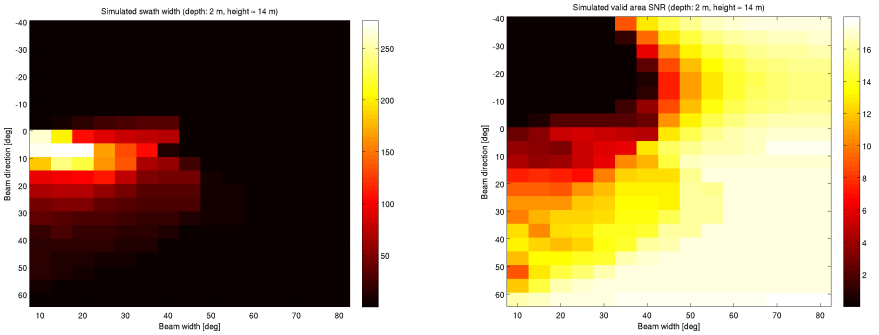

(a) Depth: 2 m. Altitude: 14 m.

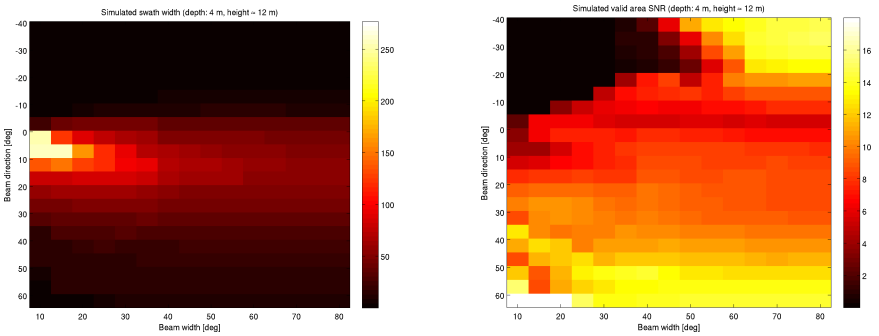

(b) Depth: 4 m. Altitude: 12 m.

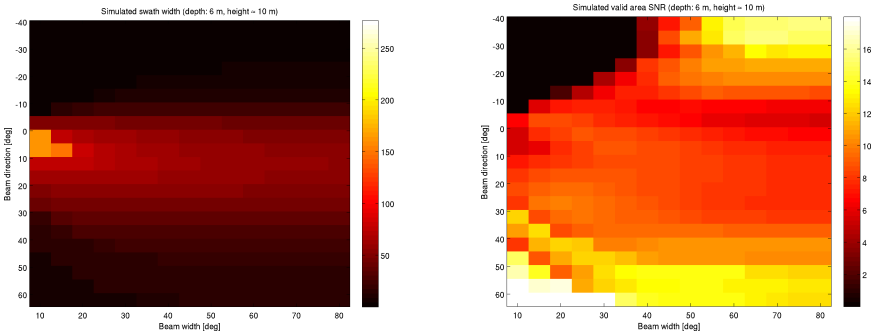

(c) Depth: 6 m. Altitude: 10 m.

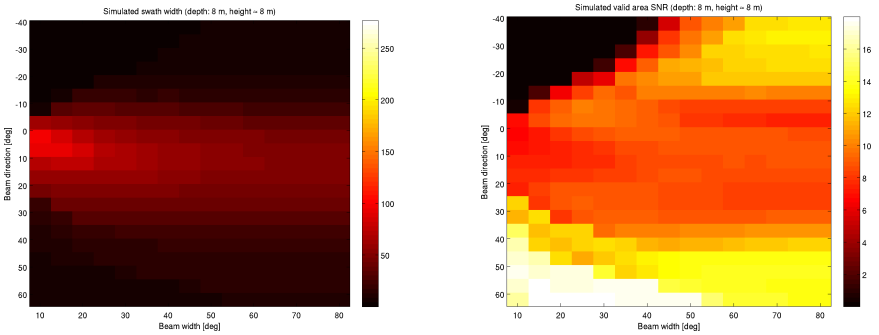

(d) Depth: 8 m. Altitude: 8 m.

Figure 9.10: Simulated swath width (left) and valid area mean SNR (right) for dataset 080814_1. The values are average values from estimations on each of the lines.

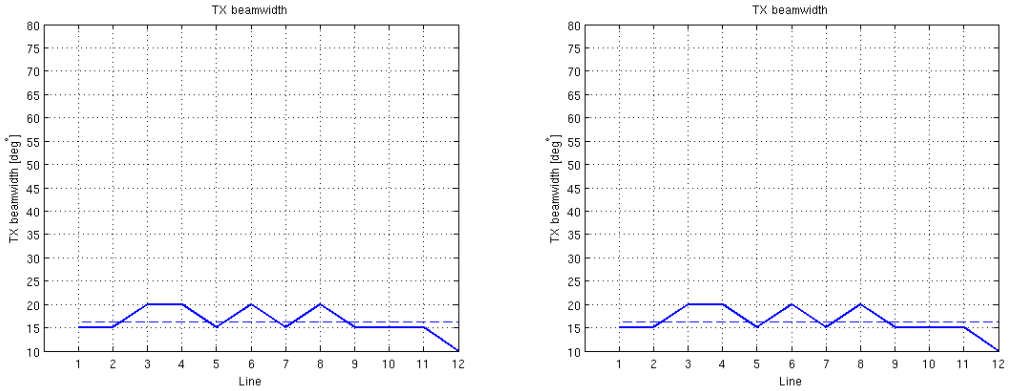

(a) Transmit beam width.

(b) Transmit beam direction.

Figure 9.11: Transmit beam sonar settings for overall best swath on each line for dataset 080814_1.

9.2.3 Shallow Water Dataset 120918_2

Figure 9.12 shows a scatter plot of the swath mean SNR as a function of swath lower (LL) and upper (UL) limits. As with the other datasets, the characteristic lines of constant lower limits can be seen, caused by the altitude. This simulation was run with four different altitudes, whose values correspond to the four lines of constant lower limit seen in the plot.

To maximize the swath width, the lower and upper limit coordinates that are as far apart as possible need to be found. This corresponds to the upper points in the scatter plot. Comparing this to the deep water result in Figure 9.6, the limitations when in shallow water is again clear. The highest mean SNR levels are achieved for very small swath widths. For the largest swath widths, the SNR level drops to around 4-5 dB, or even lower. Comparing this to the other shallow water result in Figure 9.9, the best solutions are not as good for dataset 120918_2. This can be related to bathymetry, but considering that the best results for dataset 80814_1 was with higher altitudes, it is likely that the water depth is an important factor here. Dataset 120918_2 has a sea floor depth of about 10 meters, while dataset 080814_1 has a sea floor depth of about 16 meters.

Maximizing SNR is analogous to picking the brightest yellow data point from the scatter plot. As with the other results, the trade-off between SNR and swath width is clear here, as it is hard to find a bright yellow dot with more than 15 meters swath width in this case.

For a minimum required swath width, the SNR decreases quickly, but a few swath widths of over 150 meters can be found with mean SNR values of more than 5 dB.

Limiting the SNR and picking the best swath width available is illustrated e.g. by removing all reddish data points and selecting the best swath width as before. Doing so for this shallow water case will quickly limit the available choices.

Figure 9.13 shows the simulated swath width and valid area mean SNR as a function of beam width and beam direction for different depths.

The best swath widths are achieved at 8 meters altitude, or 2 meters depth, with a beam width of 10 degrees, steered slightly down from the horizon by 5 degrees. They are the white areas in the images. These do not, however, correspond to the highest SNR values. Higher SNR values are achieved by further steering down towards the sea floor. The best SNR values are achieved at low altitudes for larger beam widths, directed down towards the sea floor. They result in very narrow swath widths.

Picking the best simulated swath width from each line, which has varying solutions to the environment, the transmit beam width and electronic steering are shown in Figure 9.14. Ideally these should be the same value for all lines. The result here is not as bad as one might have expected from the large variance seen before.

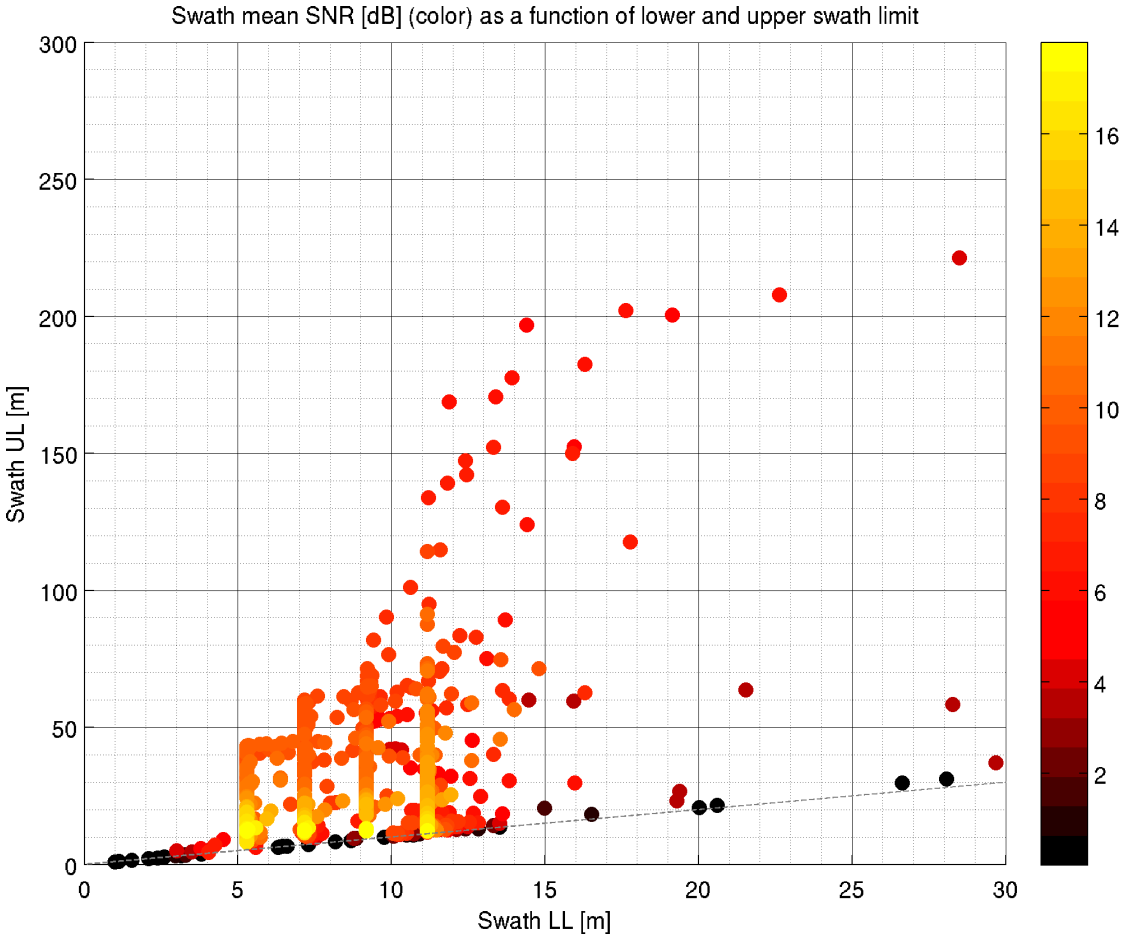

Figure 9.12: Result of brute force simulation for dataset 120918_2. Color indicates mean swath SNR [dB] plotted for swath lower limit (LL) and swath upper limit (UL). Ideal solution is top left with bright yellow color.

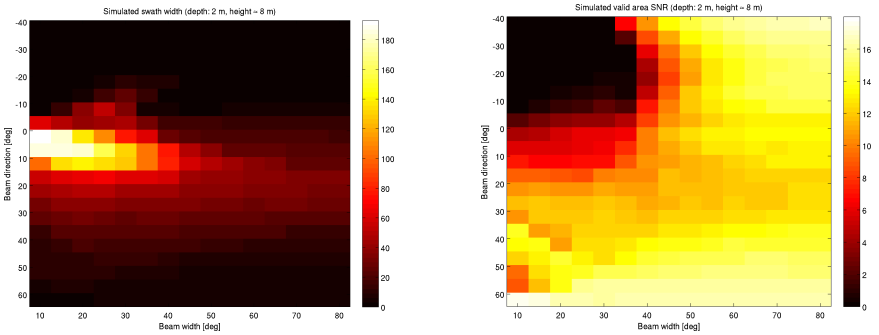

(a) Depth: 2 m. Altitude: 8 m.

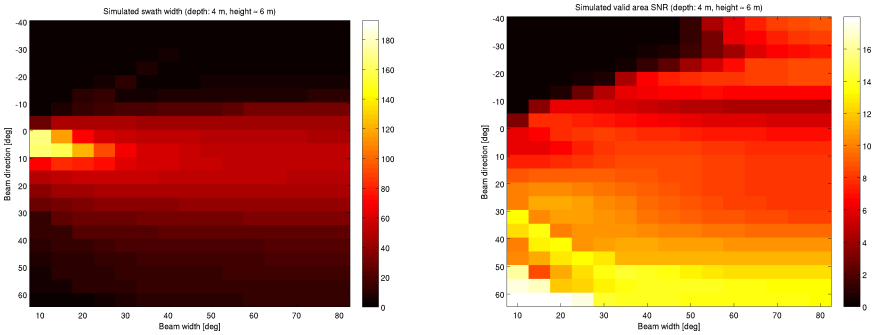

(b) Depth: 4 m. Altitude: 6 m.

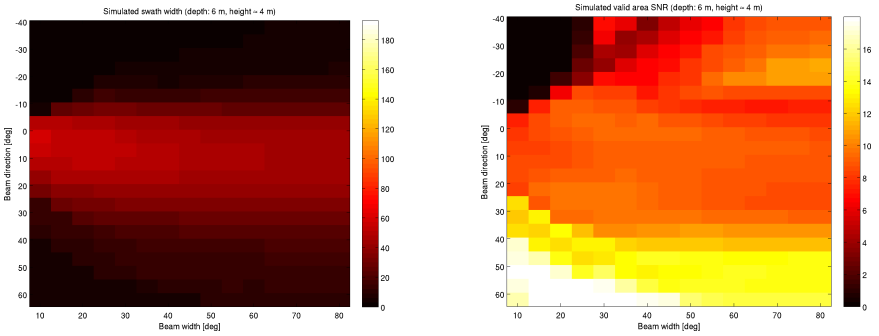

(c) Depth: 6 m. Altitude: 4 m.

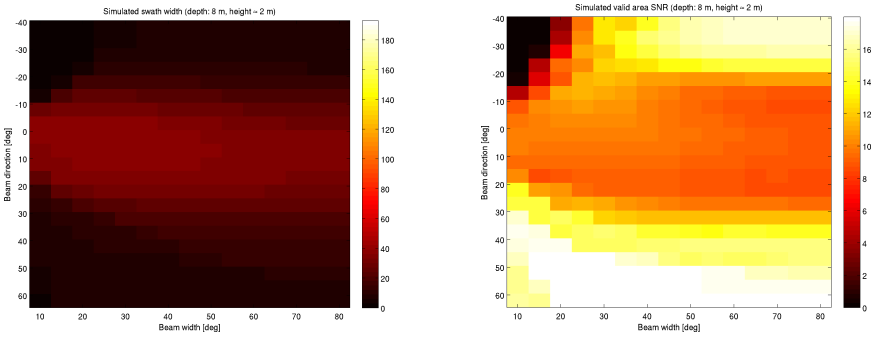

(d) Depth: 8 m. Altitude: 2 m.

Figure 9.13: Simulated swath width (left) and valid area mean SNR (right) for dataset 120918_2. The values are average values from estimations on each of the lines.

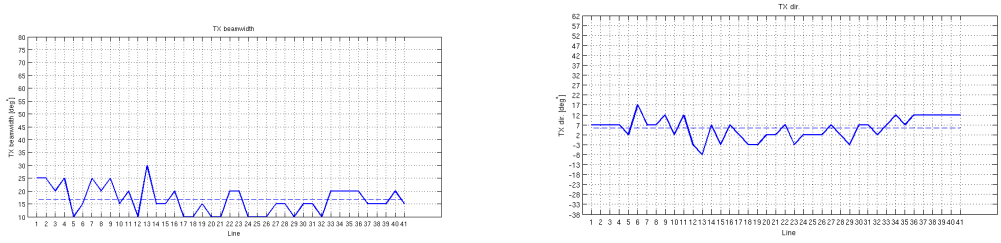

(a) Tx beam width.

(b) Tx beam direction.

Figure 9.14: Tx sonar settings for overall best swath on each line for dataset 120918_2.

9.2.4 Adaptation Summary

When comparing the results from deep water in Section 9.2.1 to the shallow water results in Sections 9.2.2 and 9.2.3, it is obvious that sonar imaging in shallow water is harder than in deep water. The range of sonar settings and altitudes that give large swath widths with high SNR are much more limited the more shallow the water gets.

It has been seen that increasing the swath width involves trading off SNR. This can be partly explained by how large an area our finite amount of energy is spread out over. Spreading it over a small area, e.g. a narrow beam directed downwards, results in a small swath width and high SNR. Spreading it over a larger area, e.g. a wider beam or a more horizontal beam direction, results in a wider swath with lower SNR. This can change with bathymetry or multipaths, but no convincing examples of this is seen.

The simulations for all the datasets show that a beam directed slightly down from the horizon is the best result. The measurements, however, indicate the opposite trend with the measured swath width, i.e. it decreases when the beam is steered up closer to the horizon, as was seen in Chapter 5. This might be an indication that the beam pattern used for the simulations is not correct, and that more energy is transmitted upwards. This would cause both better range with a lower direction in deep water, and more multipath with a horizontal direction in shallow water. Tank measurements of the current antennas could confirm this theory, but are not available in time for writing this thesis.

The criteria discussed in Section 8.2 are reviewed for shallow water based on the results.

The first suggested criteria, maximizing the swath width and then the SNR, works well, even though the swath lower limits are unpredictable, and it can results in relatively low SNR.

The second suggested criteria, maximizing the SNR first and then the swath width, does not seem to work well at all because it results in very small swath widths, often less than 10 meters.

The third suggested criteria, requiring a minimum swath width and then maximizing the SNR, is an approach that allows to dynamically trade SNR for range by varying the minimum swath width. The lower swath limit is, however, still unpredictable.

The other way around, with the fourth criteria of requiring a minimum SNR level and then maximizing the swath width, is less predictable in terms of swath width. In shallow water, the obtainable SNR can potentially be low, and setting a threshold might result in a solution of a small swath width.

The fifth suggested criteria, setting a minimum swath by requiring a maximum lower limit and a minimum upper limit and then maximizing the SNR, has the same drawbacks as the third suggested criteria, except that the lower swath limits are more predictable. The cost of this limits the options further, so the SNR obtained for the third suggested criteria will often be higher than in this case.

The sixth suggested criteria, requiring a maximum lower limit and a minimum SNR and then trying to maximize the upper limit, controls the lower limit well. If the SNR requirement is set low, this criteria will maximize the swath width while keeping the

lower limit predictable. This might not result in a very large swath width, since it has been seen that higher lower limits are required, but if the lower swath limit is more important than swath width, this suggested criteria seems to be the best choice.

The best choice of criteria is dependent on the objective of the data collection. For pure imaging, maximizing the swath width can result in faster coverage rate. If, however, aperture synthesizing will be done, there might be a need to perform micro-navigation, which benefits from samples at shorter range (Hansen et al. 2011). In that case, limiting the maximum range for the lower limit is appropriate. For creating bathymetric maps, higher signal to noise ratios are required than for pure imaging (Sæbø, T. O. 2010). Thus, ensuring sufficient signal to noise ratio is more important in this application. In conclusion, the objective of the data collection needs to be decided and used as a premise for selecting the appropriate optimization criteria.

Part V

Implementation

Chapter 10

Adaptive Sonar Algorithm

A full implementation, including environment estimation and adaptation, is discussed in this chapter. First, the search algorithm is discussed by analyzing a few example search spaces in Section 10.1. Then, the algorithm is described in Section 10.2, and the results of a sample run on a few datasets are shown in Section 10.3.

10.1 Search Method

Examples of search spaces for environment modeling from each dataset is shown in Figure 10.1. Bottom type and sea state are at the x- and y-axes, and the error between measured and simulated SNR is on the z-axis. For the deep water dataset 120515_1, this is a one-dimensional search problem where only the bottom type is significant. Minimizing the error in this case is an easy task, and can be done well with a greedy search algorithm, i.e. always move towards the next better value until you can't find any better values. For the shallow water datasets 080814_1 and 120918_2, the search spaces are more complicated. There are large areas of small errors, which contain several local minima. These have a tendency to cause large variations in the results with search algorithms that are prone to getting stuck at a local minimum, like hill climbing is. Using a hill climber algorithm for the environment estimation also shows this behavior in practice. Since it is important for the adaptation that the environment is well estimated, this is a major drawback and the extra computational cost of a brute force approach is considered instead. In order to slightly decrease the number of function evaluations, the search space is divided into twelve different parts by the sea state. Then, a greedy search algorithm is used on each part, starting at the middle of the search space, since mid-space values should occur more often than extreme values. The winning result is the minimum error found after these twelve greedy searches are done.

Figure 10.2 shows examples of search spaces for the swath width from each dataset. This corresponds to using the search criteria of maximizing swath width, as discussed in Section 8.2. These are comparable to the mean data shown in Section 9.2, but the

visualization here is for a single line only. It illustrates the search space for hill climbing based on a single measurement line. Beam direction and beam widths are on the x- and y-axes, and the resulting swath widths are on the z-axis. The example from dataset 120515_1 looks continuous and is mostly increasing, with the exception of a few plateaus. For the datasets 080814_1 and 120918_2, there are large areas of no swath width. A similar ridge to the one for dataset 120515_1 is present and increasing towards the maximum swath widths. These search spaces have characteristics which should work well with a hill climber algorithm, as long as the initial value is not in the areas with zero swath width. Considering that an initial guess at what a good setting would be is available, i.e. the standard settings, these settings can be used as initial parameters to start hill climbing from. More often than not, these initial parameters should be coordinates from which there is a strictly increasing way to the maximum. With this requirement of a good initial value for success, the hill climber is used in this algorithm for the adaptation.

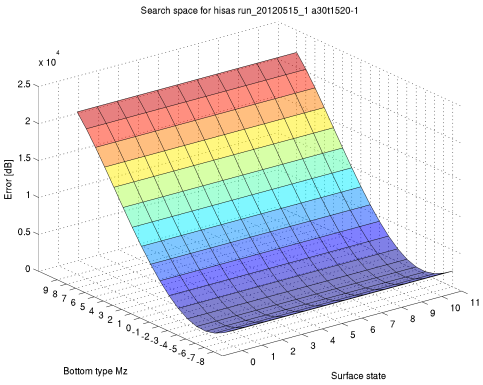

(a) Dataset 120515_1, line a30t1520-1.

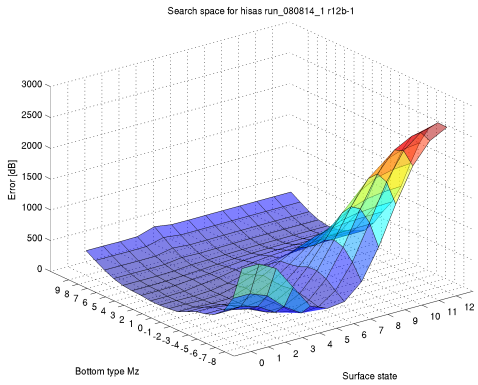

(b) Dataset 080814_1, line r12b-1.

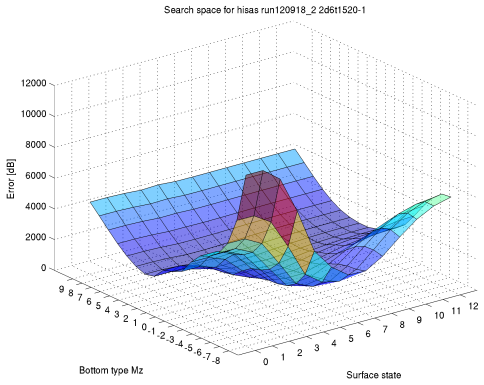

(c) Dataset 120918_2, line 2d6t1520-1.

Figure 10.1: Example search spaces of environment estimations.

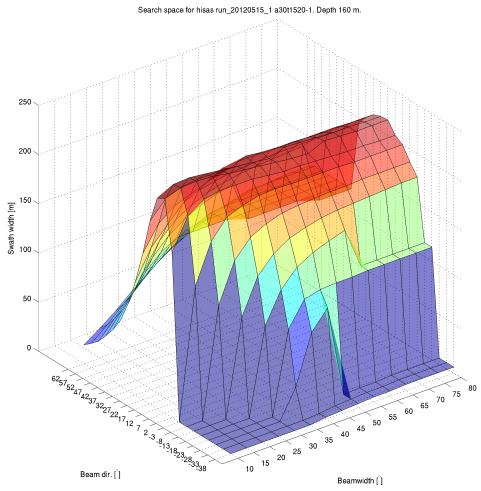

(a) Dataset 120515_1, line a30t1520-1.

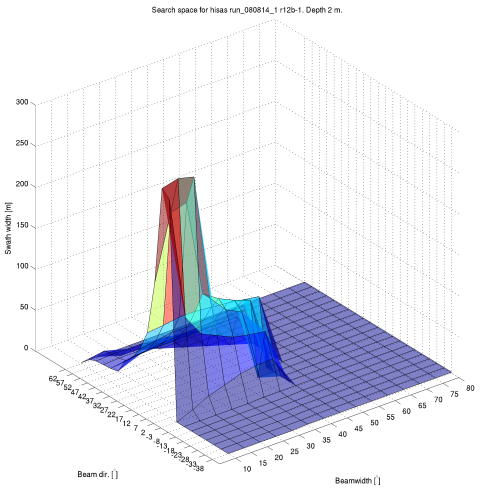

(b) Dataset 080814_1, line r12b-1.

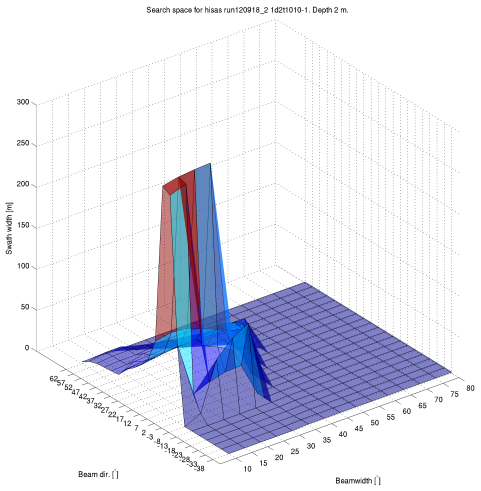

(c) Dataset 120918_2, line 1d2t1010-1.

Figure 10.2: Example search spaces of adaptation with swath width on z-axis. Note that there is a third dimension, depth, that is not displayed here, but fixed to an arbitrary value for the sake of displaying an example.

10.2 Algorithm

The flowchart in Figure 10.3 shows the entire environmentally adaptive sonar process, with data input and output from each step. The algorithm takes a measurement as input, including the measured bathymetry, coherence, vehicle control (e.g. altitude and

depth), sound speed profile and the sonar settings used for the measurement. Then, the environment estimation is done as described in Chapter 6 and Section 10.1. The best resulting bottom type and sea state are then used for adaptation, as described in Chapter 8 and Section 10.1. Finally, a check is done to evaluate whether or not the simulation claims to improve the performance, in this case the swath width. If the swath width is improved, the new parameters are the output from the algorithm, ready to be applied to the sonar system. If not, the process starts over.

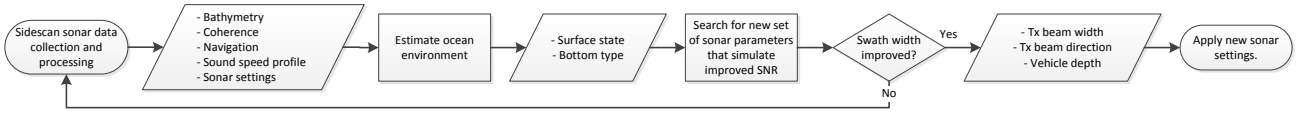

Figure 10.3: Flowchart of the environmentally adaptive sonar process.

10.3 Algorithm Results

In this section, sample runs of the algorithm on each line in each of the datasets are presented in tables. The runtime is given in seconds, and the parameters, both for the environment estimation and the adaptation, are listed for each line. Finally, the old and new swath widths, along with the improvement in percent, are listed. For some lines, the adaptation parameters are shown as *NaN*. These are the cases where the algorithm has failed to produce an improved result, as is clearly seen by the negative improvement percentage. This can be caused by both errors in the environment estimation, or simply that the search algorithm failed, e.g. by getting stuck at a local maximum.

The self-noise max-range was set to 200 meters and the valid area threshold to -5 dB. The search space boundaries was bottom types from -8 to 9 and sea states from 0 to 12 for the environment estimation. The search space boundaries for the adaptation was beam widths from 10 to 80 degrees, beam directions from 42 to -28 degrees (positive down from the horizon) and altitudes from 3 meters above the sea floor up to maximum 80 meters, depending on the sea floor depth. For dataset 120515_1, 30 pings were used for each line. For dataset 080814_1, 100 pings were used for each line. For dataset 120918_2, 60 pings were used for each line.

10.3.1 Deep Water Dataset 120515_1

Results from the EAS-algorithm for each line in dataset 120515_1 are listed in Table 10.1. Notice that the surface parameter is set to 1 because it does not affect this simulation for deep water.

Because these measurements are collected in deep water, the measured swath width is already high. The improvement is large for the lines that had initially worse settings, less for lines with better settings, and ends up failing to improve the best measurement in line 19. Comparing the sonar parameters found, the beam width and beam direction seems to correspond well with the best results, shown in Section 9.2.1.

The runtime is very low for this dataset. This is because no multipaths needs to be calculated, as the water depth is about 190 meters.

The results here show that the algorithm can find trustworthy improved settings from a single line, but also that it is not particularly useful in deep water if good standard settings are already being used. How much the best settings vary with varying bottom type and bathymetry is an interesting question, but could not be investigated with this dataset.

10.3.2 Shallow Water Dataset 080814_1

Results from the EAS-algorithm for each line in dataset 080814_1 are listed in Table 10.2.

The algorithm fails to improve one of the twelve lines, for which the estimated bottom type is an outlier. For the rest, however, the suggested beam width, beam direction and depth come very close to the best known settings, as found in Section 9.2. The improved swath widths are not as high as those found in Section 9.2, which might be explained by the steepness of the hill close to these maxima, as seen in Figure 10.2(b), but also by the fact that varying bathymetry gives varying results, even for relatively slight changes. Bottom types of 1-1.5 and sea states of 1-3 are estimated, which correspond to the lines that seemed to be the best fits in the model verification analysis in Section 9.1.2. The average runtime is about 38 seconds per line.

10.3.3 Shallow Water Dataset 120918_2

Results from the EAS-algorithm for each line in dataset 120918_2 are listed in Table 10.3.

The algorithm fails to improve six of the 41 lines. For the rest, the suggested beam width, beam direction and depth are mostly the same as found in Section 9.2, with a narrow beam directed a few degrees down from the horizon at about two meters depth. The beams are narrow (10-30 degrees) and steered slightly down from the horizon. The average runtime is about 34 seconds per line.

10.4 Discussion and Recommendations

The simple environmentally adaptive sonar implementation provided in this chapter connects the dots from the other parts of this thesis. It shows that it is possible to perform environment estimation and use simulations to make a recommendation for improved settings, and that it is possible to do so within about half a minute on a reasonably powerful computer.

Table 10.1: Results of running the environmentally adaptive sonar algorithm for dataset 120515_1. The average sea floor depth is approximately 190 meters.

Line	Runtime [s]	Mz	Surface	Beam width [°]	Beam dir. [°]	Depth [m]	Measured swath [m]	New swath [m]	Improvement
1	4.2	-3.5	1	22	11	153.8	161	199	23.6 %
2	4.1	-4	1	20	12	148.2	133	211	58.6 %
3	3.9	-4	1	22	10	147.5	123	212	72.4 %
4	4.2	-4	1	20	10	150.4	129	210	62.8 %
5	4.2	-5.5	1	16	9	160	110	244	121.8 %
6	4.1	-4.5	1	20	11	150.6	114	223	95.6 %
7	4.7	-4.5	1	18	10	156.6	184	224	21.7 %
8	4.3	-4.5	1	20	12	147.5	157	225	43.3 %
9	4.2	-4.5	1	17	10	151	174	224	28.7 %
10	4.3	-4.5	1	20	10	145.7	159	224	40.9 %
11	4.1	-5.5	1	20	10	158.2	133	246	85 %
12	4.1	-4.5	1	20	12	144.8	146	225	54.1 %
13	4.5	-4.5	1	21	12	147.8	204	228	11.8 %
14	4.6	-5	1	20	12	150.7	196	238	21.4 %
15	4.4	-4.5	1	21	10	146.6	189	227	20.1 %
16	4.6	-5	1	20	10	152.7	188	237	26.1 %
17	4.3	-5	1	21	10	151.5	163	238	46 %
18	4.5	-6	1	20	8	163.7	174	256	47.1 %
19	4.7	-5	1	NaN	NaN	NaN	244	240	-1.6 %
20	4.7	-5	1	26	13	147.9	212	238	12.3 %
21	4.6	-4.5	1	19	13	147.2	221	230	4.1 %
22	4.6	-4.5	1	23	10	147.6	196	227	15.8 %
23	4.5	-5	1	23	11	152	194	240	23.7 %
24	4.5	-4.5	1	20	13	143.8	195	227	16.4 %
25	4.8	-5.5	1	25	9	155.1	230	251	9.1 %
26	4.8	-5	1	20	11	151.2	239	240	0.4 %
27	4.8	-5	1	18	10	155.3	226	240	6.2 %
28	4.8	-5	1	20	10	153.5	233	239	2.6 %
29	4.6	-5	1	20	12	149.7	204	239	17.2 %
30	4.7	-5	1	20	10	153.7	226	238	5.3 %

Table 10.2: Results of running the environmentally adaptive sonar algorithm for dataset 080814_1. The average sea floor depth is approximately 16 meters.

Line	Runtime [s]	Mz	Surface	Beam width [°]	Beam dir. [°]	Depth [m]	Measured swath [m]	New swath [m]	Improvement
1	33.3	1.5	1	10.5	7	2.6	85	102	20 %
2	39.4	1.5	1	10.5	7	3.5	79	99	25.3 %
3	38.6	1	1	10.5	7	2.6	84	101	20.2 %
4	43.7	1.5	1	10.5	10	2.6	111	129	16.2 %
5	32.9	1.5	1	10.5	8	2.5	79	101	27.8 %
6	40.5	3	2	10.5	10	2.6	94	119	26.6 %
7	35.2	1.5	3	10.5	8	2.7	103	118	14.6 %
8	37.3	1.5	3	10.5	7	2.6	104	113	8.7 %
9	31.7	1.5	1	11.5	9	2.7	65	101	55.4 %
10	49.9	-5.5	1	NaN	NaN	NaN	84	81	-3.6 %
11	38.7	-1.5	4	10.5	7	2.7	83	152	83.1 %
12	36.9	1.5	3	11.5	7	2.6	103	111	7.8 %

The environment estimation is decisive for the reliability of the improved settings. Therefore, it is recommended to put sufficient computational resources into making this estimate a good one. An example of how to do this is the semi brute force approach implemented here. Another would be to do the same method, but with multiple measurements. This would require a history of the last measurements, which can be used to minimize the total error. Further research is needed towards whether this will converge to exact or biased environment parameters, or if it converges at all. Doing this improved the results with dataset 120918_2.

The hill climber used here performs fairly well in these sample runs. It usually finds solutions that simulate large swath width improvements.

The average runtime of the algorithm for shallow water, i.e. with multipaths, was approximately 35 seconds per line. For dataset 120918_2, this means that all 41 lines took about 23 minutes to complete. This is quick compared to the brute force search earlier, which for this dataset took approximately 30 hours to complete for all 41 lines when not computed in parallel. It can be quick enough, e.g. for delayed real-time by running the algorithm for the previous measurement line before finishing with the collection of the next line. Further search optimization, including method and model optimizations, parallelization and faster CPUs or GPU implementations could probably cut down the runtime additionally, maybe even down to a few seconds, which will allow real time operation.

On board an autonomous underwater vehicle, this example algorithm could run in delayed real time by processing the previously collected line while collecting the current one. After collecting one line of measurements, the algorithm could be run while the vehicle carries on to the next line. Then, the algorithm finishes and applies the improved sonar settings on the third line, under the assumption that the lines are long enough for the computations to complete. This process can be repeated continuously. However, there will be no convergence to good settings as long as no history of

Table 10.3: Results of running the environmentally adaptive sonar algorithm for dataset 120918_2. The average sea floor depth is approximately 10 meters.

Line	Runtime [s]	Mz	Surface	Beam width [°]	Beam dir. [°]	Depth [m]	Measured swath [m]	New swath [m]	Improvement
1	31.5	1.5	1	10	6	2.3	72	87	20.8 %
2	39.5	-1	1	NaN	NaN	NaN	74	50	-32.4 %
3	32.6	1.5	1	10	5	2.3	75	85	13.3 %
4	40.1	-5	1	NaN	NaN	NaN	67	38	-43.3 %
5	30.8	2.5	2	11	5	2.3	73	88	20.5 %
6	38.7	3.5	5	NaN	NaN	NaN	88	59	-33 %
7	26	3	3	10	6	2.1	73	100	37 %
8	33.7	1.5	3	10	6	2.1	81	109	34.6 %
9	37.4	2.5	2	NaN	NaN	NaN	78	67	-14.1 %
10	16	3.5	1	10	7	2.1	72	98	36.1 %
11	51.7	1.5	4	30	10	2.1	76	104	36.8 %
12	34	3	4	26	5	2.2	73	90	23.3 %
13	35.4	3	4	20	5	7.1	78	116	48.7 %
14	46.4	-0.5	5	17	0	7.1	79	159	101.3 %
15	34.4	2.5	3	30	8	6.1	70	115	64.3 %
16	38.3	-5	6	19	12	6.1	66	214	224.2 %
17	34.2	1.5	6	10	4	6.1	74	105	41.9 %
18	29.9	1.5	5	11	3	6.2	57	130	128.1 %
19	29.2	2.5	5	10	5	4.2	53	93	75.5 %
20	27.4	2.5	6	11	5	2.2	55	93	69.1 %
21	31.1	1.5	6	22	5	2.2	45	99	120 %
22	31.2	2.5	3	20	9	2.2	42	87	107.1 %
23	30.1	2.5	7	11	5	3.2	54	95	75.9 %
24	31.6	2.5	1	10	5	2.7	79	93	17.7 %
25	32.8	0.5	4	10	5	2.4	98	111	13.3 %
26	32.6	2.5	1	10	8	2.4	99	104	5.1 %
27	32.4	2.5	2	10	7	2.3	83	104	25.3 %
28	41.8	1.5	3	29	14	3.4	82	93	13.4 %
29	37	1.5	4	NaN	NaN	NaN	87	62	-28.7 %
30	34.3	1.5	5	10	6	2.2	111	121	9 %
31	32.1	1	7	10	5	2.2	103	126	22.3 %
32	41.4	2.5	3	NaN	NaN	NaN	108	78	-27.8 %
33	32.2	1.5	5	10	4	4.2	88	118	34.1 %
34	45.8	-3.5	6	10	1	6.1	85	236	177.6 %
35	36.3	0	6	10	5	2.1	89	135	51.7 %
36	31.3	2.5	6	10	6	2.5	96	105	9.4 %
37	29.3	1.5	9	10	5	2.1	94	116	23.4 %
38	31.7	1.5	7	10	5	3.1	91	117	28.6 %
39	33.4	2.5	6	10	5	3.1	84	104	23.8 %
40	27.5	1.5	6	10	5	3	80	115	43.8 %
41	32.2	1.5	7	10	5	2.1	80	115	43.8 %

measurements and results are taken into account, or alternatively a growing set of measured data is used by finding environment parameters based on all the previously collected data, as done in Section 9.1.3. Convergence to good settings is important for a successful implementation, and assuring this is an interesting topic for future work.

Part VI

Conclusion

Chapter 11

Conclusion

This chapter recapitulates the discussions and conclusions in this thesis, and briefly discusses topics which would be interesting and useful for future work.

11.1 Environmentally Adaptive Sonar

The aim of this thesis was to dynamically adapt the sonar settings to the sensed ocean environment in order to improve performance. This concept of *environmentally adaptive sonar* has been investigated, developed and tested with real measurements.

I have shown that the ocean environment can be estimated from a single or multiple measurements using the sonar performance model SMURF in Part III, *Modeling the ocean environment*. Based on this, I have further shown that the same model can accurately predict measurements with other sonar settings in Part IV, *adapting to the ocean environment*. I have suggested and implemented an environmentally adaptive sonar algorithm for finding improved settings in Part V, *Implementation*. Example runs of this algorithm shows that it successfully improves the sonar parameters automatically. Showing that the sonar settings can be dynamically adapted to the sensed ocean environment in order to improve performance is a successful proof of concept for environmentally adaptive sonar.

Developing and describing a proof of concept for environmentally adaptive sonar and showing that it works with real measurements are the main contributions of this thesis. Additionally, examples of sonar performance in both shallow and deep water can be useful as partial information when deciding which sonar settings to use in similar environments. For further development of environmentally adaptive sonar, the discussions provided on robustness and optimization are useful.

11.2 Future Work

This chapter lists suggestions for future work based on the results and experiences in this thesis.

Verify improved settings: While the model verification analysis in Part IV, *Adapting to the ocean environment*, shows that the available measurements can be accurately simulated, it has not been verified that the best simulated results found here actually provide a real performance increase when applied. Ultimately, this needs to be done automatically in-mission, otherwise the environment might change between runs.

Adding history to the algorithm: Even though the analysis in this thesis shows that averaging multiple environment estimations is less effective than using more pings for one estimation, remembering the results from other lines in the current area and using them to improve the estimate should be a natural addition to the algorithm. This is important in order to assure convergence to good settings.

Advanced beam forming: More advanced transmit beam forming, e.g. with asymmetrical beams, could be applied in order to improve the adaptive sonar performance further.

Extreme environments: This thesis has generally considered shallow waters with benign bathymetry. Environments with extreme bathymetry could benefit from adaptive sonar, both in shallow and deep water.

Search algorithms: The environmentally adaptive sonar algorithm presented in this thesis uses a greedy search and a simple hill climbing algorithm, both of which are not necessarily the optimal search algorithms for neither speed, nor to find the optimal result. Using better search algorithms could potentially increase the speed and robustness of the full algorithm. Investigating this by surveying existing literature and performing simulations, and testing them on real data, is an interesting research topic.

Multi-objective search: For adaptation, it is desirable to optimize more than one criterion at the same time, as discussed in Section 8.2. New insight could be gained by investigating this, e.g. by analyzing dominance and Pareto optimality (Eiben and Smith 2007, p. 166). A survey of existing literature on multi-objective search, followed by application to the multipath problem would be interesting.

Model optimization: It might be possible to optimize the model for increased speed. Optimizing the ray tracer should be studied initially, as this is the most time consuming part of the simulations.

Self-noise: The variations in self-noise levels that best fits the measurements may be an indication that the self-noise calculations are incorrect. Further research is needed on how the self-noise could be properly measured and modeled.

Model accuracy at small grazing angles: The sonar performance model's accuracy is known to decrease with lower altitude and longer range, because the reflectivity model is no longer valid at small grazing angles. This is believed to have a large

impact, since this application is for shallow water, and thus low altitudes with small grazing angles are usually the case. Improving this would improve the accuracy of the end result.

Modeled beam pattern: For the simulated results to be correct, the beam pattern used must be accurately modeled. In the case of this thesis, it is believed that the beam pattern used for simulations does not accurately model the real beam pattern. This is being investigated further.

Appendix A

Curve Fitting Results

Table A.1: Results from the curve fitting test for dataset 080814_1.

(a) Mean values over all the lines for each combination.

Threshold [dB]	Self-noise max-range [m]	Mz	Surface	RMSE [dB]	UL [m]	UL error [m]
0	200	1.83	2.33	1.30	105	-12.58
0	400	1.17	2.17	1.38	179.67	-87.25
-5	200	1.67	2	1.44	98.67	-6.25
-5	400	-0.83	1.92	2.14	123.33	-30.92
-10	200	2.33	1.92	1.68	93.92	-1.50
-10	400	-2.08	1.83	3.04	111.50	-19.08

(b) Standard deviations over all the lines for each combination.

Threshold [dB]	Self-noise max-range [m]	Mz	Surface	RMSE [dB]	UL [m]	UL error [m]
0	200	2.44	1.25	0.53	28	22.20
0	400	2.51	1.28	0.48	94.75	89.74
-5	200	2.17	1.41	0.37	25.49	19.80
-5	400	0.80	1.19	0.56	74.36	70.49
-10	200	1.75	1.44	0.54	14.71	9.93
-10	400	0.76	1.21	0.80	76.77	75.23

Table A.2: Results from the curve fitting test for dataset 120515_1.

(a) Mean values over all the lines for each combination.

Threshold [dB]	Self-noise max-range [m]	Mz	RMSE [dB]	UL [m]	UL error [m]
0	200	-4.47	1.78	210.23	-0.50
0	400	4.70	1.63	214.37	-4.63
-5	200	-4.60	2.66	212.63	-2.90
-5	400	4.43	2.45	216.57	-6.83
-10	200	-4.97	3.16	217.90	-8.17
-10	400	4.20	2.84	218.50	-8.77

(b) Standard deviations over all the lines for each combination.

Threshold [dB]	Self-noise max-range [m]	Mz	RMSE [dB]	UL [m]	UL error [m]
0	200	0.72	0.48	49.07	11.74
0	400	1.37	0.47	48.30	9.88
-5	200	0.61	1.13	47.26	8.93
-5	400	1.26	0.96	46.04	9.60
-10	200	0.95	1.71	40.78	11.73
-10	400	1.45	1.40	41.03	10.81

Table A.3: Results from the curve fitting test for dataset 120918_2.

(a) Mean values over all the lines for each combination.

Threshold [dB]	Self-noise max-range [m]	Mz	Surface	RMSE [dB]	UL [m]	UL error [m]
0	200	-0.13	4.61	2.39	101.70	-13.22
0	400	3.61	3.17	2.10	140.43	-51.96
-5	200	-0.91	5.04	3.47	98.35	-9.87
-5	400	3.04	3.52	3.19	124.96	-36.48
-10	200	-2.09	5.04	6.07	89.74	-1.26
-10	400	0.74	2.83	5.49	114.61	-26.13

(b) Standard deviations over all the lines for each combination.

Threshold [dB]	Self-noise max-range [m]	Mz	Surface	RMSE [dB]	UL [m]	UL error [m]
0	200	3.42	3.27	1.11	29.15	28.64
0	400	2.68	1.81	1.04	69.61	62.33
-5	200	3.50	2.61	1.82	23.47	20.09
-5	400	4.10	2.72	1.25	61.60	55.83
-10	200	4.20	2.99	4.63	21.15	23.43
-10	400	4.73	2.18	2.40	60.37	61.28

Appendix B

Bottom Type and Sea State Estimation Results

Table B.1: Mz estimation over entire dataset 120515_1 for fixed self-noise with valid area attenuation limit 0 dB.

	Mz		UL error [m]		SNR error [dB]	
Self-noise [m]	Mean	STD	Mean	STD	Mean	STD
150	-7.53	0.57	7.09	8.03	2.44	0.66
160	-7.03	0.49	8.32	8.08	2.25	0.60
170	-6.63	0.67	7.36	8.32	2.26	0.63
180	-6.10	0.61	8.87	7.92	2.17	0.58
190	-5.70	0.70	6.18	5.45	2.14	0.60
200	-5.13	0.63	8.65	7.53	2.10	0.57
210	-4.80	0.81	5.81	4.59	2.02	0.57
220	-4.33	0.66	7.24	5.98	2.04	0.58
230	-3.83	0.79	6.42	4.76	1.94	0.55
240	-3.53	0.78	7.25	6.24	1.94	0.58
250	-2.93	0.83	7.61	6.40	1.89	0.55
260	-2.67	0.92	7.08	6.27	1.84	0.56
270	-2.10	0.92	7.24	5.96	1.87	0.55
280	-1.73	0.94	6.65	5.56	1.76	0.54
290	-1.37	1	7.74	6.93	1.80	0.55
300	-0.77	0.97	6.23	5.61	1.72	0.54
310	-0.50	1.07	8.37	6.91	1.73	0.54
320	0.13	0.97	6.23	5.56	1.72	0.54
330	0.33	1.12	8.14	6.21	1.69	0.52
340	0.93	1.14	7.80	6.57	1.71	0.55
350	1.27	1.05	7.47	6.18	1.66	0.52
360	1.63	1.16	8.22	7.74	1.68	0.54
370	2.20	1.16	6.81	5.79	1.65	0.52
380	2.53	1.20	8.06	7.14	1.66	0.54
390	3.07	1.23	7.39	6.52	1.66	0.53
400	3.43	1.28	7.91	6.27	1.66	0.53
410	3.90	1.37	6.98	6.92	1.67	0.54
420	4.30	1.26	7.25	5.10	1.67	0.54
430	4.80	1.35	7.25	7.06	1.68	0.55
440	5.17	1.09	7.58	6.45	1.72	0.55
450	5.60	1.30	8.55	7.96	1.75	0.58
460	6	1.05	7.84	8.01	1.82	0.61
470	6.27	0.98	10	10.44	1.90	0.69
480	6.60	0.81	10.26	11.78	2.05	0.76
490	6.73	0.64	13.52	13.73	2.22	0.87
500	6.80	0.61	16.99	15.34	2.46	0.96

Table B.2: Mz estimation over entire dataset 120515_1 for fixed self-noise with valid area attenuation limit -5 dB.

	Mz		UL error [m]		SNR error [dB]	
Self-noise [m]	Mean	STD	Mean	STD	Mean	STD
150	-7.77	0.43	7.01	8.36	3.41	1.39
160	-7.33	0.55	7.36	6.39	3.20	1.17
170	-6.90	0.61	6.37	8.25	3.05	1.04
180	-6.50	0.78	7.73	6.03	2.96	0.97
190	-6	0.74	6.60	6.88	2.86	0.97
200	-5.50	0.90	7.69	5.89	2.82	0.91
210	-5.07	0.74	7.07	6.12	2.72	0.94
220	-4.63	0.93	6.33	5.26	2.68	0.88
230	-4.17	0.83	7.09	5.61	2.60	0.91
240	-3.70	0.99	7.10	6.54	2.54	0.87
250	-3.30	0.88	8.23	7.11	2.51	0.85
260	-2.83	0.99	7.26	6.21	2.44	0.86
270	-2.40	1	7.88	6.96	2.44	0.81
280	-1.97	1.16	6.79	5.53	2.34	0.84
290	-1.60	1.07	8.99	7.16	2.36	0.81
300	-0.97	1.16	6.20	5.69	2.29	0.80
310	-0.73	1.11	9.15	7.06	2.29	0.80
320	-0.13	1.11	6.87	7.36	2.28	0.76
330	0.10	1.18	9.35	6.43	2.22	0.78
340	0.63	1.27	8.26	7.89	2.25	0.75
350	1.07	1.17	7.92	6.30	2.18	0.76
360	1.43	1.41	8.93	7.67	2.21	0.76
370	2.03	1.19	7.25	6.07	2.19	0.75
380	2.33	1.45	9.33	6.79	2.17	0.75
390	2.87	1.31	8.05	7.24	2.20	0.74
400	3.27	1.44	8.31	5.99	2.17	0.74
410	3.60	1.48	8.07	7.40	2.20	0.74
420	4.13	1.31	7.72	5.89	2.19	0.75
430	4.43	1.45	8.56	7.76	2.20	0.75
440	4.93	1.39	8.65	6.41	2.21	0.75
450	5.23	1.28	10.17	7.95	2.25	0.76
460	5.70	1.37	9.03	8.40	2.30	0.77
470	6	1.14	11.31	9.94	2.37	0.83
480	6.40	1.13	11.12	11.38	2.48	0.87
490	6.57	0.97	14.12	13.38	2.61	0.95
500	6.67	0.76	17.68	14.73	2.83	1.01

Table B.3: Mz estimation over entire dataset 120515_1 for fixed self-noise with valid area attenuation limit -10 dB.

	Mz		UL error [m]		SNR error [dB]	
Self-noise [m]	Mean	STD	Mean	STD	Mean	STD
150	-7.90	0.31	8.22	9.20	4.47	2.94
160	-7.57	0.50	8.23	6.34	4.12	2.53
170	-7.10	0.61	7.71	8.87	3.87	2.19
180	-6.73	0.78	9.21	6.58	3.65	1.95
190	-6.27	0.83	8.54	7.92	3.51	1.77
200	-5.83	0.99	9.23	7.06	3.38	1.63
210	-5.43	1.07	9.78	7.93	3.29	1.54
220	-5.03	1.16	9.91	8.33	3.22	1.46
230	-4.53	1.17	10.22	7.56	3.12	1.43
240	-4.13	1.33	11.18	9.19	3.07	1.39
250	-3.57	1.17	10.05	8.04	3.02	1.37
260	-3.27	1.31	11.28	8.64	2.95	1.34
270	-2.77	1.36	11.63	8.97	2.93	1.30
280	-2.23	1.36	9.32	6.34	2.85	1.31
290	-1.90	1.42	11.55	9.14	2.84	1.26
300	-1.23	1.36	8.66	6.55	2.79	1.27
310	-1.03	1.43	12.13	8.50	2.76	1.23
320	-0.43	1.55	10.07	8.56	2.76	1.22
330	-0.13	1.41	11.22	8.19	2.70	1.21
340	0.33	1.52	12.02	9.18	2.72	1.18
350	0.83	1.49	10.23	8.34	2.67	1.19
360	1.13	1.61	12.01	9.23	2.68	1.17
370	1.73	1.62	10.12	8.57	2.66	1.17
380	1.97	1.47	12.85	8.91	2.65	1.16
390	2.53	1.59	11.36	8.07	2.66	1.15
400	2.83	1.58	12.35	8.49	2.63	1.15
410	3.40	1.67	11.03	8.09	2.66	1.14
420	3.80	1.65	11.03	8.43	2.63	1.14
430	4.13	1.72	12.04	9.72	2.66	1.14
440	4.67	1.65	11.03	7.98	2.66	1.13
450	4.97	1.65	12.72	9.28	2.66	1.14
460	5.47	1.61	11.56	9.31	2.71	1.14
470	5.77	1.55	13.21	10.92	2.74	1.16
480	6.10	1.49	14.26	12.06	2.85	1.17
490	6.33	1.40	16.03	13.43	2.96	1.20
500	6.43	1.30	19.76	14.13	3.15	1.20

Table B.4: Self-noise estimation over entire dataset 120515_1 for fixed Mz with valid area attenuation limit 0 dB.

	Self-noise [m]		UL error [m]		SNR error [dB]	
Mz	Mean	STD	Mean	STD	Mean	STD
-8	151.67	4.61	7	6.78	2.73	0.84
-7	162.67	12.02	6.59	5.58	2.17	0.63
-6	184.67	14.32	6.28	5.16	2.07	0.60
-5	206.67	15.39	5.94	5.11	1.98	0.60
-4	229.33	16.39	5.72	4.96	1.88	0.59
-3	253.33	19.18	6.56	6.26	1.80	0.58
-2	274.67	19.07	6.84	5.10	1.74	0.57
-1	300	22.74	6.46	6.78	1.69	0.56
0	322	24.13	6.71	6.22	1.64	0.55
1	344.67	25.15	6.42	5.90	1.62	0.54
2	368.33	27.18	6.96	6.68	1.60	0.54
3	390.67	29	6.91	6.35	1.60	0.54
4	412	29.64	5.70	5.75	1.61	0.54
5	434.33	29.09	7.36	6.55	1.64	0.54
6	454	28.24	7.66	6.33	1.70	0.56
7	471.33	24.03	7.38	5.88	1.79	0.63

Table B.5: Self-noise estimation over entire dataset 120515_1 for fixed Mz with valid area attenuation limit -5 dB.

	Self-noise [m]		UL error [m]		SNR error [dB]	
Mz	Mean	STD	Mean	STD	Mean	STD
-8	155	11.37	7.35	6.80	3.27	0.99
-7	171.33	16.76	6.29	5.80	2.95	0.99
-6	193.33	17.29	4.83	5.17	2.78	0.93
-5	214	19.40	5.50	4.67	2.63	0.89
-4	238	20.74	6.83	6.60	2.50	0.84
-3	260	22.28	7.17	6.82	2.38	0.82
-2	281.67	23.65	7.07	6.04	2.29	0.79
-1	305	26.49	6.98	6.42	2.23	0.77
0	326.67	26.95	7.44	6.26	2.18	0.76
1	350.33	30	7.85	6.09	2.15	0.75
2	373.33	31.11	7.82	6.99	2.13	0.74
3	397.33	31.29	9.05	6.90	2.13	0.74
4	419	32.20	7.44	6.47	2.14	0.75
5	440	31.73	7.39	6.28	2.18	0.78
6	459.33	27.91	7.13	6.95	2.27	0.90
7	475.33	22.70	6.65	6.26	2.43	1.08

Table B.6: Self-noise estimation over entire dataset 120515_1 for fixed Mz with valid area attenuation limit -10 dB.

	Self-noise [m]		UL error [m]		SNR error [dB]	
Mz	Mean	STD	Mean	STD	Mean	STD
-8	163.67	24.56	12.09	9.70	3.71	1.42
-7	180.67	26.77	11.03	8.29	3.40	1.42
-6	202.33	28.37	10.88	9.42	3.23	1.34
-5	223	28.91	10.83	9.04	3.08	1.28
-4	245.33	29.09	10.20	8.79	2.95	1.23
-3	267	30.98	10.92	8.96	2.83	1.20
-2	289	32.52	10.73	8.21	2.75	1.17
-1	312.67	32.79	10.64	8.86	2.68	1.15
0	334.67	35.11	10.87	8.97	2.63	1.15
1	358	37.18	11.28	8.54	2.61	1.14
2	380	37.87	10.85	8.37	2.59	1.13
3	404.67	39.10	11.86	8.79	2.59	1.14
4	425.33	35.01	9.91	8.15	2.62	1.18
5	444.33	30.59	9.25	7.84	2.72	1.33
6	463.33	25.51	9.32	7.97	2.88	1.59
7	480.33	20.25	9.27	7.86	3.09	1.93

Table B.7: Mz and self-noise estimation over dataset 120515_1, one averaged 30-ping section per line with valid area attenuation limit 0 dB.

Line	Mz	Self-noise [m]	UL error [m]	SNR error [dB]
1	3	330	8.24	1.96
2	3	340	13.14	0.78
3	3	370	12.43	1.40
4	2	330	6.14	1.17
5	3	420	3.84	1.38
6	4	390	8.13	1.32
7	2	350	21.46	2.12
8	5	410	24.28	1.71
9	2	350	4.64	1.82
10	2	350	6.28	1.27
11	2	400	0.28	1.97
12	2	360	1.73	1.22
13	3	370	0.44	2.07
14	3	390	6.42	1.79
15	3	390	2.50	1.53
16	4	410	2.39	1.91
17	4	450	2.53	1.19
18	2	440	1.45	1.23
19	3	390	0.03	1.17
20	2	380	11.66	1.64
21	2	350	2.09	1.60
22	3	400	13.62	1.58
23	3	410	7.21	1.48
24	2	380	0.62	1.41
25	3	400	11.86	3.94
26	3	400	4.05	1.49
27	2	380	19.94	1.79
28	2	380	1.07	1.36
29	3	420	1.94	1.29
30	4	440	3.20	1.31
Mean:	2.80	386	6.79	1.60
STD:	0.79	31.47	6.47	0.53

Table B.8: Mz and self-noise estimation over dataset 120515_1, one averaged 30-ping section per line with valid area attenuation limit -5 dB.

Line	Mz	Self-noise [m]	UL error [m]	SNR error [dB]
1	3	340	14.24	2.52
2	2	320	13.14	2.28
3	3	380	18.43	2.86
4	5	390	4.14	1.36
5	2	400	2.84	1.33
6	4	390	8.13	1.76
7	3	380	26.46	2.24
8	4	390	25.28	2.12
9	3	390	1.36	2.42
10	4	400	9.28	2.28
11	3	460	14.28	4.28
12	3	390	2.27	2.42
13	3	380	6.56	2.07
14	3	400	13.42	2.09
15	3	400	7.50	2.16
16	2	370	5.39	1.92
17	3	450	7.47	3.55
18	3	480	7.45	2.43
19	3	390	0.03	1.14
20	-2	280	3.66	1.72
21	3	380	2.09	1.66
22	5	440	9.62	1.65
23	2	400	6.21	2.35
24	3	400	1.38	1.46
25	2	370	6.86	3.88
26	2	380	2.05	1.45
27	2	380	19.94	1.76
28	4	430	0.93	1.34
29	3	430	6.94	1.79
30	3	420	1.20	1.38
Mean:	2.87	393.67	8.29	2.12
STD:	1.20	38.43	6.96	0.73

Table B.9: Mz and self-noise estimation over dataset 120515_1, one averaged 30-ping section per line with valid area attenuation limit -10 dB.

Line	Mz	Self-noise [m]	UL error [m]	SNR error [dB]
1	3	350	18.24	2.81
2	3	350	20.14	2.92
3	3	400	28.43	3.91
4	3	360	11.14	2.90
5	2	480	27.16	5.85
6	3	400	25.13	4.34
7	2	350	21.46	2.18
8	0	300	22.28	2.23
9	3	390	1.36	2.58
10	3	380	11.28	2.69
11	3	490	26.28	5.05
12	2	380	9.27	3.28
13	3	380	6.56	2.05
14	4	420	11.42	2.09
15	3	400	7.50	2.11
16	4	420	8.39	1.89
17	2	440	13.47	3.79
18	3	500	15.45	2.64
19	3	390	0.03	1.14
20	-4	230	1.34	1.83
21	4	400	2.09	1.67
22	7	480	8.62	1.64
23	2	400	6.21	2.37
24	4	420	2.38	1.75
25	2	370	6.86	3.88
26	2	380	2.05	1.45
27	2	380	19.94	1.76
28	4	430	0.93	1.34
29	3	430	6.94	1.77
30	3	420	1.20	1.38
Mean:	2.70	397.33	11.45	2.58
STD:	1.68	53.79	8.78	1.12

Table B.10: Mz estimation over entire dataset 080814_1 for fixed self-noise with valid area attenuation limit 0 dB.

	Mz		Surface		UL error [m]		SNR error [dB]	
Self-noise [m]	Mean	STD	Mean	STD	Mean	STD	Mean	STD
150	-1.25	1.96	4.17	4.17	9.73	6.22	1.20	0.62
200	2.42	2.78	2.92	2.92	12.24	10.17	1.17	0.62
250	3.25	3.77	2.92	2.92	27.05	33.47	1.21	0.59
300	1.33	2.53	2.58	2.58	67.76	55.12	1.42	0.56
350	0.42	1.08	2.58	2.58	111.84	78.26	1.46	0.58
400	0.42	1.08	2.58	2.58	132.34	92.20	1.46	0.58

Table B.11: Mz estimation over entire dataset 080814_1 for fixed self-noise with valid area attenuation limit -5 dB.

	Mz		Surface		UL error [m]		SNR error [dB]	
Self-noise [m]	Mean	STD	Mean	STD	Mean	STD	Mean	STD
150	-1.33	0.89	4.17	4.17	9.14	5.71	1.43	0.72
200	1.83	1.47	2.42	2.42	7.98	5.91	1.37	0.62
250	3.67	3.80	2.42	2.42	9.69	12.20	1.74	0.65
300	4.08	4.87	2.58	2.58	23.56	33.54	2.17	0.60
350	-0.58	0.90	2.00	2.00	56.90	65.70	2.59	0.80
400	-0.75	0.97	2.08	2.08	54.77	74.62	2.60	0.80

Table B.12: Mz estimation over entire dataset 080814_1 for fixed self-noise with valid area attenuation limit -10 dB.

	Mz		Surface		UL error [m]		SNR error [dB]	
Self-noise [m]	Mean	STD	Mean	STD	Mean	STD	Mean	STD
150	-1.83	0.94	4.17	4.17	11.34	6.47	1.68	0.69
200	1.75	1.22	2.08	2.08	11.69	7.76	1.62	0.63
250	5.83	2.89	3.83	3.83	14.74	9.23	2.25	0.64
300	7.08	4.25	3.83	3.83	22.35	7.88	2.70	0.71
350	1.75	5.36	2.17	2.17	25.95	7.01	3.57	0.80
400	0.17	4.22	1.75	1.75	26.57	7.51	3.75	0.74

Table B.13: Mz, surface and self-noise estimation over dataset 080814_1, valid area attenuation limit -5 dB.

Line	Mz	Surface	Self-noise [m]	UL error [m]	SNR error [dB]
1	-1	0	180	3.71	2.14
2	1	1	200	8.44	1.17
3	2	0	180	6.40	1.10
4	2	2	240	11.56	1.78
5	1	2	180	13.32	1.49
6	0	5	150	3.68	0.73
7	2	3	180	9.28	1.07
8	1	4	190	18.31	1.25
9	2	0	190	19.22	1.54
10	1	4	160	5.80	1.25
11	0	4	180	4.23	1.36
12	0	4	170	14.29	1.13
Mean:	0.92	2.42	183.33	9.85	1.34
STD:	0.95	1.83	21.34	5.26	0.35

Table B.14: Mz estimation over entire dataset 120918_2 for fixed self-noise with valid area attenuation limit 0 dB.

	Mz		Surface		LL error [m]		UL error [m]		SNR error [dB]	
Self-noise [m]	Mean	STD	Mean	STD	Mean	STD	Mean	STD	Mean	STD
150	-2.56	2.19	6.59	6.59	2.41	2.08	15.20	11.05	2.26	1.31
200	0.34	3.25	5.02	5.02	2.53	2.09	16.25	13.77	2.05	1.27
250	2.41	3.30	3.54	3.54	2.35	2.10	20.96	15.53	2	1.23
300	3.93	2.88	3.32	3.32	2.26	1.81	29.08	24.04	2.01	1.21
350	4.07	3.19	3.20	3.20	2.30	1.85	46.79	45.68	2.05	1.20
400	3.85	3.09	3.32	3.32	2.28	1.80	68.09	63	2.10	1.19
450	3.83	3.06	3.29	3.29	2.31	1.81	90.81	72.64	2.12	1.18
500	3.83	3.06	3.29	3.29	2.31	1.81	104.64	78.72	2.13	1.18

Table B.15: Mz estimation over entire dataset 120918_2 for fixed self-noise with valid area attenuation limit -5 dB.

	Mz		Surface		LL error [m]		UL error [m]		SNR error [dB]	
Self-noise [m]	Mean	STD	Mean	STD	Mean	STD	Mean	STD	Mean	STD
150	-2.90	2.14	6.56	6.56	2.37	2.01	14.81	10.83	3.13	1.95
200	-0.05	3.06	5.29	5.29	2.37	2.03	16.69	14.94	2.90	1.66
250	2.29	3.80	3.44	3.44	2.36	2.12	19.20	15.25	2.79	1.50
300	3.44	4.27	3.68	3.68	2.21	1.91	22.73	21.37	2.90	1.40
350	3.83	4.36	3.41	3.41	2.30	1.84	31.19	38.88	3.06	1.28
400	4.02	4.23	3.20	3.20	2.27	1.76	40.87	48.35	3.21	1.21
450	3.68	4.08	3.10	3.10	2.37	1.80	54.46	58.66	3.31	1.17
500	3.37	3.95	3	3	2.44	1.89	61.58	70.06	3.36	1.15

Table B.16: Mz estimation over entire dataset 120918_2 for fixed self-noise with valid area attenuation limit -10 dB.

	Mz		Surface		LL error [m]		UL error [m]		SNR error [dB]	
Self-noise [m]	Mean	STD	Mean	STD	Mean	STD	Mean	STD	Mean	STD
150	-3.59	2.60	6.37	6.37	2.42	2.07	16.63	10.02	5.68	5.48
200	-0.93	3.71	5.15	5.15	2.37	1.99	16.52	9.48	4.91	4.10
250	1.34	4.71	3.29	3.29	2.41	2.10	17.88	10.51	4.57	3.28
300	3.56	5.61	3.49	3.49	2.39	2.12	18.87	12.80	4.64	2.73
350	2.95	5.40	2.61	2.61	2.37	1.79	22.54	12.83	4.88	2.34
400	2.88	5.27	2.63	2.63	2.40	1.78	28.08	19.33	5.25	2.04
450	2.54	5.08	2.41	2.41	2.53	1.84	38.65	40.87	5.56	1.91
500	1.66	4.40	2.05	2.05	2.53	1.90	46.20	54.06	5.79	1.86

Table B.17: Bottom type, sea state and self-noise estimation over dataset 120918_2, valid area attenuation limit -5 dB.

Line	Mz	Surface	Self-noise [m]	UL error [m]	SNR error [dB]
1	2	2	270	8.74	2.43
2	2	0	290	67.24	2.28
3	2	0	250	27.28	2.02
4	2	2	390	9.69	1.97
5	-2	6	150	2.67	1.74
6	3	2	190	34.93	2.54
7	3	3	210	8.34	1.30
8	3	2	230	19.36	2.18
9	3	0	190	14.85	4.78
10	4	2	270	12.81	1.87
11	4	2	250	12.22	1.70
13	5	5	210	32.37	2.53
16	4	4	350	16.12	2.08
17	4	3	370	9.88	3.26
22	6	3	490	6.98	6.37
24	9	4	270	4.30	1.49
25	4	0	290	8.47	1.71
26	2	0	270	24.38	2.77
27	3	0	230	17.35	2.08
28	2	2	470	24.75	2.29
29	3	1	270	15.68	3.59
30	1	6	190	5.30	0.71
31	3	6	230	2.28	0.88
32	4	3	190	41.62	4.30
33	-3	8	150	17.42	1.06
34	4	3	350	4.55	1.69
35	3	4	270	9.46	0.99
36	1	8	170	5.12	1.38
37	-2	9	150	29.12	1.69
38	3	6	230	8.12	1.52
39	3	6	210	12.11	1.52
40	4	5	310	3.88	1.24
41	4	6	230	5.89	1.02
Mean:	2.82	3.42	260.30	15.86	2.15
STD:	2.18	2.52	82.26	13.44	1.17

Bibliography

APL-UW (1994). *High-frequency ocean environment acoustic models handbook*. Technical Report APL-UW TR 9407. Applied Physics Laboratory, University of Washington.

Blomberg, A. E. A., A. Austeng, R. E. Hansen, and S. A. V. Synnes (2012). Improving sonar performance in shallow water using adaptive beamforming. *IEEE Journal of Oceanic Engineering (Accepted for release)*.

Blondel, P. (2009). *The Handbook of Sidescan Sonar*. Springer.

Burden, R. L. and J. D. Faires (2010). *Numerical Analysis*. Cengage Learning.

Burdic, W. S. (1984). *Underwater Acoustic System Analysis*. Prentice-Hall.

Capon, J. (1969). High-resolution frequency-wavenumber spectrum analysis. *Proceedings of the IEEE 57*(8), pp. 1408 – 1418.

Carter, G., C. Knapp, and A. Nuttall (1973). Statistics of the estimate of the magnitute-coherence function. *IEEE Transactions on Audio and Electroacoustics 21*(4), pp. 388 – 389.

Chen, Q., W. Xu, X. Pan, and J. Li (2009). Wideband multipath rejection for shallow water synthetic aperture sonar imaging. *IET Radar, Sonar & Navigation 3*(6), p. 620.

Crosby, F. and J. T. Cobb (2005). Sonar processing for short range, very-high resolution autonomous underwater vehicle sensors. In *Proceedings of MTS/IEEE OCEANS, 2005*, Volume 1, pp. 398 – 402.

Eiben, A. E. and J. E. Smith (2007). *Introduction to Evolutionary Computing*. Springer.

Fish, J. P. and H. A. Carr (2001). *Sound Reflections: Advanced Applications of Side Scan Sonar Data*. Lower Cape Pub Co.

Hansen, R. E. (2011). Introduction to synthetic aperture sonar. In N. Z. Kolev (Ed.), *Sonar Systems*, pp. 3 – 28. Intech.

Hansen, R. E., H. J. Callow, T. O. Sæbø, and S. A. V. Synnes (2011). Challenges in seafloor imaging and mapping with synthetic aperture sonar. *IEEE 49*(10), pp. 3677 – 3687.

Hanssen, R. F. (2001). *Radar Interferometry: Data Interpretation and Error Analysis*. Dordrecht, The Netherlands: Kluwer Academic Publishers.

Hayes, M. P. (2004). Multipath reduction with a three element interferometric synthetic aperture sonar. In *Proc. European Conf. Underwater Acoustics (ECUA)*, pp. 1151 – 1156.

Hayes, M. P. and P. T. Gough (2009). Synthetic aperture sonar: A review of current status. *IEEE J. Oceanic Eng. 34*(3), pp. 207 – 224.

Johnson, D. H. and D. E. Dudgeon (1993). *Array Signal Processing: Concepts and Techniques*. Prentice Hall.

Kay, S. M. (1993). *Fundamentals of Statistical Signal Processing: Estimation Theory*. Prentice Hall International Editions.

Kirsteins, I. P. (2003). Blind separation of signal and multipath interference for synthetic aperture sonar. In *OCEANS 2003*, pp. 2641 – 2648, Vol. 5.

Kraeutner, P. H. and J. S. Bird (1999). Beyond interferometry, resolving multiple angles-of-arrival in swath bathymetric imaging. In *OCEANS '99 MTS/IEEE. Riding the Crest into the 21st Century*, Volume 1, pp. 37 – 45.

Le Bas, T. P., D. C. Mason, and N. C. Millard (1995). TOBI image processing-the state of the art. *IEEE Journal of Oceanic Engineering 20*(1), pp. 85 – 93.

LeBlond, P. H. and L. A. Mysak (1978). *Waves in the Ocean*. Elsevier.

Li, J., P. Stoica, and Z. Wang (2003). On robust capon beamforming and diagonal loading. In *2003 IEEE International Conference on Acoustics, Speech, and Signal Processing, 2003. Proceedings. (ICASSP '03)*, Volume 5, pp. 337 – 340.

Lurton, X. (2002). *An Introduction to Underwater Acoustics*. Springer Praxis Publishing.

Marsland, S. (2009). *Machine Learning: An Algorithmic Perspective*. CRC Press.

Pinto, M., A. Bellettini, L. S. Wang, P. Munk, V. Myers, and L. Pautet (2004). A new synthetic aperture sonar design with multipath mitigation. *AIP Conference Proceedings 728*(1), pp. 489 – 496.

Stewart, R. H. (2009). *Introduction to Physical Oceanography*. University Press of Florida.

Synnes, S. A. V. (2009). Potensiale for 60% auka rekkevidde for HISAS ved eckernförde. FFI reference 09/02034/FFI. Fortrolig.

Synnes, S. A. V. (2011). Sonar performance modeling for seafloor imaging in shallow waters - concept and implementation in SMURF 1.0 and SPRAY 1.0. FFI-rapport 2011/00582, Forsvarets forskningsinstitutt. Unntatt offentlighet.

Synnes, S. A. V., R. E. Hansen, and T. O. Sæbø (2009). Assessment of shallow water performance using interferometric sonar coherence. In *UAM 2009*, Nafplion, Greece.

Synnevåg, J. F., S. Holm, and A. Austeng (2008). A low complexity data-dependent beamformer. In *IEEE Ultrasonics Symposium, 2008. IUS 2008*, pp. 1084–1087.

Sæbø, T. O. (2010). *Seafloor depth estimation by means of Interferometric synthetic aperture sonar*. Ph. D. thesis, University of Tromsø.

The Norwegian Meteorological Institute (2012). Date search for observation station number 17280 Gullholmen, Moss (Østfold). http://www.yr.no/place/Norway/Vestfold/Horten/Horten/almanakk.html.

Urick, R. J. (1983). *Principles of underwater sound* (3d ed.). Los Altos, CA, USA: Mcgraw-Hill Book Company.

Van Trees, H. L. (2002). *Optimum Array Processing*. Wiley-Interscience.

Xu, W. and W. K. Stewart (1999). Coherent source direction estimation for three-row bathymetric sidescan sonars. In *OCEANS '99 MTS/IEEE. Riding the Crest into the 21st Century*, Volume 1, pp. 299 – 304.

Zebker, H. A. and J. Villasenor (1992). Decorrelation in interferometric radar echoes. *IEEE Trans. Geosci. Remote Sensing. 30*(5), pp. 950 – 959.

Ziomek, L. J. (1985). *Underwater Acoustics: A Linear Systems Theory Approach*. Academic Press.